LUND UNIVERSITY

Radiation and radionuclide measurements at radiological and nuclear emergencies. Use of instruments and methods intended for clinical radiology and nuclear medicine.

Ören, Ünal

2016

Document Version:
Publisher's PDF, also known as Version of record

Radiation and radionuclide measurements at radiological and nuclear emergencies

Use of instruments and methods intended for clinical radiology and nuclear medicine

Ünal Ören

LUND
UNIVERSITY

DOCTORAL DISSERTATION
by due permission of the Faculty of Medicine, Lund University, Sweden.
To be defended at room 2005-7, DC, SUS, Malmö, 2016-12-15, 9:00

Faculty opponent
Professor Christer Fröjdh,
Mid Sweden University, Sundsvall

Organization LUND UNIVERSITY	Document name DOCTORAL DISSERTATION
	Date of issue 2016-12-15
Author(s) Ünal Ören	Sponsoring organization

Title and subtitle: Radiation and radionuclide measurements at radiological and nuclear emergency situations - Use of instruments and methods intended for clinical radiology and nuclear medicine

Abstract

In this thesis, applications of radiation detectors and imaging modalities, intended for clinical radiology and nuclear medicine were investigated for applications in radiological and nuclear emergency (RN) situations.

The suitability of self-developing radiochromic films were investigated as real-time visually readable dosemeters for first responders in radiation emergency situations (Paper I). It was shown that the Gafchromic RTQA2 type film was suitable for use in RN scenarios due to its relatively low energy dependence in dose response for the relevant radiation qualities.

The response characteristics of a solid-state x-ray detector, widely available at hospitals and used in diagnostic radiology, were investigated for radiation safety applications (Paper II). The results show that the x-ray detector has a relative energy response of a factor of < 2 when normalized to ^{60}Co and could thus be applied in a broad range of photon energies.

Paper III describes the feasibility of using a silicon detector, available in hospitals and used for quality control of Computed Tomography (CT) systems, as a portable hand-held alpha particle spectrometer for field measurements. The results demonstrate that spectrometric measurements were achievable after a modification of the silicon detector and the detector efficiencies and minimum detectable activity (MDA) values were calculated.

In Paper IV it was evaluated whether, from a radiation risk perspective, it is justified to use diagnostic imaging modalities such as CT and Digital Radiography (DR) to detect radioactive fragments in the body. It was concluded that imaging could be justified for individuals with incorporated radioactive fragments where the activity levels are on the order of megabecquerel.

In Paper V, the use of an easilly constructed conical-cylindrical phantom as a replacement for an anthropomorphic phantom was tested by deriving calibration coefficients MDA values for ^{131}I and ^{137}Cs *in-vivo* when using a dual-headed gamma camera for internal contamination assessment purposes.

In conclusion, this thesis provides insights of the capacity and role of radiation detectors and imaging modalities that could be applied in radiation emergencies and could thus strengthen the emergency preparedness plans in health care facilities.

Key words		
Classification system and/or index terms (if any)		
Supplementary bibliographical information		Language: English
ISSN and key title		ISBN 978-91-7619-375-4
Recipient's notes	Number of pages 50	Price
	Security classification	

Signature 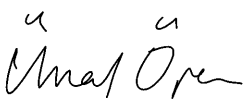 Date 2016-11-07

Radiation and radionuclide measurements at radiological and nuclear emergencies

Use of instruments and methods intended for clinical radiology and nuclear medicine

Ünal Ören

LUND
UNIVERSITY

Lund University, Faculty of Medicine Doctoral Dissertation Series 2016:148
Department of Translational Medicine
Medical Radiation Physics Malmö
Skåne University Hospital
SE-205 02 Malmö, Sweden

ISBN 978-91-7619-375-4
ISSN 1652-8220

Printed in Sweden by Media-Tryck, Lund University
Lund 2016

Till Gülay, Atilla, Timur

Content

Acknowledgements

My sincere appreciation and thankfulness goes to:

- My supervisors:
  - *Christopher L Rääf* for your continuous support, guidance, mentorship, patience and for giving me the opportunity to participate in a stimulating research environment.
  - *Sören Mattsson* for your inspiration and sharing your vast knowledge, endless encouragement, enthusiasm and constructive feedback.
- My co-authors:
  - *Mats Hansson, Martin Andersson, Jonas Nilsson, Lars Herrnsdorf and Mikael Gunnarsson* for close collaboration, support at all levels and contribution to this work.
- Present and past colleagues at the Medical Radiation Physics Malmö, Lund University and Radiation Physics, Skåne University Hospital, Malmö:
  - *LEO, Jonas J, Christian B, Karl Ö, Mattias J, Therese GB, Marcus P, Hanna H, Maria C, Hannie P, Simon K, Lena T, Magnus D, Pontus T, Daniel F, Marcus S, Kurt S, Peder K, Gertie J, Pernilla P, Sven M, David M, Kai N, Peter W, Veronica NL, Sven B, Viveca F, Sigrid LS, Anders T et al.* for creating a pleasant work atmosphere.
- My family for your love and support

This research was financially supported by the Swedish Radiation Safety Authority (SSM).

List of figures

Abbreviations

CT	Computed tomography
CTDIvol	Volume computed tomography dose index
CTDP	CT Dose Profiler
DAP	Dose area product
DR	Digital radiography
HVL	Half value layer
IAEA	International Atomic Energy Agency
ICRP	International Commission on Radiological Protection
LiF:Mg, Ti	Lithium fluoride doped Mg and Ti
MDA	Minimum detectable activity
MPV	Mean pixel value
NDCT	Non-diagnostic computed tomography
NOD	Net optical density
OD	Optical density
PHA	Pulse-height analyzer
PMMA	Polymethyl methacrylate
QA	Quality assurance
RDD	Radiological dispersal device
RN	Radiological and nuclear
ROI	Region of interest
RTQA	Radiotherapy quality assurance
SD	Standard deviation
SDCT	Standard-dose computed tomography
SDD	Source to detector distance
SPECT	Single-photon emission computed tomography
TLD	Thermoluminescent dosemeter
WBC	Whole-body counter
XRQA	X-ray quality assurance

Original papers

This thesis is based on the following five publications, which will be referred to by their Roman numerals:

I. Gafchromic film as a fast visual indicator of radiation exposure of first responders. Ören, Ü., Rääf, C.L., Mattsson, S. *Radiat. Prot. Dosimetry* 150(1), 119-23 (2012)

II. Can an energy-compensated solid-state x-ray detector be used for radiation protection applications at higher photon energies? Ören, Ü., Herrnsdorf, L., Gunnarsson, M., Mattsson, S., Rääf, C.L. *Radiat. Prot. Dosimetry* 169(1–4), 292–96 (2016)

III. Silicon diode as an alpha particle detector and spectrometer for direct field measurements. Ören, Ü., Nilsson, J., Herrnsdorf, L., Gunnarsson, M., Rääf, C.L., Mattsson, S. *Radiat. Prot. Dosimetry* 170(1–4), 247–51 (2016)

IV. Detection of radioactive fragments in patients after radiological or nuclear emergencies using computed tomography and digital radiography. Ören, Ü., Hansson, M., Mattsson, S., Rääf, C.L. *J. Radiol. Prot.* 34(1), 231-47 (2014)

V. A phantom for determination of calibration coefficients and minimum detectable activities using a dual-head gamma camera for internal contamination monitoring following radiation emergency situations. Ören, Ü., Andersson, M., Rääf., C.L, Mattsson, S. *Radiat. Prot. Dosimetry* 169(1–4), 297–302 (2016)

Preliminary reports

Preliminary reports were presented at the following meetings:

Gafchromic as a fast visual indicator of radiation exposure of first responders at radiological or nuclear accidents. NSFS Conference Current Challenges in Radiation Protection, Reykjavik, Island, 22-25 Aug 2011

Using computed tomography and digital radiography of the human body to visualize metal fragments from bomb explosions – A preliminary report. 10th International Conference Medical Physics in the Baltic States 2012, Kaunas, Lithuania, 8-10 Nov 2012

Effective dose from a cobalt-60 hot particle following nuclear events. International Scientific Conference "Radiation Environment and Technosphere", Gomel, Belarus, 26-27 Sept 2013

Silicon diode as a dosemeter for radiation emergency situations. The Third Annual Sweray's Workshop, Malmö, Sweden, 20-22 Aug 2014

Silicon photodiode as a dosemeter for first responders in radiation emergency situations. Third International Conference on Radioecology and Environmental Radioactivity, Barcelona, Spain, 7-12 Sept 2014

A portable charged particle detector and spectrometer based on silicon diodes. International Conference on Individual Monitoring of Ionising Radiation, Bruges, Belgium, 20-24 April 2015

Can an energy compensated solid-state x-ray detector be used for radiation protection applications at higher energies? Optimisation in X-ray and Molecular Imaging, Gothenburg, Sweden, 28-30 Maj 2015

A phantom for determination of calibration coefficients and minimum detectable activities using a SPECT/CT for internal contamination monitoring following radiation emergency situations. Optimisation in X-ray and Molecular Imaging, Gothenburg, Sweden, 28-30 Maj 2015

Related publication

Ören, Ü., Hiller, M., Andersson, M. IDACstar: A MCNP application to perform realistic dose estimations from internal or external contamination of radiopharmaceuticals. *Radiat. Prot. Dosimetry* (2016) doi: 10.1093/rpd/ncw22 First published online: July 29, 2016

Abstract

In this thesis, applications of radiation detectors and imaging modalities, intended for clinical radiology and nuclear medicine were investigated for applications in radiological and nuclear emergency (RN) situations.

The suitability of self-developing radiochromic films were investigated as real-time visually readable dosemeters for first responders in radiation emergency situations (Paper I). It was shown that the Gafchromic RTQA2 type film was suitable for use in RN scenarios due to its relatively low energy dependence in dose response for the relevant radiation qualities.

The response characteristics of a solid-state x-ray detector, widely available at hospitals and used in diagnostic radiology, were investigated for radiation safety applications (Paper II). The results show that the x-ray detector has a relative energy response of a factor of < 2 when normalized to ^{60}Co and could thus be applied in a broad range of photon energies.

Paper III describes the feasibility of using a silicon detector, available in hospitals and used for quality control of Computed Tomography (CT) systems, as a portable hand-held alpha particle spectrometer for field measurements. The results demonstrate that spectrometric measurements were achievable after a modification of the silicon detector and the detector efficiencies and minimum detectable activity (MDA) values were calculated.

In Paper IV it was evaluated whether, from a radiation risk perspective, it is justified to use diagnostic imaging modalities such as CT and Digital Radiography (DR) to detect radioactive fragments in the body. It was concluded that imaging could be justified for individuals with incorporated radioactive fragments where the activity levels are on the order of megabecquerel.

In Paper V, the use of a simple conical-cylindrical phantom as a replacement for an anthropomorphic phantom was tested by deriving calibration coefficients and MDA values for ^{131}I and ^{137}Cs *in-vivo* when using a dual-headed gamma camera for internal contamination assessment purposes.

In conclusion, this thesis provides insights of the capacity and role of radiation detectors and imaging modalities that could be applied in radiation emergencies and could thus strengthen the emergency preparedness plans in health care facilities.

Populärvetenskaplig sammanfattning

Syftet med avhandlingen är att undersöka sjukvårdsutrustnings potential för snabb bestämning av intern och extern-exponering och kontaminering av personer i händelse av nukleära- eller radiologiska (RN) krishändelser och nödsituationer. Avhandlingen består av fem delarbeten och fokuserar på lättillgängliga mätresurser inom sjukvården vilka skulle kunna förstärka nationella strålskyddsberedskapen och vars mätpotential i händelse av större RN krishändelser och nödhändelser hittills inte alls till fullo utforskats.

Film, som utan efterföljande framkallning ändrar färg vid bestrålning används för stråldosmätningar inom röntgendiagnostik och strålbehandling. I Arbete I har sådan film undersökts med avseende på responsen för strålkvalitéer som är aktuella vid RN-händelser. Det påvisades att Gafchromic RTQA2 filmtyper kan t.ex. användas som direktvisande dosimetrar av räddningspersonal och medge snabb visuell indikation på dostillskott ner till 35 mSv.

I arbete II demonstrerades det att ett kiselelement som används för kvalitetssäkring inom röntgendiagnostik även kan användas för dosimetri i beredskapssammanhang. Det påvisades att detektorn med dess energikompenserande filter kan utnyttjas för bestämning av absorberad dos inom energiområdet 29 keV – 1.25 MeV med en mätnoggrannhet inom en faktor 2.

Ett liknande men filterlöst kiselelement användes också för att testa förmågan att detektera alfastrålning (Arbete III). Syftet var att utforska om en enkel och bärbar baskonfiguration av denna detektor kan användas för att detektera alfastrålning spektrometriskt, d.v.s. att kunna särskilja energierna på de infallande alfapartiklarna och därmed identifiera vilken alfastrålande radionuklid det rör sig om. Tillämpningar skulle kunna vara mätningar på hud och kläder på personer på en skadeplats och i öppna sår och på hud hos patienter som skadats och genomgår kirurgiska ingrepp.

I Arbete IV genomfördes experiment med datortomografi (CT, ”skiktröntgen”) och digital röntgenteknik för att fastställa detektionsgränser för radioaktiva fragment i individer. Partikelfragment ner till 100-180 µm skulle kunna påvisas till en effektiv dos som ej överstiger 6 mSv. Det fastställdes vilka effektiva doser som minst skulle krävas för att detektera dessa partiklar och detta ställdes i relation till de effektiva doser som det radioaktiva fragmentet skulle ge om man inte avlägsnade det kirurgiskt.

Ett lättillverkat och billigt fantom applicerbart för gammakameror togs fram i Arbete V i syfte att bestämma omräkningstal från mätvärde till aktivitet av radionuklider för att fastställa eller utesluta intern kontamination. Fantomet kan ersätta dyrare mera människoliknande fantom och kan reproduceras på kliniker som vill använda gammakameror och SPECT/CT utrustningar i sina beredskapsplaner.

Den viktigaste slutsatsen är att den kliniska utrustning som idag används av sjukvården har en unik potential för kartläggning av radioaktiva föroreningar och kartläggning av stråldoser till individer i samband med storskaliga och allvarliga RN händelser.

1.Introduction

In case of radiological and nuclear (RN) emergency scenarios, such as accidents at nuclear facilities, transportation accidents involving radioactive material or radiological dispersal device (RDD) attacks, it will be essential to assess the radiological situation. Individuals could be subject to ionizing radiation by external exposure or by contamination, which could occur internally or externally. Internal contamination due to radioactive material can occur through inhalation, ingestion or through open wounds [1]. Individuals in the vicinity of a RDD explosion will also sustain injuries from embedded radioactive fragments [2].

Following radioactivity release situations where a large number of people are affected, appropriate emergency management measures would be required. In the management of mass casualty scenarios due to RN events it is anticipated that hospitals, emergency departments and first responders from the local community will have an important role at an initial stage [3]. One of the major goals of the response to radiation emergencies is to protect the public and the emergency response personnel from radiation exposure and its consequences. Following the aforementioned scenarios, where large amounts of radionuclides could be released, large groups of people could be affected and rapid measurements are required in order to identify people who need further care. Also, the first responders need to be prepared to work in environments with elevated radiation levels and healthcare workers face the challenge to manage radiological contaminated victims.

Hospitals, especially the larger ones, are equipped with a variety of radiation detectors and imaging modalities used in clinical radiology and nuclear medicine departments. During the aftermath of RN incidents the potential of efficiently deploy available hospital equipment has to be considered and this thesis explores the possibility of using commonly available hospital resources in RN scenarios. Deployable equipment includes gamma cameras, computed tomography and digital radiography systems, which could be used for internal contamination assessment whereas external exposures could be assessed with radiochromic films and solid-state x-ray detectors. Paper I and II focus on radiochromic films and x-ray silicon detectors for external exposure situations whereas Paper III utilizes silicon diodes for external contamination assessment. Paper IV and V investigate the possibility of using computed tomography, digital radiography and gamma cameras for internal or external contamination measurements. The results in this thesis are of interest for radiation accident management plans.

Utilizing already existing radiation detection instruments available at most hospitals could increase the radiation emergency response capability where well trained health

professionals such as emergency physicians, nuclear medicine technologists, diagnostic radiology personnel and medical physicists could play an active role in the management of potentially contaminated individuals. In this respect, the management of equipment, its adaptation and calibration is the responsibility of the medical physicists.

1.1 Objectives

The overall objective of this PhD thesis was to investigate possible applications of radiation detectors and imaging modalities intended for clinical radiology and nuclear medicine in radiation emergency situations.
In order to achieve this objective, five studies were conducted where each study has the following more specific aims:

- To evaluate the potential use of self-developing radiochromic films as real-time visually readable dosemeters for first responders in radiation emergency situations (Paper I).
- To investigate the response characteristics of a solid-state x-ray detector, widely available at hospitals and used in diagnostic radiology, for radiation safety applications (Paper II).
- To investigate the feasibility that a silicon detector, available in hospitals and used for quality control of computed tomography systems, after some modifications could be used as a portable hand-held alpha particle spectrometer for field measurements and under realistic ambient conditions (Paper III).
- To investigate whether, from a radiation risk perspective, it is justified to use imaging modalities utilizing ionizing radiation to detect radioactive fragments in the body with the intention to remove them (Paper IV).
- To test a simple conical-cylindrical phantom as a replacement for an anthropomorphic phantom by deriving calibration coefficients and minimum detectable activity values for ^{131}I and ^{137}Cs *in-vivo* when using a dual-headed gamma camera for internal contamination assessment purposes (Paper V).

2. Material and methods

2.1 Radiation detectors

2.1.1 Radiochromic films

In Paper I, three types of radiochromic films were studied for use as personal dosemeters and the films were of Gafchromic type [4]. In contrast to traditional radiographic films, which are based on silver bromide (AgBr) crystals, which has a high atomic number Z_{eff}, the Gafchromic films are nearly tissue-equivalent and are self-developing, eliminating the need for additional chemical processing [5]. The radiosensitive layer of Gafchromic films consists of components of monomers and a polymerization process occurs upon irradiation which is observed as a progressive darkening of the films as the radiation dose increases [6]. In order to be a possible candidate as a personal dosimeter in RN scenarios several criteria, such as real-time response and energy independency across a wide range of radiation qualities, have to be met.

The first radiochromic film (RTQA2) investigated was specifically designed for use in radiation therapy quality assurance procedures whereas the two other film types, XRQA and XRQA2, were intended for quality assurance procedures in diagnostic radiology [7]. The characterization of the films consisted of studying the response to different radiation qualities, the time dependency and visual readout tests. The sensitivity of multiple film layers and sensitivity to environmental conditions were also investigated. The reader is referred to Paper I for detailed description of these tests.

Two photon radiation sources were used to assess the energy dependence of the dose response: i) an X-ray unit (A-196, Varian Medical Systems, USA), operating at a tube voltage of 80 kV and ii) a ^{60}Co-unit (Gammatron-3, Siemens, Germany), with primary photon energies of 1.17 and 1.33 MeV. High-energy β-particles, using a sealed ^{90}Sr/^{90}Y source (E_{Max}=2.27 MeV; Risø TL-15 reader, Risö National Laboratory, Roskilde, Denmark), were also used for irradiations. The films, originally with an area of 25 x 25 cm^2, were cut into 2 x 2 cm^2 pieces. For the x-ray irradiations, the film pieces were placed on the surface of a 30 x 30 x 15 cm^3 water equivalent phantom (RW3, PTW Freiburg, Germany). For ^{60}Co exposures, the films were placed at a depth of 0.5 cm inside the phantom to ensure charge particle equilibrium at the position of the film layer. For both experimental setups, the films were irradiated, one at a time, at the center of 10 x 10 cm^2 field while placed perpendicular to the central beam axis. Two type of ionization chambers were exposed at the same positions as the films in order to relate

the signal (in terms of optical density [OD]) to the absorbed dose at the film plane. For ^{60}Co, absorbed doses were measured in the radiation field center with an Roos type chamber (TW34001 PTW, Freiburg, Germany) and for the 80 kV x-ray exposures a Radcal chamber (Model 2186, Monrovia, CA, USA) was used. For these measurements, the OD of the films were evaluated three hours post-irradiation in order to ensure completion of the polymerization. At least two hours after irradiation is recommended by the manufacturer before evaluating the films. For the relatively low absorbed doses in the current application, the response was however very fast (as shown in this study) and the evaluation could have been done immediately after exposure.

A portable densitometer (X-Rite 331 Grand Rapids, MI, USA) was used to assess the change in OD of the films and the net OD (NOD) were calculated for all films by subtracting the background levels from the results. Background levels required to obtain the NOD were determined from unexposed areas of the film sheet from the same batch. Subsequently, the NOD values were plotted against the dose values.

To determine the time dependence of the response, the RTQA2 films were irradiated to 91 mGy and 277 mGy and the NOD was evaluated at different time points (1- 300 min) post-irradiation.

Then, visual readout evaluation was performed with ten participants. First, the participants were presented ten randomly ordered Gafchromic RTQA2 films and each participant was asked to grade the film pieces from the lowest to highest dose where the films were previously exposed to absorbed doses ranging from 0 – 100 mGy from the X-ray unit. Then, each participant was shown an exposed film next to a reference background film, in a twin-film configuration, and the task was to identify the exposed film.

2.1.2 Semiconductor detectors

Silicon based detectors are common in various fields of medical physics such as conventional radiotherapy and radiology, proton and heavy charged particle radiotherapy, nuclear spectroscopy as well as in high energy physics [8, 9, 10, 11, 12, 13, 14, 15, 16, 17]. Two solid-state radiation detectors commonly available at hospitals were selected for the experiments: In Paper II, the R100 Dose probe (R100, RTI Electronics AB, Mölndal, Sweden) was used for photon detection in the energy range 29 to 1332 keV and in Paper III the CT Dose profiler (CTDP, RTI Electronics AB, Mölndal, Sweden), was used for the spectrometric detection of alpha particles. Both the R100 and the CTDP are based on silicon (Si) and the R100 detector has a 1x1 cm^2 sensitive area and a thickness of 0.36 mm whereas the CTDP has a 4 mm^2 active area and a thickness of 0.36 mm. The silicon sensor of the CTDP is manufactured by the Mid Sweden University, Sundsvall, Sweden. Furthermore, the R100 includes an inherent energy compensating filter whereas the CTDP was modified by uncovering the Si diode in order to detect alpha particles by milling a hole in the package cap.

2.1.2.1 Silicon detector – Dose probe R100

In Paper II, the R100 detector was evaluated for use as a real-time personal radiation monitor following RN events. As previously mentioned, the R100 is dedicated for quality assurance in diagnostic x-ray applications and it has a built-in energy correction filter [18]. This results in an energy compensation due to the attenuation of the lower energy photons by the correction filter. It is important to determine the detector response as a function of energy since RN emergencies can be associated with radionuclides emitting a broad range of gamma-ray energies (keV). Thus, basic dosimetric properties of the R100 detector such as energy dependence and linearity in dose response were examined in Paper II.

Irradiations of the R100 detector were carried out free in air to x-ray beams and high energy gamma photons from ^{60}Co and the exposure was expressed in terms of air kerma (Gy). The air kerma was measured using a calibrated cylindrical ionization chamber with a 6 cm^3 active volume (Model 10X5-6, Radcal, Monrovia, Ca, USA). The R100 and the ionization chamber were connected to an electrometer (Barracuda, RTI, Mölndal, Sweden) for readout and were simultaneously irradiated. R100 was operated in photovoltaic mode, i.e. no external bias (V) was applied whereas a high-voltage (300 V) was applied to the ionization chamber. The measured charge (nC) was used to evaluate the dosimetric characteristics of the detector.

The energy response was assessed utilizing a conventional X-ray unit (A-196, Varian Medical Systems, USA) as well as high-energy photons from a ^{60}Co source (Gammatron-3, Siemens, Germany). The source-to-detector (SDD) distance was 1 m for the x-ray measurements and the following tube voltages were applied: 40 kVp, 60 kVp, 80 kVp, 100 kVp and 120 kVp. The corresponding effective photon energies for each tube voltage were estimated to 29 keV, 31 keV, 40 keV, 46 keV and 49 keV. The half-value layer (HVL) for each tube voltage was used to derive the effective photon energies. The HVL values were determined using a Si based detector (Unfors RaySafe Xi R/F, Billdal, Sweden). For the ^{60}Co irradiations, the SDD was 0.5 m. In order to achieve charge-particle equilibrium for the ^{60}Co irradiations a 0.5 cm build-up cap made of polymethyl methacrylate (PMMA) was used. The response per unit air kerma of the ionization chamber [nC Gy^{-1}] varies ± 5% in the energy range of 30 keV up to 1333 keV when a build-up cap is used according to the specifications. A 0.5 cm thick PMMA plate was used in front of the R100 for ^{60}Co exposures. The detector response per unit air kerma was normalized to the ^{60}Co readout value.

Furthermore, the detector response was compared to the ratio of the mass energy-absorption coefficient (μ_{en}/ρ [cm^2/g]) taken from the NIST database of Si to that of dry air [19].

The linearity of the detector signal with respect to air kerma was tested where the detector was exposed to ^{60}Co gamma rays to air kerma values ranging from 21 to 208 mGy and the accumulated charge was plotted against the air kerma. This range of air kerma can be said to represent the external exposures relevant for radiological protection of workers in both normal and emergency exposure situations [20, 21]. Five consecutive

measurements were performed to obtain an average detector reading for the given exposure level.

2.1.2.2 Silicon detector – CT Dose profiler (CTDP)

In Paper III, a silicon (Si) diode was evaluated as a portable alpha particle detector and spectrometer for measurements under normal air conditions. The original use of the detector was to perform point dose profile measurements in computed tomography applications (CT Dose Profiler [CTDP], RTI Electronics AB, Mölndal, Sweden) [8]. The CTDP was modified by the manufacturer to a shorter version (length 15 mm, diameter 12 mm) and the Si was uncovered in order to detect alpha particles. The procedure where the encapsulation of the detector is removed can be performed by a medical physicist or engineer. In Fig. 1 (left), the CTDP is placed next to an ion-implanted planar Si detector (ISD) commonly used for alpha spectrometric measurements. In the electronic chain, the CTDP was connected to a preamplifier (Canberra, Model 2003BT, Meriden, CT, USA) and a handheld digital multichannel analyzer (MCA, DigiDartTM, Ortec, Oak Ridge, TN, USA) for a spectrometric evaluation (Fig. 1, right).

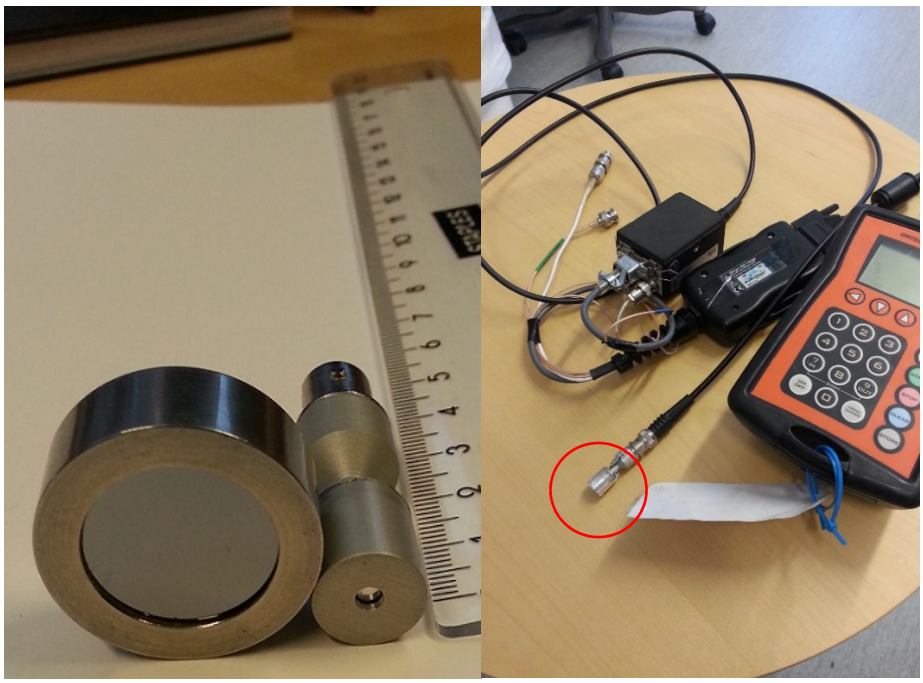

Figure 1. A 300 mm^2 ion implanted silicon detector (ISD) next to the 4 mm^2 Si CT dose profiler (CTDP), here without aluminum Mylar foil. The CTDP is contained within a cylinder with a 2.5 mm (Ø) aperture (left picture). The CTDP, indicated by a circle, connected to a charge-sensitive preamplifier (2003BT) and a digital portable multichannel analyzer (DigiDart™) (right picture).

Aluminum Mylar foil (3 μm) was used to cover the CTDP in order to protect it from contamination and ambient light. The MCA data was analyzed using a commercial software (ORTEC, Gammavision 32 v-6.01). Bias voltage was not used and the detector response, energy resolution (keV), detection efficiency [cps Bq^{-1}] and minimum detectable activity (MDA) [Bq] values were evaluated at normal (ambient) air pressure and room temperature.

The detector response as a function of SDD were investigated for the CTDP using two alpha emitting sources (^{241}Am and ^{210}Po) and the source characteristics are summarized in Table 1. The ^{241}Am standard source from the National Institute for Standards and Technology (NIST; Gaithersburg, MD, USA) was used to irradiate the detector with alpha particles and the changes in energy resolution was investigated as with increasing SDD (0.5, 1.0, and 1.8 cm). The energy resolution of the alpha peaks was specified as the full width at half maximum (FWHM) in terms of energy (keV). Measurements were performed for 100 s. The experiment was repeated using the ^{210}Po source at the three distances mentioned above.

Table 1
Summary of the alpha emitting sources used in Paper III.

Radionuclide	Energy (keV)	Activity (kBq)	Area (mm^2)	Geometrical form	Type
^{241}Am	5486 and 5443	2.3	33	Circular (6.5 mm diameter)	Electrodeposited onto a 0.16 mm thick platinum foil
^{210}Po	5304	9	90	Rectangular (5x18 mm^2)	Coated with 3 μm Au

The detection efficiency (ε) was determined as a function of the SDD by

$$\varepsilon(\%) = \frac{N}{A_\alpha \cdot t} \cdot 100 \quad (1)$$

where N is the total number of counts registered under the peak, A_α is the activity (in Bq) for a given radionuclide, and t is the measurement time (100 s). The efficiency measurements were performed using the ^{241}Am source at 0.5, 1.0, and 1.8 cm source-detector distance. It should be noted that the efficiency values are valid for contamination areas comparable to the ^{241}Am source area (33 mm^2). Once ε was established, the MDA values of the specific source-detector geometries, expressed in Bq and defined at the 95% confidence level, were calculated by the following [22]:

$$MDA = \frac{2.71+4.65\sqrt{B \cdot t_m}}{t_m \times \varepsilon} \quad (2)$$

where B denotes the background count rate, t_m is the measurement time (100 s), and ε is the efficiency value obtained with the ^{241}Am source. The background acquisition time was 11200 s.

2.2 Imaging modalities

Imaging modalities in hospitals such as computed tomography and digital radiography equipment as well as gamma cameras could potentially also be a part of the hospital's disaster preparedness for patient management in the event of RN emergencies. In such scenarios, rapid measurements are required to determine internal contaminations when radioactive fragments have been inhaled, ingested or penetrated into human tissue or organs. In Paper IV computed tomography (CT) and digital radiography (DR) systems were used to detect potentially radioactive fragments. Subsequently, the relationship between the effective dose (mSv), from the imaging modality applied and the averted dose if a surgical extraction of a radioactive fragment is carried out was established. Calibration coefficients and MDA values (kBq), for ^{131}I and ^{137}Cs and for different body sizes ranging from 10-30 cm in diameter were determined when using a dual–headed gamma camera in Paper V.

2.2.1 Computed tomography and digital radiography

2.2.1.1 Fragments

A set of nonradioactive fragments, substituting radioactive material, of different densities and sizes were used to assess the minimum detectable size [µm] utilizing CT and DR. Table 2 summarizes the fragment materials used in Paper IV. Fragment sizes in the range of 100 µm to 700 µm were used. A wide spectrum in size for radioactive fragments and particles, varying from a few mm down to some µm are found in the literature [23, 24, 25]. These fragments could be incorporated in subjects through inhalation or ingestion or through wound.

Table 2
Fragments used in Paper IV.

	Fragment material			
	Volcanic ash	**Fe**	**Cu**	**U**
Density (g·cm^{-3})	2.65	7.87	8.96	19.1
Sieve aperture size (µm)	←		700-500 500-400 400-300 300-250 250-180 180-100	→

2.2.1.2 Imaging, quantitative analysis and radiation dose measurements

A standard-dose CT (SDCT) (Somatom Definition AS+, Siemens, Erlangen, Germany), a non-diagnostic CT (NDCT) (SPECT/CT, Symbia Truepoint, Siemens, Erlangen, Germany) and a digital radiography (DR) system (A-196, Varian Medical Systems, USA) were evaluated for the detection of the fragments mimicking radioactive entities.

The NDCT is only used for attenuation correction of SPECT data and localization of organs and thus utilizes a lower mAs than the SDCT. In order to simulate an individual, that is internally contaminated with radioactive material, the fragments were placed in the lungs and in the abdomen of an Alderson Rando phantom (Radiology Support Devices, Long Beach, CA, USA), which was filled with water to simulate tissue equivalent attenuation. The fragments were positioned 1 cm apart from each other at each location and the phantom was exposed to a combination of acquisition parameters (Table 3) and sizes as given in Table 2 (using each one of the aforementioned imaging systems). After each exposure, the volume CT dose index ($CTDI_{vol}$ [mGy]) and dose-area product (DAP [mGy cm^2]) values were recorded. Table 3 includes the acquisition parameters used for the imaging modalities.

Table 3
The imaging modalities and the scan parameters utilized in Paper IV.

	Imaging modalities		
Scan parameters (units)	SDCT	NDCT	DR
Tube voltage (kVp)	100, 120, 140	130	70, 90, 110, 130
Effective mAs (CT) and mAs (DR)	90, 120, 150, 180, 210, 230	17	10, 20, 40 80, 160
Scan time [s]	3.5	96	
Slice [mm]	0.6	1.0	
Rotation time [s]	0.5	0.8	
Pitch	1.2	1.5	

The detection threshold (DT) for the fragments was determined, for a 95% confidence level, if the mean pixel value of the fragment (MVP_{frag}) was more than $3.29\sigma_{\mu}$ over the mean of the background, where σ_{μ} is the standard deviation of the mean of the background pixel value [26]. The MVP_{frag} ($\pm$ SD) were registered by positioning circular region of interests (ROIs) on the axial images encompassing the fragments. The ROIs, with a constant shape and size, were placed in the identical locations for each series of images and detection thresholds were calculated for each set of scanning parameters since the detection threshold would be affected by the tube potential (kVp) and tube load (mAs). The MVP_{frag} of the fragments were compared with the detection threshold by means of their quotient, MPV_{frag}/DT, i.e. fragments with a quotient higher than unity were considered as detectable. Image processing was performed using ImageJ [27].

The absorbed dose required to detect the fragments in the Alderson Rando phantom by the different imaging modalities was recorded using thermoluminescent dosemeters (TLDs) (Harshaw TLD-100, Thermo Fisher Scientific Inc, Erlangen, Germany). The TLDs were distributed throughout the Alderson Rando phantom (Fig. 2). A standard protocol, using a TLD reader (Harshaw 5500, Gammadata Bycron NE, Wermelskirchen, Germany), was followed to read out the TLDs post-irradiation [28].

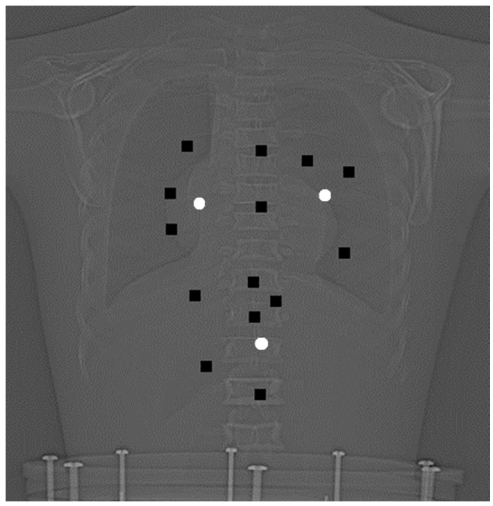

Figure 2 The approximate locations of the thermoluminescent dosemeters (LiF: Mn, Ti) (indicated as black squares) and the radionuclide positions (indicated as white circles) shown in a CT scout radiography of the Alderson Rando phantom.

From the protocols in Table 3, the combination of tube voltage and tube load which optimized detection of the fragments and which resulted in the lowest $CTDI_{vol}$ and DAP values, were chosen for the TLD measurements.

Furthermore, gamma emitting point sources of ^{137}Cs, ^{60}Co and ^{99m}Tc, summarized in Table 4, were positioned in the same places in the Alderson Rando phantom as the fragments used in Table 3 to mimic the irradiation caused if the fragments were radioactive. The radionuclides were chosen due to their relevance in several RN emergency scenarios.

Table 4
Summary of the gamma emitting sources used in Paper IIV

Radionuclide	Energy (keV)	Activity (MBq)	Half-life	Type
^{137}Cs	662	31.7	30.2 y	Sealed point source
^{60}Co	1173, 1333	15.5	5.27 y	Sealed point source
^{99m}Tc	141	97	6.01 h	Sealed point source

In addition to the geometry of the aforementioned measurements, the point sources were also placed on the surface of the torso in order to simulate skin deposition (Fig. 2). TLDs were used to derive the resulting absorbed doses (mGy) due to the gamma radiation from the radionuclides and each experiment was repeated for a specific radionuclide. A 24 h irradiation time was chosen for the radionuclides and the same TL-reading procedure was followed as for the radiographic imaging of the phantom. Subsequently, the equivalent organ doses (mSv) and the effective doses, for both the imaging modalities and radionuclides exposures, were determined using the absorbed doses and by utilizing the radiation weighting coefficients as defined by ICRP publication 103 [20].

2.2.2 Gamma camera

2.2.2.1 Phantoms

In Paper V, an easy to produce in-house developed phantom, intended for calibration of *in-vivo* body burden of gamma emitting radionuclides using gamma cameras, was tested and compared against a standard anthropomorphic phantom. In the first step of the study, humans and body parts of different sizes (Fig. 3, left) were simulated using the in-house developed PMMA phantom which consists of one cylindrical and one conical part. The reader is referred to Paper V for detailed specifications. This phantom was used to derive calibration coefficients (cps kBq^{-1}) and MDA values for different body sizes. The second phantom, the Alderson Rando nuclear medicine thorax phantom (Radiology Support Devices, Long Beach, Ca, USA) was used to verify the calibration coefficients obtained with the conical-cylindrical phantom. The Alderson Rando phantom corresponds to an average male adult (74 kg) and it includes organs mimicking the lungs, liver, rib cage and the spinal cord with attenuating properties comparable with those of human anatomical structure. The phantoms are illustrated in Fig. 3.

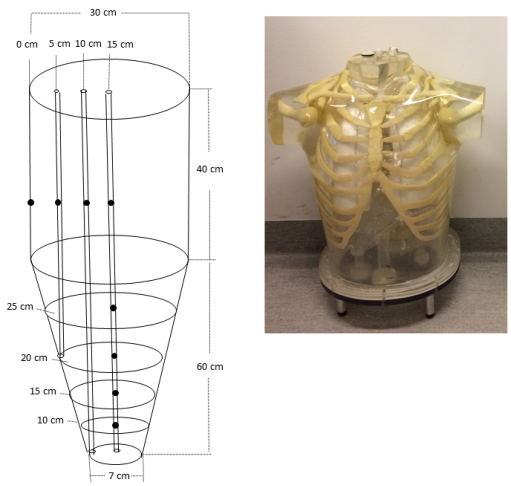

Figure 3 The conical-cylindrical phantom used in Paper V (left) and the Alderson Rando thorax phantom used in Paper IV and V (right). The cylindrical part of the phantom corresponds to the Alderson phantom whereas the conical part can be used to mimic body parts with different thicknesses.

2.2.2.2 Calibration coefficients and minimum detectable activities

The dual-headed gamma camera in a hybrid SPECT/CT scanner (Symbia TruePoint T2, Siemens Medical Solutions, Erlangen, Germany) was used in combination with the conical-cylindrical phantom to derive calibration coefficients between body content of gamma emitter (Bq) and count rate in a specified energy window of the gamma camera (cps). The calibration coefficients were derived from point sources located at various phantom diameters and depths in the conical-cylindrical phantom, with the phantom placed in a lying position on the imaging couch. The MDA (kBq) for the source-

phantom geometries were also determined. The camera heads of the SPECT system consist of thallium-activated sodium iodide (NaI[Tl]) scintillation detectors with a detector thickness of 9.5 mm. The field of view is 53.3 x 38.7 cm^2.

The collimators of the gamma camera were removed and static planar images were acquired for 300 s with a 180° detector configuration.

Gamma emitting point sources of ^{131}I (737 kBq [22 Dec 2014]) and ^{137}Cs (167 kBq [22 Dec 2014]) were selected on basis of their potential risk in radiation emergency situations. The greatest source of internal exposure to a population following nuclear power plant accidents is from intake of ^{131}I and ^{137}Cs and therefor these radionuclides are considered among the most important in RN events [29, 30].

The sources were inserted in the central drill hole in the cylindrical and conical phantom one at a time, using shortest possible detector- phantom surface distance (2.5 cm) for the measurements.

The following phantom diameters were selected for the count rate registrations with the conical-cylindrical phantom: 10, 15, 20, 25 and 30 cm. Since 690 keV is the upper limit of the pulse-height analyzer (PHA) of the gamma camera system the energy window for ^{137}Cs counts could not be symmetrically centred on the full energy peak at 661.6 keV. Instead the energy window was set at the 588 keV peak with a window width of 34%, covering energies in the range of 490-690 keV. The corresponding energy window settings for ^{131}I were 364 keV with a 15 % window width (energy window of 337 - 391 keV). Using these energy window settings, calibration coefficients were calculated as the ratio between the background-corrected count rate (counts per second [cps]) and the activity of the radionuclides (kBq). Due to the high count rate, the MDA was calculated applying the following equation:

$$MDA_{t_m} = \frac{3}{t_m \times \varepsilon} \times SD_{bkg} \quad (3)$$

where ε refers to the calibration coefficients (cps kBq^{-1}), SD_{bkg} is the standard deviation of the background count rate and t_m is the acquisition time.

2.2.2.3 Verification measurement

The Alderson Rando phantom was used to verify the determined calibration coefficients. The ^{137}Cs source was positioned on the right lung surface and a measurement was performed using the same settings as for the conical-cylindrical phantom with the exception of the detector-phantom surface distance which was 4 cm due to practical limitations.

3. Results and comments

3.1 Radiation detectors

3.1.1 Radiochromic films

The usefulness of the RTQA2 of the Gafchromic films as a dosemeter is demonstrated in Paper I. In parallel to visual inspection, the dose response relationships of the XRQA, XRQA2 and RTQA2 film models, exposed to 80 kV, ^{60}Co and ^{90}Sr/^{90}Y beams, were obtained by plotting net optical density (NOD) values against corresponding absorbed doses and the results are compared in Fig. 4. For the XRQA and XRQA2 films, there is a pronounced dependency on radiation quality with an elevated response for lower (<100 keV) photon energies, which is consistent with reported results for XR-type films [31, 32]. For these films, a sensitivity change is apparent with beam quality where the sensitivity [optical units mGy^{-1}] increases with decreasing radiation energy, since these films contain high-Z halides in the sensitive layer, with the intention to increase the response to lower energies (< 200 kVp) [33]. This makes the films more suitable for diagnostic radiology but makes them unsuitable as generally applicable personal dosemeters due to the large energy dependency in a broader energy range. On the other hand there is less pronounced difference in response in a broad range of beam qualities for the RTQA2, which is thus most suitable, among the three films studied, for use as a dosemeter.

The film response (NOD) as a function of post-irradiation time was evaluated and no time dependence of the signal was observed, with a fully developed signal when the NOD was recorded in the first minute post-irradiation (Fig. 5). No further change in the NOD was observed in a time frame of 1 – 300 min suggesting a rapid and immediate full developed response. For high single dose administrations this film is expected to exhibit a gradually increasing NOD-value as a function of time until reaching an asymptotic value. However, the observation in this study is consistent with other data which reveal that the total dose affects the post-irradiation kinetics with faster development at lower doses and thus a much less pronounced time dependence is shown [34].

Fig. 6 illustrates the results when ten participants were asked to identify exposed films placed next to an unexposed film. A 0.05 criterion value would mean that 5% of the observations would result in false negatives at ~ 35 mGy. This means that there is a 95% probability that the film is identified as exposed to radiation compared to an unexposed

film for absorbed doses > 35 mGy. This finding shows that visual evaluation can be performed to estimate the absorbed dose, down to approximately 35 mGy.

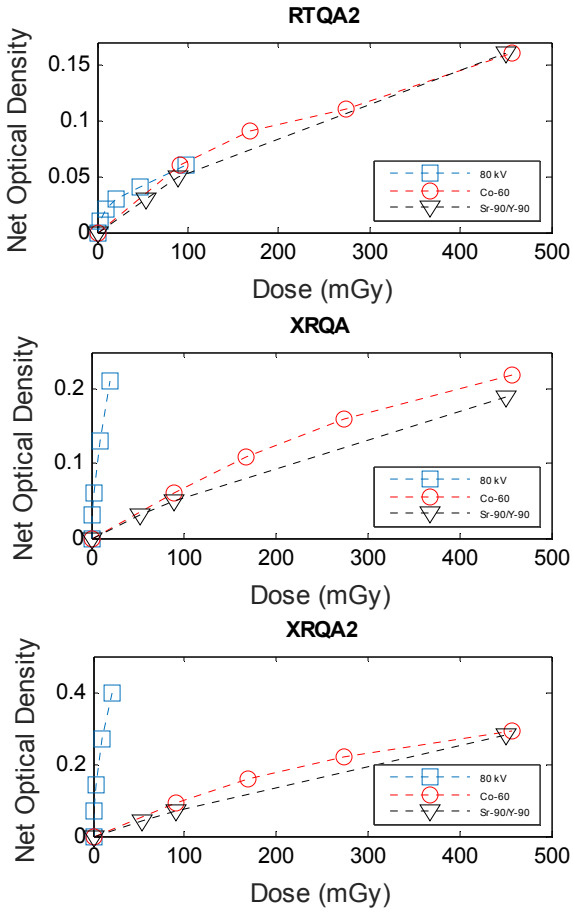

Figure 4 Measured dose response curves for the Gafchromic films to different radiation qualities.

The focus of Paper I is to investigate the suitability of radiochromic films as emergency dosemeters and the findings suggest that the RTQA2 film type can be applied as a real-time dosemeter in large scale RN events for first responders and health care personnel. The real-time response and the visually detectable measure of absorbed dose of RTQA2 make it a promising tool for personal dosimetry or as a complement to electronic personal dosimeters. The RTQA2 film is thus suitable for the aforementioned personnel whose actions in areas with elevated or unknown radiation levels could expose them to potential radiation hazards. Other works in recent years show that there is an increased interest in using radiochromic films for radiation protection purposes [35, 36].

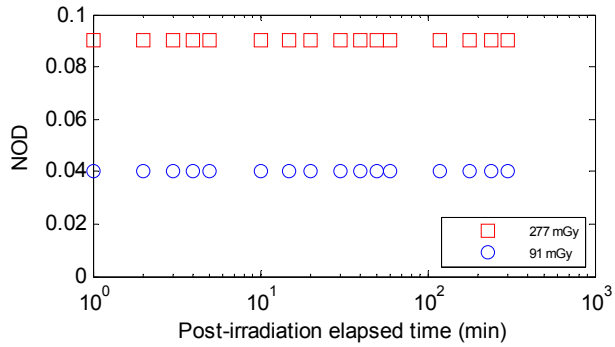

Figure 5. The net optical density (NOD) as a function of time for 91 mGy and 277 mGy irradiations with a ^{60}Co beam for the RTQA2 film.

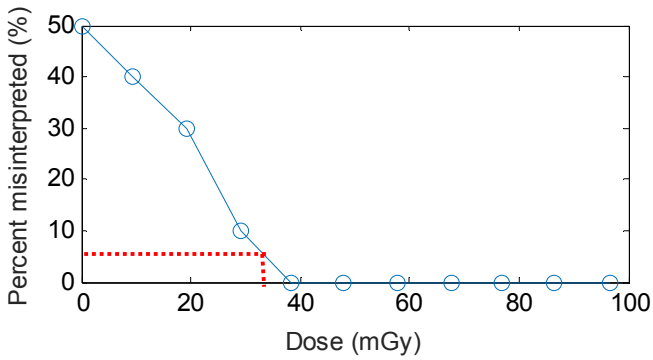

Figure 6 Ranking by participants of the exposed films placed next to unexposed ones. The red line shows the 5% likelihood of misinterpretation.

3.1.2 Semiconductor detectors

3.1.2.1. Silicon detector – Dose probe R100

In paper III, a silicon detector (R100) was evaluated for radiation protection applications. The main goal was to determine whether the detector could be used in hospitals at RN-events for a reliable determination of absorbed dose and/or air kerma. The dosimetric characteristics of the R100 detector were investigated in Paper III in terms of energy dependence and dose linearity. The response of the R100 detector in terms of charge released (nC) was determined for different effective x-ray energies (29 - 49 keV) and was normalized to the response for ^{60}Co. A weak dependence of the response on the photon energy is depicted in Fig. 7 with an increasing sensitivity with decreasing photon energy.

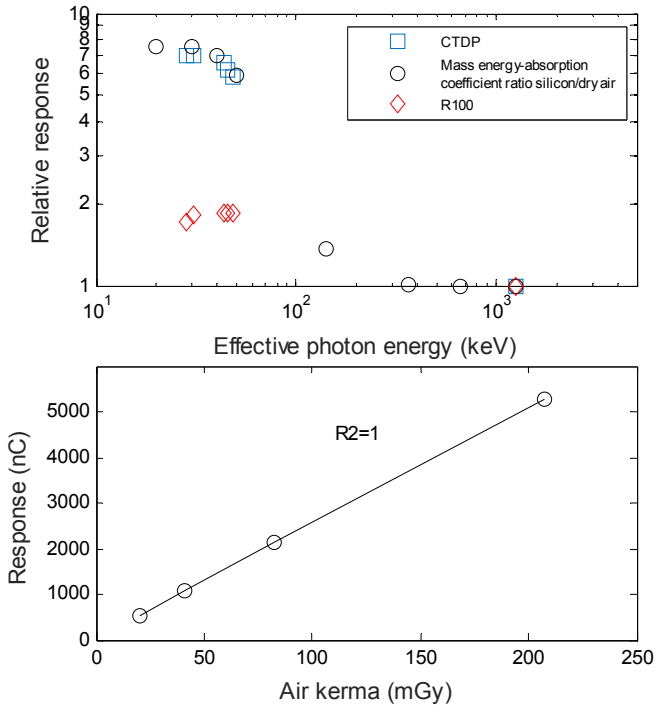

Figure 7 The relative energy response of the Si Dose probe R100 (R100) and the Si CT dose profiler (CTDP) and the mass energy-absorption coefficient ratio of silicon to that of dry air as a function of effective photon energy (upper figure). The response in terms of collected charge as a function of air kerma (lower figure).

In the x-ray energy range, the energy dependence is larger compared to that of the high energy ^{60}Co gamma photons (mean 1.25 MeV), as expected due to the larger cross-section for photoelectric interactions of low energy photons. The sensitivity peaks with an over-response of approximately 1.8 times at 49 keV relative to ^{60}Co. This is comparable with published data where maximum sensitivities are reported at 30-50 keV for both energy compensated and naked Si detectors [37, 38, 39]. In those studies, the over-responses were in the range of 3.5-5 for energy compensated Si detectors. This is a factor of approximately 2 - 3 times higher than observed for the R100-detector and the disagreement is explained by the different filter compositions of these detectors compared to the R100 detector.

Also shown in Fig. 7 are the values of the ratio of the mass energy-absorption coefficient for Si and for dry air as a function of photon energy (from 20 keV – 1.25 MeV). In this curve, the energies for ^{99m}Tc, ^{131}I and ^{137}Cs are also plotted in order to theoretically cover the whole energy range of interest. Furthermore, in order to compare the energy compensated R100 detector to bare Si detectors, identical irradiations were performed where the naked Si detector (CTDP) used in Paper III was also exposed to the same energy range as the R100. These results are also presented in Fig. 7. The result for the CTDP detector corresponds fairly well to the mass energy-absorption ratio of Si/dry air, both exhibiting over-responses with a factor of > 7 in the low energy range

compared to photons from ^{60}Co. For the R100 detector the corresponding value is approximately 4 times lower than the response predicted by the Si/dry air mass energy-absorption ratio normalized to the response for ^{60}Co. A more uniform response over the photon energy range is thus provided by the R100 with a reduction in the over-response at low photon energies due to the inherent energy compensating filter.

The sensitivity for the R100 was in the range of 44 – 26 nC mGy^{-1} (for 29 keV x-rays and 1173 and 1333 keV for ^{60}Co), resulting in an over-response by a factor of 1.7 for the lowest energy (29 keV) relative to ^{60}Co. The sensitivity of the naked CTDP is 0.8 nC mGy^{-1} at the ^{60}Co photon energies, which is approximately 33 times lower than the R100 values. This is attributed to the smaller area of the CTDP compared to the R100. Other authors have reported a sensitivity of approximately 1 nC mGy^{-1} for naked diodes and for ^{60}Co photon beams [40].

The right side of Fig. 7 shows the measured charge (nC) of the Si detector with respect to air kerma in the range of 21 mGy to 208 mGy for ^{60}Co gamma photons. The R100 detector displays a linear response with a correlation coefficient (R^2) equal to 1.0 of the linear fit. This is consistent with results published for other Si detectors [41, 42].

In conclusion, the R100 detector is proved to be useful for radiation protection purposes due to its energy compensation feature and ability to detect high energy photons such as those from ^{60}Co that could be encountered in RN emergencies.

3.1.2.2 Silicon detector – CT Dose profiler (CTDP)

In Paper III, the CTDP detector combined with a portable MCA was used to test whether the device could be useful for field alpha spectrometry. Fig 8 shows a comparison in the pulse height distribution between the ^{241}Am and ^{210}Po sources as a function of SDD. For ^{241}Am, a peak is observed at channel 130 for 0.5 cm SDD with a corresponding energy resolution (FWHM) of 281 keV. The energy resolution improves to 148 keV and 113 keV at 1.0 cm and 1.8 cm, respectively. An improved energy resolution is thus observed as the SDD increased with the best resolution at the longest SDD. The energy resolution is thus influenced by the SDD since at large SDD a larger fraction of the emitted alpha particles propagate perpendicularly to the detector and pass the entrance window at a small angle resulting in a reduced energy straggling. This is also consistent with other published results [43].

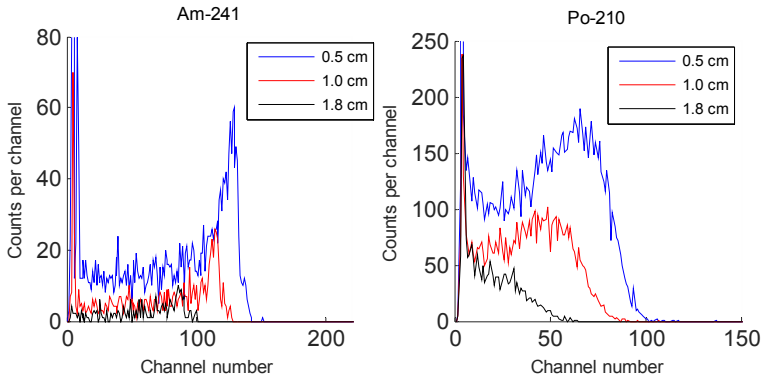

Figure 8 Pulse height distribution measured with the Si CT dose profiler (CTDP) for an electrodeposited ^{241}Am source (Eα= 5486 and 5443 keV) (left) and an encapsulated ^{210}Po source (Eα= 5304 keV) (right) at various SDD (0.5, 1.0, and 1.8 cm).

The peaks indicate that the CTDP can detect and differentiate alpha particles by energy under normal air conditions. The measurements also demonstrate a broader pulse height distribution than for the ^{241}Am source and the peak occurs in a lower channel number for ^{210}Po (Fig. 8). This is caused by energy loss processes as the alpha particles interact and loose energy while passing through the protective layer of the source. The energy resolution could further be improved by applying collimators which is indicated by the results above and also demonstrated by other authors [44, 45].

The MDA values were determined using the efficiency data for the ^{241}Am sources. The MDAs were in the range of 3.3 - 33 Bq for SDD in the range of 0.5 - 1.8 cm SDD, respectively. In this case, MDAs were also calculated in terms of surface activity (Bq/cm^2) and the corresponding values were 11 Bq/cm^2, 34 Bq/cm^2, and 101 Bq/cm^2 for the 0.5, 1.0, and 1.8 cm SDD. The above mentioned MDAs values are valid for sources with thin surfaces and with extensions in similar sizes as the ^{241}Am source used in Paper III. However, the lower MDA vales were obtained when measuring a sample or a surface at a short SDD but at a cost of a degraded energy resolution.

Various parameters, such as the exit window of the source, the source thickness, SDD, thickness of the dead layer (entrance window) of the Si detector will influence the energy resolution of this device. These parameters also explain the asymmetric shape of the alpha peaks, with the characteristic tail on the lower energy side.

In conclusion, a Si detector (CTDP) commonly available at hospitals, is utilized in Paper III, to measure alpha particles from two sources, an electrodeposited ^{241}Am source and a ^{210}Po source coated with a 3 µm thick gold foil. The CTDP allows an energy separation in the case of thin sources as demonstrated for the sources used.

The straightforward method described in Paper III could be applied for monitoring for wound or skin contaminations. For example, the NCRP provides guidance regarding skin contamination with alpha emitting radionuclides, where intervention is required for > 1000 Bq/cm^2 [46]. These requirements are demonstrated to be achievable with the CTDP which has MDAs of a few tens of Bq/cm^2.

Other possible applications could be direct surface monitoring and smear tests at nuclear fuel facilities, nuclear power plants, and facilities handling radioactive waste.

3.2 Imaging modalities

3.2.1 Computed tomography and digital radiography

Paper IV was a two-part study where the aim of the first part was to explore the detection threshold for fragment types of various sizes and densities (U, Cu, Fe, Ash) (Table 2) utilizing the imaging modalities in Table 3, for fragments positioned at the different anatomical positions. Part two deals with determination of the effective doses from the imaging modalities and the radionuclides mimicking radioactive fragments where a comparison is made.

3.2.1.1 Imaging and quantitative analysis

Paper IV shows that the SDCT and DR are more suitable compared to NDCT in the localization of embedded fragments. For the SDCT, the detection threshold for both anatomical positions (the right lung and inner abdomen surface) was 100-180, 250-300 and 300-400 μm for U, Cu and Fe, whereas the ash particles were not detectable. For the NDCT the corresponding values for U, Cu and Fe fragments were 180-250, 300-400, and 400-500 μm respectively and smaller fragments were not separable from the background. For DR, the smallest U fragments (100-180) μm were also easily detected at the right lung. For Cu and Fe the values were 300-400 μm and the results for the abdomen position were similar. For Fe, fragments in size of 400-500 μm were detected at the inner abdomen surface.

Figure 9 summarizes the detection ability of the imaging modalities and the effective doses required for the detection of the fragments with respect to material type and size. The density influences the detection and as a result smaller high-density fragments can be detected for all imaging modalities and consequently the detection is degraded for material with lower densities. It illustrates that smaller fragments can be detected at higher densities for all the imaging modalities. These results imply that the detection of fragments embedded in individuals is affected by material size and composition. This is also illustrated by the fact that the volcano ash particles were not detected with neither of the imaging modalities and the dashed line in Fig. 9 illustrates that with decreasing density, the size of the material has to increase in order to be detected.

The results in Paper IV are in accordance with other studies where metal fragments down to sizes of 0.5 - 1.00 mm have been detected [47, 48]. Other findings report metallic entities with diameters of 0.36 and 0.4 mm respectively [49, 50].

The SDCT offers the ability to localize the fragments in three-dimensions whereas in DR, the detection of fragments could be complicated since a two- dimensional image of a tree-dimensional volume is generated. However, an additional lateral projection with the DR could also result in a three dimensional image. Disadvantages of using the SDCT compared to DR are the higher radiation doses and the image artefacts generated by high density metallic fragments. The radiation doses from the SDCT could be reduced

by further optimizing the scanning parameters. Compared to the NDCT, the SDCT offers superior detectability and shorter imaging times.

Previous reports have utilized other imaging modalities such as ultrasonography in detecting foreign bodies with low densities [51]. There are however limitations with ultrasonography due to the range of ultrasound waves, resulting in failure to detected fragments deposited deeper than 2 cm [52]. Other options such as magnetic resonance imaging (MRI) could also be considered to image non-metallic fragments [53].

3.2.1.2 Dose measurements for imaging modalities and remaining radionuclide sources

TLDs were used in order to determine the absorbed doses generated by the imaging modalities and the imaging parameters were established on the basis of the lowest measured $CTDI_{vol}$ (7 mGy and 1.5 mGy for SDCT and NDCT respectively) and DAP ($\sim 1.7 \cdot 10^3$ mGy cm^2) values with respect to the smallest detected fragments. The resulting equivalent organ and effective doses for the imaging modalities are depicted in Table 5.

Fig. 9 illustrates the effective doses needed from the imaging modalities in order to detect the smallest fragments with different densities positioned in the inner abdomen region. The smallest fragments (100-180 μm) detected by the SDCT required an effective dose of 5.6 mSv, which is approximately a factor of seven times higher than for DR, where the effective dose was 0.76 mSv. For NDCT the effective dose was 1.9 mSv for the detection of the smallest fragments (180-250 μm) for this modality. Imaging with the CT systems resulted in higher equivalent organ doses compared to DR as shown for the different organs in Table 5.

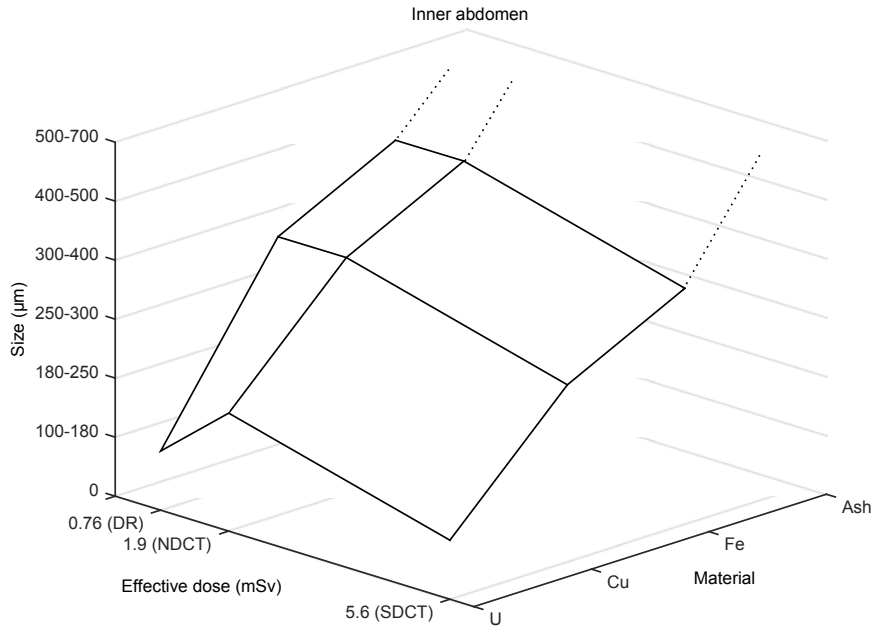

Figure 9 The relationship between the smallest fragments detected and the effective doses from digital radiography (DR), non-diagnostic CT (NDCT) and standard-dose CT (SDCT) is illustrated.

The organ equivalent and effective doses for the point sources, in terms of mSv per MBq for the first 24 h (mSv MBq^{-1} d^{-1}), were recorded for three different anatomical positions and are included in Table 6. The effective doses for the ^{137}Cs source (31.7 MBq) were 0.07, 0.08 and 0.1 mSv MBq^{-1} d^{-1} when the source was placed at the right lung, the inner abdomen area and the breast surface.

The corresponding effective doses for ^{60}Co (15.5 MBq) were 0.32, 0.43 and 0.45 mSv MBq^{-1} d^{-1}, respectively. For ^{99m}Tc (97 MBq) there was little difference in the effective doses for the different positions (0.008 - 0.009 mSv MBq^{-1} d^{-1}). These values could be used for comparison with the effective doses generated by the imaging modalities. For example, assuming a 24-hour exposure for ^{137}Cs it would require activity levels in the range of 56-80 MBq for the different positions to reach the 5.6 mSv levels of the SDCT. The corresponding values are in the range of 19-27 MBq and 8-11 MBq in order to equal the effective dose levels of SDCT and DR, respectively. For the corresponding values for the other radionuclides the reader is referred to Paper IV. For the gamma emitting radionuclides in Paper IV the effective doses are comparable to those from the imaging modalities assuming that the activity is in the order of MBq levels and within days the effective dose from a radioactive fragment would exceed the effective dose from an imaging modality. Based on averted dose, utilizing imaging would be justified.

For internal contamination with ^{60}Co and ^{137}Cs, several documents recommend intervention when the magnitude of order of activity levels exceeds > MBq [54, 1]. The

recommended annual effective dose limit of 1 mSv for members of the public would equate to activity levels in the range of 27-39 kBq for ^{137}Cs and 6-9 kBq for ^{60}Co respectively. This indicates that for fragment in the activity levels in the above mentioned ranges imaging techniques resulting in effective dose levels of < 1 mSv would not be justified. The activity levels of embedded fragments needs to exceed the above mentioned levels in order to justify the additional exposure to ionizing radiation form imaging modalities. However, other considerations, such as chemical toxicity and vicinity to critical organs, have to be taken into account [55]. The results in Paper IV can be applied in the management of individuals with incorporated radioactive fragments.

Table 5 Organ equivalent dose and effective doses (E) in millisievert (mSv) estimated using TLDs when the phantom was imaged by the SDCT,NDCT and DR. In addition are given values for equivalent and effective dose values per unit activity and day (mSv/MBq, day) for the organs using radionuclides of ^{137}Cs, ^{60}Co and ^{99m}Tc placed i) on the mediastinal part of the right lung ii) on the inner surface of the abdomen and iii) on the breast surface of the phantom.

Imaging modalities				Point sources								
	SDCT	NDCT	DR	^{99m}Tc			^{137}Cs			^{60}Co		
				Right lung	Inner abdomen	Breast surface	Right lung	Inner abdomen	Breast surface	Right lung	Inner abdomen	Breast surface
Organs												
Gonads	0.0E+00	0.0E+00	0.0E+00	5.3E-04	1.1E-03	1.5E-05	4.0E-03	8.6E-03	1.5E-04	2.7E-02	5.3E-02	8.3E-04
Red bone marrow	8.2E+00	2.3E+00	3.7E-01	6.2E-03	1.1E-02	1.5E-03	3.6E-02	8.7E-02	1.4E-02	2.2E-01	3.8E-01	7.0E-02
Lung	8.8E+00	2.7E+00	1.1E+00	3.3E-02	2.8E-03	7.0E-03	3.3E-01	2.7E-02	8.5E-02	1.3E+00	1.3E-01	4.6E-01
Colon	9.3E-01	5.9E-01	2.0E-01	1.5E-03	5.7E-03	1.3E-03	1.2E-02	4.9E-02	1.1E-02	7.4E-02	2.6E-01	6.4E-02
Stomach	2.0E+00	1.2E+00	2.2E-02	3.1E-03	2.2E-02	1.2E-03	2.5E-02	2.1E-01	1.3E-02	1.4E-01	9.5E-01	7.3E-02
Breast	1.1E+01	4.8E+00	2.7E+00	4.2E-03	1.3E-03	5.2E-02	4.1E-02	1.9E-02	6.3E-01	2.6E-01	1.0E-01	2.0E+00
Bladder	0.0E+00	0.0E+00	0.0E+00	7.0E-04	1.8E-03	3.3E-05	5.3E-03	1.4E-02	3.4E-04	3.5E-02	8.4E-02	1.9E-03
Liver	1.1E+01	3.3E+00	1.3E+00	1.5E-02	5.9E-02	2.9E-03	1.3E-01	5.0E-01	3.2E-02	5.2E-01	3.3E+00	1.6E-01
Esophagus	1.1E+01	3.0E+00	1.4E+00	6.4E-03	1.5E-03	4.5E-03	5.5E-02	1.2E-02	4.8E-02	2.9E-01	7.1E-02	2.7E-01
Thyroid	1.5E-02	0.0E+00	0.0E+00	2.2E-03	1.1E-03	2.6E-03	2.1E-02	8.2E-03	2.3E-02	1.2E-01	5.1E-02	1.3E-01
Skin	1.1E+01	3.8E+00	1.7E+00	6.6E-03	4.4E-03	1.6E-02	6.9E-02	6.1E-02	1.8E-01	3.4E-01	3.1E-01	6.7E-01
Bone surface	8.2E+00	2.3E+00	3.7E-01	6.2E-03	1.1E-02	1.5E-03	3.6E-02	8.7E-02	1.4E-02	2.2E-01	3.8E-01	7.0E-02
Brain	0.0E+00	0.0E+00	0.0E+00	9.9E-04	4.8E-04	4.0E-04	7.7E-03	3.6E-03	4.2E-03	4.8E-02	2.4E-02	2.3E-02
Salivary glands	0.0E+00	0.0E+00	0.0E+00	2.1E-03	8.7E-04	1.6E-03	1.7E-02	6.7E-03	1.7E-02	1.0E-01	4.2E-02	9.4E-02
Remainder	4.8E+00	1.4E+00	5.2E-01	5.8E-03	1.0E-02	2.8E-03	5.3E-02	9.6E-02	3.0E-02	2.6E-01	4.5E-01	1.7E-01
E	5.6E+00	1.9E+00	7.6E-01	7.7E-03	9.2E-03	9.0E-03	7.0E-02	8.2E-02	1.0E-01	3.2E-01	4.3E-01	4.5E-01

3.2.2 Gamma camera

Paper V demonstrates the feasibility of using gamma cameras together with a cylindrical-and cone-shaped phantom (mimicking different patient sizes and body parts) to obtain calibration coefficients (cps kBq^{-1}) and MDA (kBq) values, for gamma emitting radionuclides associated with RN events. Gamma cameras have previously been demonstrated to be useful to monitor internal contamination associated with radiation emergencies [56, 57]. The calibration coefficients and the MDA values obtained could be applied to estimate the activity in internally contaminated individuals involved in RN incidents.

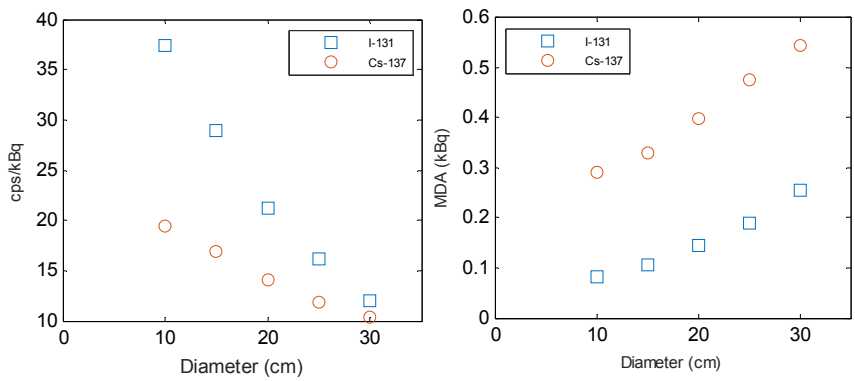

Figure 10 The derived calibration coefficients (cps kBq-1) (left) and MDA values (kBq) (right) as a function of phantom diameter for the cylindrical-conical phantom.

Fig. 10 illustrates the variation of the calibration coefficients and the MDAs for ^{131}I and ^{137}Cs as a function of phantom diameter. The calibration coefficients for ^{131}I were in the range of 12 - 37 cps kBq^{-1} (30 - 10 cm phantom diameter). For ^{137}Cs the corresponding values were 10 – 19 cps kBq^{-1} (30 - 10 cm phantom diameter). The lowest MDAs were achieved at the smallest phantom diameter for both ^{131}I (0.08 kBq) and ^{137}Cs (0.29 kBq) as illustrated to the right side of Fig. 10. There is an increase in the values of the calibration coefficients and a decrease in MDAs as the phantom diameter decreases. This means that for a given intake of a radionuclide, the count rate will vary with body size since a larger portion of the emitted and scattered gamma rays will be attenuated in thicker bodies.

The obtained MDA values for the gamma camera are thus substantially lower than the activity levels corresponding to doses exceeding 1 mSv (see paper IV).

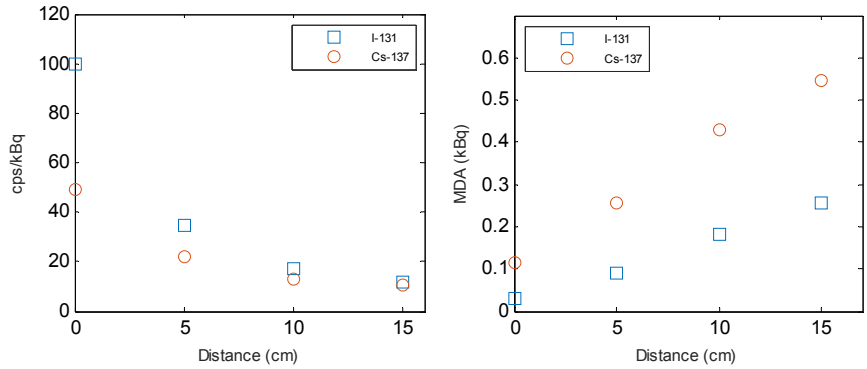

Figure 11 The derived calibration coefficients (cps kBq^{-1}) and the MDA values (kBq) for the radionuclides as a function of different depths in the 30 cm diameter phantom where 0 cm corresponds to the phantom surface and 15 cm to the center of the phantom.

The calibration coefficients and the MDAs at various depths in the cylindrical phantom, representing activities incorporated at different depths in subjects, are depicted in Fig. 11. For these positions, the highest calibration coefficients (49 and 100 cps kBq^{-1} for ^{137}Cs and ^{131}I, respectively) are found at the surface, representing skin contamination. This is also valid for the MDAs, which are lowest (0.11 and 0.03 kBq ^{137}Cs and ^{131}I) when the radionuclides are positioned on the surface, nearest to one of the gamma camera heads.

For the verification measurement, where the ^{137}Cs (167 kBq) source was placed on the lung surface in an Alderson phantom (described in Section 2) to mimic a lung deposition, a total count rate of approximately $3 \cdot 10^3$ cps was registered. Subsequently, a background correction was performed and the calibration coefficient derived from Fig. 10 was used to estimate the activity. The resulting activity estimation (215 kBq) overestimated the true activity by 29 % and this level of accuracy is fit for purpose where the primary aim of the *in-vivo* monitoring is to identify contaminated individuals who require medical care and follow-up. The discrepancy in the activity estimation could depend on differences between the conical-cylindrical phantom and the Alderson phantom and the different distances between the detector and phantom which will affect the sensitivity. With those uncertainties in activity estimation taken into consideration, an activity estimation within 30% can be achieved for internally contaminated individuals. For comparison, dedicated whole body-counters (WBC) can estimate the activity concentrations by ±8% [58]. However, facilities with WBCs are rare which limits the patient throughput when rapid radiological assessment is needed and gamma cameras could be applied in order to enhance the monitoring capacity.

The calibration coefficients obtained in Paper V are comparable to published data. For instance, for ^{137}Cs other authors obtained values in the range of 2.2 – 12 cps kBq^{-1} in phantoms weighting between 14 – 93 kg [57]. The source of discrepancies may be influenced by parameters such as the different shape, material and density of the conical-cylindrical phantom compared to phantoms used in that study as well as different energy

window settings and detector-source distances. Hansson and Rääf established 210 cps kBq^{-1} for a lung deposition of ^{137}Cs for an Alderson Rando phantom and the difference between that study and the results in Paper V is attributed to a larger energy window setting [56].

Published results using gamma cameras accompanied with dedicated thyroid phantoms exhibited a calibration coefficient value of 39 cps kBq^{-1} using a ^{133}Ba source as a surrogate for ^{131}I [59]. This is comparable with the 37 cps kBq^{-1} for ^{131}I in Paper V for the 10 cm phantom diameter, which could be approximated to a thyroid phantom diameter. The MDA in that study was 0.081 kBq compared to 0.082 kBq in Paper V. The reader is referred to Paper V for details on comparisons with the annual effective dose limits as well as comparisons with MDA values with WBC.

Paper IV demonstrates that gamma cameras could be applied in monitoring of internally contaminated individuals. The method described, using an in-house developed phantom for establishing calibration coefficients for various body sizes could be of value for nuclear medicine departments that could produce phantoms at low costs compared to more dedicated and expensive phantoms such as the Alderson phantom. A recent work shows that gamma cameras have an important role to play in national policies as part of emergency preparedness plans by being used as screening devices and body monitors in large-scale RN scenarios [60]. Moreover, gamma cameras and experienced personnel are available in most hospitals, especially in areas with higher population densities. It would be of interest to identify the various types and geographical distribution of gamma camera models and derive calibrations coefficients for different gamma emitting radionuclides, especially in hospitals located in the vicinity of nuclear facilities.

4. Conclusion and outlook

4.1 Conclusion

The aim of this thesis was to investigate the feasibility of radiation detectors and imaging resources that are available at hospitals for radiation emergency situations. The results presented in this thesis provide insight into the capabilities of commonly available hospital equipment for use in RN scenarios. Based on the results from the present studies (Paper I – V), the conclusion is drawn that radiation detectors and imaging modalities can be used without large modifications in radiation emergencies. Emergency preparedness plans of hospitals could comprise modification and preparation of equipment as well as procedures to facilitate radiation measurements. Table 6 summarizes the radiation detectors and imaging modalities studied and their use in external or internal exposure scenarios. The radiation detectors and imaging modalities investigated in this thesis could play a crucial role in the response to RN emergencies.

Table 6 Summary of the monitoring equipment used in this thesis and their capability to detect external and internal exposure.

Capable of detecting	Gafchromic films (Paper I)	R100 (Paper II)	CTDP (Paper III)	CT/DR (Paper IV)	Gamma camera (Paper V)
External exposure	X	X	X		X
Internal exposure				X	X
Surface contamination	X		X		X

For the radiochromic films investigated in Paper I, the Gafchromic RTQA2 type film was found to be preferable compared with the other films due to its uniform dose response with respect to various radiation qualities.

In Paper II, it was demonstrated that an energy compensated 100 mm^2 Si-detector used for quality assessment of diagnostic radiology has an energy response of a factor of < 2 in the energy range of interest in RN emergencies.

Paper III shows that a small Si-detector used as a CT dose profiler and commonly available in hospitals could be modified for detection and spectrometry of alpha particles under normal air conditions.

In Paper IV it was shown that x-ray imaging modalities can be used to anatomically locate radioactive fragments at sizes down to a few hundred μm, requiring less than 6 mSv. A relationship between the effective dose per time-integrated activity for radionuclides deposited in various anatomical positions versus the effective dose from the imaging modalities is also provided in Paper IV. The results could be used to determine whether imaging utilizing ionizing radiation is justified in the medical response of subjects with embedded radioactive fragments.

An in-house developed phantom was presented in Paper V, and was shown to be useful for rapid calibration of clinical gamma cameras to enable quantitative assessment of *in-vivo* body burdens of gamma emitting radionuclides relevant for RN emergencies. Together with the determined MDA values, which are enough to detect activity levels corresponding to effective doses less than 1 mSv/year, it was shown that an acceptable precision in the activity determination of 30% could be attained.

4.2 Outlook

Although not investigated in Paper I, other publications show that radiochromic films could also be used for the detection of hot particles or skin contamination [61]. This is primarily of interest for beta emitting radionuclides due to the potential skin hazard resulting from the localized dose depositions. Furthermore, the Gafchromic films could also be used as dosemeters for measurements of the eye lens doses [62].

For the R100 detector and RTQA2 film, further investigations with other gamma sources emitting photons relevant for radiological protection, such as from ^{131}I and ^{137}Cs, are necessary in order to better cover the entire investigated range of photon energies. Also, vital parameters for dosemeters used for personal dosimetry such as dose rate dependence and the angular dependence for the R100 and RTQA2 should be evaluated. The filter configuration could be optimized further for the R100 by Monte Carlo simulations or in collaboration with the manufacturer in order to obtain an even flatter energy response.

The energy resolution of the CTDP could also be improved using collimation [43, 44, 45]. However, this would be at the expense of lower efficiency. Other applications for a portable alpha spectrometer could be for forensic follow-up measurements and contamination mapping in a field environment for situations such as the Litvinenko case where large areas were contaminated with ^{210}Po. The CTDP could also be utilized for neutron detection in combination with converters such as ^{6}LiF or ^{10}B. This would be of interest in particle accelerator facilities such as MAX IV and ESS (European Spallation Source), both located in Lund, Sweden.

For computed tomography imaging, the individual absorbed dose could be optimized by applying dose-reducing techniques such as tube current modulation compared to the fixed parameters used in Paper IV [63, 64]. Detection limits could also be established for other imaging modalities such as Cone-beam CTs (CBCT) and Dual-Energy CT

(DECT) since an advantage of these modalities is an artifact reduction which could be generated by high density fragments when imaged with conventional CT [65, 66, 67].

The derived calibration coefficients and MDA are valid for the specific gamma camera type used in Paper V and the conical-cylindrical phantom can be used to determine the corresponding values for other gamma camera models with other scintillator thicknesses. It could also be applied for gamma cameras with other detector material such as cadmium zinc telluride (CdZnTe). These modalities have advantages such as better energy resolution than conventional gamma cameras (usually consisting of NaI(Tl)) and the possibility to utilize these devices as spectrometers. Furthermore, calibration coefficients and MDA could also be derived for pure-beta emitters such as ^{90}Sr by measuring the bremsstrahlung. Moreover, for higher gamma energies such as from ^{60}Co where the full-energy peaks are above the maximum range of the PHA of a gamma camera the Compton scattered events could be registered and used for determination of calibration coefficients and MDA. Nevertheless, the straightforward methodology used in Paper V could be used as a template for other vendors. Also, the phantom could be used to calibrate *in-vivo* body burdens with traditional hand-held radiation protection instruments at hospitals in order to derive instrument specific calibration coefficients. This would be useful when there is a need to rapidly screen a large number of people and to identify individuals who further need medical attention.

There is also other equipment available at hospitals, such as numerous types of hand-held beta and gamma detecting probes and even miniaturized gamma cameras [68, 69]. The devices are used for radiosurgery applications and medical imaging utilizing various types of detectors, such as NaI(Tl), thallium-activated cesium iodide (CsI(Tl)), bismuth germanate (BGO), cadmium telluride (CdTe) or CdZnTe. The dosimetric properties of these instruments could be tested for radiation safety applications. Other probe types that could be evaluated in the future are silicon photomultiplier (SiPM) based scintillators [70, 71].

References

[1] Rojas-Palma, C., Liland, A., Jerstad, A.N., Etherington, G., Pérez, M.R., Rahola, T., Smith, K., Eds. TMT Handbook - Triage, Monitoring and Treatment of people in the event of malevolent use of radiation. Norwegian Radiation Protection Authority Österås, Norway Available at www.tmthandbook.org (2009).

[2] Williams, G., O'Malley, M., Nocera, A. Ensuring safety of surgical teams when managing casualties of a radiological dirty bomb. Injury 41(9), 938-42 (2010).

[3] IAEA (International Atomic Energy Agency) Manual for first responders to a radiological emergency, EPR-FIRST RESPONDERS. IAEA, Vienna (2006).

[4] Available at http://online1.ispcorp.com/_layouts/Gafchromic/index.html.

[5] Devic, S. Radiochromic film dosimetry: Past, present, and future. Physica Medica 27, 122 – 134 (2011).

[6] Niroomand-Rad, A., Blackwell, C.R., Coursey, B.M., *et al.* Radiochromic film dosimetry: recommendations of AAPM Radiation Therapy Committee Task Group 55. American Association of Physicists in Medicine. Med Phys 25(11), 2093-2115 (1998).

[7] Butson, M.J., Yu, P.K.N,. Cheung, T., Metcalfe P. Radiochromic film for medical radiation dosimetry. Mater Sci Eng R 41, 61-120 (2003).

[8] AAPM. Diode in vivo dosimetry for patients receiving external beam radiation therapy. AAPM report no. 87. Report of AAPM Task Group 62 of the Radiation Threapy Committe. College Park, MD, USA (2005).

[9] Herrnsdorf, L., Björk, M., Cederquist, B., Mattsson, C.G., Thungström, G. and Fröjdh, C. Point dose profile measurements using solid-state detectors in characterization of computed tomography systems. Nucl Instr Meth A 607, 223-25 (2009).

[10] Palm, Å., Nilsson, E., Herrnsdorf, L. Absorbed dose and dose rate using the Varian OBI 1.3 and 1.4 CBCT system. J Appl Clin Med Phys 11(1), 3085 (2010)

[11] Åsard, P.E., Baarsen. G. Commercial photodiodes as gamma and roentgen ray dosimeters. Acta Radiol Ther Phys Biol 7, 49-58 (1968).

[12] Kaiser, F.J., Bassler, N., Jäkel, O. COTS silicon diodes as radiation detectors in proton and heavy charged particle radiotheraphy 1. Radiat Environ Biophys 49(3), 365-71 (2010).

[13] Grusell, E., Medin, J. General characteristics of the use of silicon diode detectors for clinical dosimetry in proton beams. Phys Med Biol 45, 2573-82 (2000).

[14] Gramsch, E., Lynn, K.G., Weber, M., DeChillo, B., McWilliams, J.R. Silicon PIN photodetectors in high resolution nuclear spectroscopy. Nucl Instr And Meth A 311(3), 529-38 (1992).

[15] Lindström, G., Moll, M., Fretwurst, E. Radiation hardness of silicon detectors - challenge from high-energy physics. Nucl Inst and Meth A 426, 1-15(1999)

[16] Fröjdh, A., Thungström, G., Fröjdh, C., Petersson, S. An optimized system for measurement of radon levels in buildings by spectroscopic measurement of radon progeny. JINST C12018 (2011).

[17] Fröjdh, A., Fröjdh, E., Thungström, G., Fröjdh, Norlin, B. Processing and characterization of a MEDIPIX2-compatible silicon sensor with 220 μm pixel size. Nucl Instr And Meth A 633, 578-80 (2011).

[18] Available at http://rtigroup.com/content/downloads/manuals.

[19] Hubbell, J.H., Seltzer, S.M. Tables of x-ray mass attenuation coefficients and mass energy-absorption coefficients (Version 1.4). National Institute of Standards and Technology, Gaithersburg, MD (online) Available (2004) http://physics.nist.gov/xaamdi.

[20] ICRP (International Commission on Radiological Protection) Recommendations of the International Commission on Radiological Protection ICRP Publication 103; Ann. ICRP 37 (2007).

[21] IAEA (International Atomic Energy Agency) Criteria for use in preparedness and response for a nuclear or radiological emergency. General Safety Guide No. GSG-2. IAEA, Vienna (2011).

[22] Currie, L.A. Limits for qualitative detection and quantitative determination. Application to radiochemistry. Analytical Chemistry 40(3), 586-93 (1968).

[23] Lang, S., Servomaa, K., Rytömaa, T. Biokinetics of nuclear fuel compounds and biological effects of nonuniform radiation. Environ Health Perspect 103, 920-34 (1995).

[24] Aragon, A., Espinosa, A., De la Cruz, B., Fernandez, J.A. Characterization of radioactive particles from the Palomares accident. J Environ Radioact 99, 1061-7 (2008).

[25] Salbu, B. Radionuclides released to the environment following nuclear events Integr Environ Assess Manag 7, 362–4 (2011).

[26] Hsieh, J. Computed Tomography Principles, Design, Artifacts (Bellingham, Wash. Hoboken, NJ SPIE; J. Wiley & Sons) pp 158-9 (2009).

[27] Rasband, W.S. ImageJ, U.S. National Institutes of Health, Bethesda, Maryland, USA, http://rsb.info.nih.gov/ij/, 1996-2016.

[28] Davis, S.D., Ross C.K, Mobit, P.N., Van der Zwan. L., Chase, W.J., Shortt, K.R. The response of LiF thermoluminescence dosemeters to photon beams in the energy range from 30 kV x rays to 60Co gamma rays. Radiat Prot Dosim 106, 33-43 (2006).

[29] Cardis, E., Howe, G., Ron, E., Bebeshko, V., Bogdanova, T., Bouville, A., Carr, Z., Chumak, V., Davis, S., Demidchik, Y et al. Cancer consequences of the Chernobyl accident: 20 years on. J Radiol Prot 26(2), 127-40 (2006).

[30] UNSCEAR (United Nations Scientific Committee on the Effects of Atomic Radiation) Sources and Effects of Ionizing Radiation—Volume II: Effects (New York: United Nations) (2000).

[31] Cheung, T., Butson, M.J., Yu, P.K.N. Experimental energy response verification of XR type T radiochromic film. Phys Med Biol 49 (21), 371-76 (2004).

[32] Tomic, N., Quintero, C., Whiting, B.R., Aldelaijan, S., Bekerat, H., Liang, L., DeBloise, F., Seuntjens, J., Devic, S. Characterization of calibration curves and energy dependence GafChromic™ XR-QA2 model based radiochromic film dosimetry system. Med Phys 41(6), 062105 (2014).

[33] Evans, M.D.C., Devic, S, Podgorsak, E.B. High dose-rate brachytherapy source position quality assurance using radiochromic film. Med Dosim 32(1), 13–15 (2007).

[34] Ali, I., Dempsey, J.F., Williamson, J.F. Dependence of radiochromic film optical density post-exposure kinetics on dose and dose fractionation. Med Phys 30, 1958-1967 (2003).

[35] Alnawaf, H., Butson, M.J., Peter K.N. Yu, P.K.N., Cheung, T. SIRAD - Personal radiation detectors. Radiat Measurements 46, 1826 – 28 (2011).

[36] Gordon, R.K., Winters, P., Patel, G., Patel, P. Self-indicating radiation alert dosemeter (SIRAD). Radiat Prot Dosim 120 (1-4), 259-62 (2006).

[37] Rikner, G., Grusell, E. Selective shielding of a p-Si detector for quality independence. Acta Radiol Oncol 24, 65-9 (1985).

[38] Gilar, P., Petro, I. Silicon photodiodes as a detector of exposure rate. Nucl. Instr Meth A 234, 566-72 (1984).

[39] Gager, L.D., Wright, A.E., Almond, P.R. Silicon diode detectors used in radiological physics measurements. Part I: Development of an energy compensating shield. Med Phys 4, 494-8 (1977).

[40] Kaiser, F.J., Bassler, N., Jäkel, O. COTS silicon diodes as radiation detectors in proton and heavy charged particle radiotheraphy 1. Radiat Environ Biophys 49(3), 365-71 (2010).

[41] Batista, E., Khoury, H.J., Melo, F.A., Barros, V., da Silva, E.F Jr. The performance of commercial photodiodes for dosimetry in mammography. Radiat Prot Dosim 115, 391-3 (2005).

[42] Khoury, H.J., Hazin, C.A., Masccarenhas, P.A., da Silva, Jr E.F. Low cost silicon photodiode for elelctron dosimetry. Radiat Prot Dosim 84, 341-43 (1999).

[43] Vaninblat, N., Pelled, O., German, U., Haquin, G., Tshuva, A., Alfassi, Z.B. Determination of parameters relevant to alpha spectrometry when employing source coating. Appl Radiat and Isotopes 61, 307-11 (2004).

[44] Pöllänen, R., Peräjärvi, K., Siiskonen, T., Turunen, J. High-resolution alpha spectrometry at ambient pressure-towards new applications. Nucl Inst and Methods A 694, 173-78 (2012).

[45] Park, S., Kwak, S-W., Kand, H-B. High resolution alpha spectrometry through collimation. Nucl Inst and Methods. 784, 470-473 (2015).

[46] National Council on Radiation Protection and Measurement. Management of persons contaminated with radionuclides. NCRP Report No. 161. Bethesda, Md, USA: National Council on Radiation Protection and Measurement; (2009).

[47] Lakits, A., Prokesch, R., Scholda, C., Nowotny, R., Kaider, A., Bankier, A. Helical and conventional CT in the imaging of metallic foreign bodies in the orbit Acta Ophthalmol Scand 78, 79-83 (2000).

[48] Dass, A.B., Ferrone, P.J, Chu, Y.R, Esposito, M., Gray, L. Sensitivity of Spiral Computed Tomography Scanning for Detecting Intraocular Foreign Bodies. Ophthalmology 108, 2326-8 (2001).

[49] Chacko, J.G., Figueroa, R.E., Johnson, M.H., Marcus, D.M., Brooks, S.E. Detection and localization of steel intraocular foreign bodies using computed tomography. A comparison of helical and conventional axial scanning. Ophthalmology 104, 319-23 (1997).

[50] Otto, P.M., Otto R.A., Virapongse, C., Friedman, S.M., Emerson, S., Li, K.C., Malot, R., Kaude, J.V., Staab, E.V. Screening test for detection of metallic foreign objects in the orbit before magnetic resonance imaging. Invest Radiol 27, 308–11 (1992).

[51] Aras, M.H., Miloglu, O., Barutcugil, C., Kantarci, M., Ozcan, E., Harorli, A. Comparison of the sensitivity for detecting foreign bodies among conventional plain radiography, computed tomography and ultrasonography. Dentomaxillofac Radiol 39, 72–8 (2010).

[52] Turkcuer, I., Atilla, R., Topacoglu, H., Yanturali, S., Kiyan, S., Kabakci, N., Bozkurt, S., Cevik, A.A. Do we really need plain and soft-tissue radiographies to detect radiolucent foreign bodies in the ED? Am J Emerg Med 24, 763–68 (2006).

[53] LoBue, T.D., Deutsch, T.A., Lobick, J., Turner, D.A. Detection and Localization of Nonmetallic Intraocular Foreign Bodies by Magnetic Resonance Imaging. Arch Ophthalmol 106, 260-61(1988).

[54] IAEA Rapid monitoring of large groups of internally contaminated people following a radiation accident Vienna, Austria IAEA-TECDOC-746 (1994)

[55] Edmond, C.A., Kalinich, J.F. Biokinetics of embedded surrogate radiological dispersal device material. Health Phys 102, 124-36 (2012).

[56] Hansson, M., Rääf, L.R. Visualisation and quantification of lung content of radionuclides associated with nuclear and radiological emergencies. Radiat Prot Dosim 145, 341–350 (2011).

[57] Wallström, E., Alpsten, M., Mattsson, S. A gamma camera for measurements of internal contamination after a radiological accident. J Radiol Prot 19, 2143–54 (1998).

[58] Andrási, A. Whole-body counter intercomparison as a tool of quality assurance. Radiat Prot Dosim 89(3-4), 229-33 (2003).

[59] Dantas, B. M., Lucena, E. A., Dantas, A. L., Araújo, F., Rebelo, A.M., Terán, M., Paolino, A., Hermida. J.C., Rojo, A.M., Puerta, J.A. et al. A protocol for the calibration of gamma cameras to estimate internal contamination in emergency situations. Radiat Prot Dosim 127(1-4), 253-7 (2007)

[60] Schuffham, J.W., Yip-Braidley, M., Schutt, A.L., Hinton, P.J., Nisbet, A., Bradley, D. A. Adapting clinical gamma cameras for body monitoring in the event of a large-scale radiological incident. J Radiol Prot 36, 363-81 (2016).

[61] Eakins, J.S., Hager, L.G., Tanner, J. Calibration of thermoluminescence and film dosemeters for skin doses from high-activity microparticles. Radiat Prot Dosim 70(1-4), 173-76 (2016).

[62] Akhilesh, P., Kulkarni, A.R., Jamhale, S.H.,, Sharma., S.D., Kumar, R., Datta, D. Estimation of eye lens dose during brain scans using gafchromic XR-QA2 film in various multidetector CT scanners. Radiat Prot Dosim doi:10.1093/rpd/ncw132 (2016).

[63] Kaira, M.K., Maher, M.M., Toth, T.L., Schmidt, B., Westerman, B.L., Morgan, H.T., Saini, S. Techniques and applications of automatic tube current modulation for CT. Radiology 233(3), 649-657 (2004).

[64] Mattsson, S., Andersson, M., Söderberg, M. Technological advances in hybrid imaging and impact on dose. Rad Prot Dosim 165(1–4), 410–415 (2015).

[65] Von See, C., Bormann, K.H., Schumann, F., Goets, F., Gellrich, N.C., Rücker, M. Forensic imaging of projectiles using cone-beam computed tomography, Forensic Sci Int 190, 38–41 (2009).

[66] Zhang, Y., Zhang, L., Zhu, X.R., Lee, A.K, Chambers, M., Dong, L. Reducing metal artifacts in cone-beam CT images by preprocessing projection data. Int. J. Radiat Oncol Biol Phys 67, 924–32 (2007).

[67] Bamberg, F., Dierks, A., Nikolaou, K., Reiser, M.F., Becker, C.R., Johnson, T.R.C. Metal artifact reduction by dual energy computed tomography using monoenergetic extrapolation, Eur Radiol 21, 1424–9 (2011).

[68] Povoski, S.P., Neff, R.L., Mojzisik, C.M., O'Malley, D.M., Hinkle, G.H., Hall, N.C., Murrey Jr, D.A., Knopp, M.V., Martin Jr, E.W. A comprehensive review of radioguided surgery using gamma detection probe technology. World J Surg Oncol 7(11) (2009).

[69] Sánchez, F., Fernández, M.M., Giménez, M., Benlloch, J.M., Rodríguez-Alvarez, M.J., García de Quirós, F., Lerche Ch., Pavón, N., Palazón, J.A., Martínez, J., Sebastiá, A. Performance tests of two portable mini gamma cameras for medical applications. Med Phys 33(11), 4210-30 (2006).

[70] Kwak, I.S., Kang, H.G., Son, J-W., Lee, J.S, Hong, J.S A feasibility study of an intraoperative beta imaging/gamma probe using a depth of interaction measurement. J Nucl Med 56(3), 1867 (2015).

[71] Herrnsdorf, L., Caccia, M., Mattsson, S. Silicon photomultipliers for medical imaging and dosimetry. Rad Prot Dosim 169(1-4), 430-435 (2016).

Paper I

Radiation Protection Dosimetry (2012), Vol. 150, No. 1, pp. 119–123 doi:10.1093/rpd/ncr374
Advance Access publication 17 September 2011

NOTE

GAFCHROMIC FILM AS A FAST VISUAL INDICATOR OF RADIATION EXPOSURE OF FIRST RESPONDERS

Ünal Ören*, Christopher L. Rääf and Sören Mattsson
Medical Radiation Physics, Department of Clinical Sciences, Lund University, Skåne University Hospital, SUS Malmö, SE-205 02 Malmö, Sweden

*Corresponding author: unal.oren@med.lu.se

Received March 29 2011, revised July 27 2011, accepted August 18 2011

Three types of Gafchromic films have been studied to investigate their potential for use as a visually readable dosemeter for persons acting as first responders in connection with radiological or nuclear emergencies. The two most sensitive film types show a pronounced variation in sensitivity by photon energy and are therefore not suitable for use in cases of unknown exposures. The third film type tested (RTQA2), which is intended for quality control in radiation therapy has a sensitivity that is independent of the radiation quality, and is therefore considered as the most optimal for visual reading *in situ*. Tests carried out on a group of 10 human observers showed that absorbed doses down to 40 mGy can be detected by the eye. Read by a portable densitometer, qualitative absorbed dose estimates down to 9 mGy can be achieved. The colour change is obtained instantaneously, giving first responders immediate information about the presence of beta-, gamma- and X-ray radiation.

INTRODUCTION

Following a radiological or nuclear accident, there is a need for the first responders to monitor their radiation exposure instantly. It is of interest to find a dosemeter that can be used across a wide range of radiation qualities. The dosemeter must be light in weight, portable, easy to use with minimal training and affordable. An instantaneous reading of exposure in the appropriate dose range is desirable, so that timely and appropriate action can be taken regarding the rescue operation and preventing overexposure. Pocket ionisation chambers for personal dose assessment, Geiger–Muller counters and other survey meters require regular charging of batteries and training for use. They are fairly expensive, making them economically non-viable for issuing to first responders on a mass scale. Radiochromic film has been found to be useful for monitoring radiation dose for emergency responders[1]. Gafchromic film (ISP, International Specialty Products, Wayne, NJ, USA), is widely used for radiation dosimetry in conventional radiotherapy and diagnostic radiology[2]. The Gafchromic films develop automatically due to radiation-induced polymeriation reactions within its sensitive layer. Upon exposure to ionising radiation, the Gafchromic film changes colour from yellow to brown and the colour intensifies as the absorbed dose increases, thereby providing the user information on cumulative radiation exposure. The change in optical density (OD) can be measured with densitometers, film scanners or spectrophotometers[3].The aim of this investigation is to study the feasibility of Gafchromic film as a potential personal dosemeter, giving a *visual* qualitative measurement of exposure for first responders.

MATERIALS AND METHODS

Initially, three types of Gafchromic film were investigated. The RTQA2 film was specifically designed for use in radiation therapy quality assurance procedures (http://online1.ispcorp.com/_layouts/Gafchromic/index.html)[4]. According to the manufacturer, the film is designed to be used in the absorbed dose range from 0.02 to 8 Gy. The films XRQA (dose range 2–500 mGy) and XRQA2 (1–200 mGy), were produced for quality assurance procedures in the kilovoltage X-ray energy range. All three types of film have a white backing material and a yellow coloured transparent polyester cover on the front, and the active layer is sandwiched between these two. They are constructed in this way to increase the visual colour change seen upon exposure. Information regarding the film constructions and characteristics are available on the website of the manufacturer (ISP).

Energy dependence

There are varying amounts of high atomic number dopants in Gafchromic products, thus creating a variable sensitivity for different radiation qualities, which may not be optimal for a mass scale application to rescue workers, who may be subject to irradiation fields of unknown photon energy composition. To evaluate the energy dependence of the dose response, two photon radiation sources were used: An X-ray unit (A-196, Varian Medical

Systems, USA), which operates at 80 kV and a ^{60}Co-unit (Gammatron-3, Siemens, Germany), with primary photon energies of 1.17 and 1.33 MeV. Irradiations were also performed with high-energy beta particles using a sealed ^{90}Sr/^{90}Y source (E_{Max}=2.27 MeV; Risø TL-15 reader, Risö National Laboratory, Roskilde, Denmark). A sheet of each of the three films was cut into multiple squares 20 mm×20 mm. At kilovoltage energy ($E_{hv,Max}$=80 keV), the films were placed at the surface of a water equivalent phantom (RW3, PTW Freiburg, Germany) of dimensions 30 cm×30 cm×15 cm. For dose delivery with ^{60}Co, the films were placed between the slabs at a depth of 0.5 cm. The films were irradiated, one at a time, at the centre of 10×10 cm^2 field while placed perpendicular to the central beam axis. Precautions in handling of radiochromic film as outlined in the AAPM Radiation Therapy Task Group TG-55 were taken (Niroomand-Rad *et al.*[4]). The film was only removed from a light tight envelope during irradiation and readout to reduce any effects of ambient light (Butson *et al.*[5]). Prior to film measurements, the absorbed dose was measured in the field centre with an ionisation chamber (Roos type TW34001 PTW, Freiburg, Germany) for ^{60}Co exposures and another ionisation chamber (Radcal, Model 2186, Monrovia, CA, USA) for exposures with kilovoltage X rays at the same location and depth, in order to correlate the signal (in terms of e.g. OD) to the absorbed dose at the film plane. After irradiation, the films were stored for 3 h before ODs were measured. This time interval was initially chosen to ensure that all polymer changes within the film due to the radiation exposure had been completed. The manufacturer recommends waiting at least 2 h post-irradiation before scanning. Our results (see below) later showed that this waiting time was unnecessary for the intended application. The ODs of the films were measured using a portable densitometer (X-Rite 331 Grand Rapids, MI, USA) and the net ODs (NODs) were calculated for all films by subtracting the background levels from the results. The NOD values were plotted against the dose values.

Time dependence

The time dependence of the film response was analysed. A post-exposure density growth of Gafchromic films occurs when exposed to ionising radiation[5].Two pieces of RTQA2 were exposed to an absorbed dose of 91 and 277 mGy, respectively, with a ^{60}Co beam. The ODs of the films were then measured at different time periods ranging from 1 to 300 min and the response was plotted as a function of time.

Sensitivity of multiple layered films

A method for increasing the sensitivity of the RTQA2 film, by using multilayer film technique, was performed. The principle used is described by the Beer–Lambert law, stating that the light absorbed by a medium varies exponentially with the path-length of the light in the medium, thus effectively increasing the change in OD with absorbed dose by layering films together. Previous results have shown that layering films together increases the sensitivity of Gafchromic films so that lower doses can be measured[6]. RTQA2 films were cut into 20 mm×20 mm pieces and films up to three layers were constructed and stuck together with a tape covering 1 mm of the outer edges of each dosemeter. To make sure that no air gaps were present between the film layers and to reduce the effect of reflected light within the film stack, care was taken that the stack was bound tightly together. The stack thicknesses of three layered films were compared with three individual layer thicknesses to ensure this. The film stacks were placed in the water equivalent phantom and were irradiated with 0.5 cm build up material, using the ^{60}Co unit. The ODs of the irradiated films were measured 3 h post-irradiation with a densitometer.

Sensitivity to environmental conditions

A field study was performed where four unirradiated RTQA2 films were deployed in three different environmental locations. Two films, where one was enclosed in a transparent plastic case and the other without protection, were placed outdoors. The other two films were placed in an office environment and in a radiotherapy simulation operation control room. The dosemeters were read after a 2-month period in the autumn of 2010 to test whether there was any change in ODs due to environmental influence over a certain time.

Visual readout

Visual readout tests were also performed where 10 individuals volunteered to participate. Four were medical physicists, two technicians, two students and two nurses. They were familiar with the Gafchromic film and its purpose but had no previous experience evaluating films. The visual test used 10 Gafchromic RTQA2 pieces, which had been exposed to absorbed doses ranging from 0 to 100 mGy from the X-ray unit. The films were placed in random order and each subject was asked to grade them from the lowest to the highest dose. The participants were also instructed to identify the exposed films from an unexposed one in a twin-film arrangement, where every film in the current dose range was placed next to a reference unexposed film.

RESULTS AND DISCUSSION

Energy dependence

Dose–response relationships of each type of Gafchromic film irradiated by a given radiation source were obtained by plotting NOD values against corresponding absorbed doses and the results are presented in Figure 1. An energy-dependent dose response is observed for the two films XRQA and XRQA2, with an elevated response for lower (<100 keV) photon energies. The film sensitivity decreases with increasing radiation energy, as expected from the original design idea. The results are consistent with previous reports for XR-type films[7]. These film models contain high-Z materials in the emulsion and have been designed to increase photoelectron interaction, thus increasing its response in the kilovoltage range and making the film more suitable for diagnostic radiology. This leads to an increased energy dependence when used in photon irradiation fields of a larger energy range. The energy dependence of these films therefore disqualifies them as personal dosemeters for first responders. The response for the film aimed for therapy applications, RTQA2, does not, however, reveal any energy dependence. The latter film type is thus, among the three films studied, the best candidate in terms of minimal energy dependence of the response.

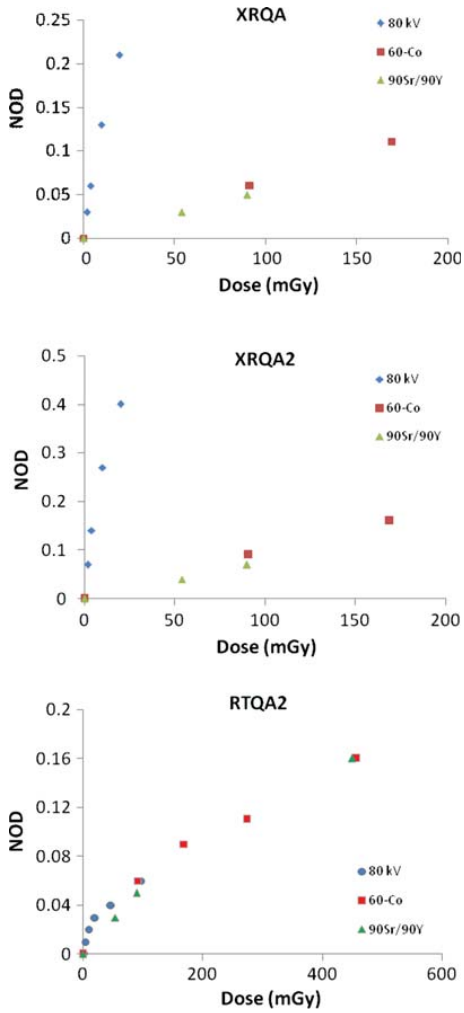

Figure 1. Dose–response curves, obtained by plotting NODs versus absorbed dose, of Gafchromic XRQA, XRQA2 and RTQA2 films irradiated with an X-ray system (80 kV), a beam of ^{60}Co (1.17 and 1.33 MeV) and a 20 MBq ^{90}Sr/^{90}Y β source.

Time dependence

NODs as a function of time for the RTQA2-film plotted for each post-irradiation time, at absorbed doses of 91 and 277 mGy respectively, are presented in Figure 2. The result indicates that there were no changes in post-irradiation ODs between 1 and 300 min after irradiation. The RTQA2 film thus responds rapidly, providing a dose estimate within less than a minute from exposure.

Sensitivity of multiple layered films

NODs for a single-, double- and triple-layer RTQA2 film exposed to ^{60}Co radiation are presented in Figure 3a. It shows that the sensitivity increases by

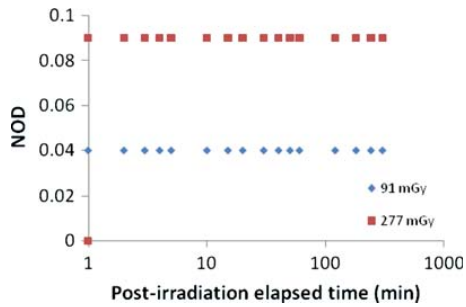

Figure 2. NODs of RTQA2 as a function of time after exposures of absorbed doses of 91 and 277 mGy, respectively.

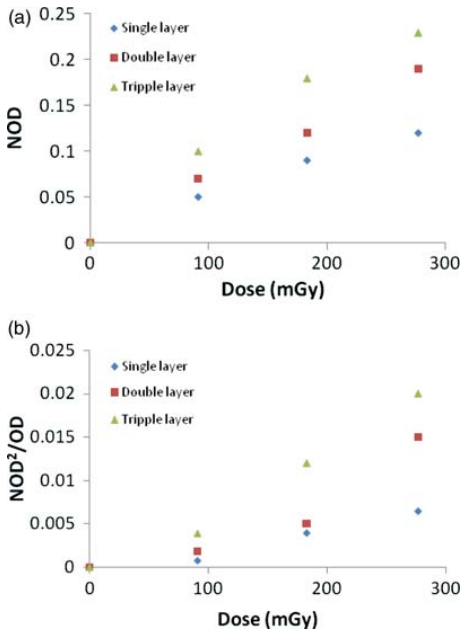

Figure 3. (a) NOD as determined by densitometer vs. absorbed dose for single-, double- and triple-layer RTQA2 films. (b) Figure-of-merit, in terms of NOD squared divided by the background OD, plotted against absorbed dose for single-, double- and triple-layer films.

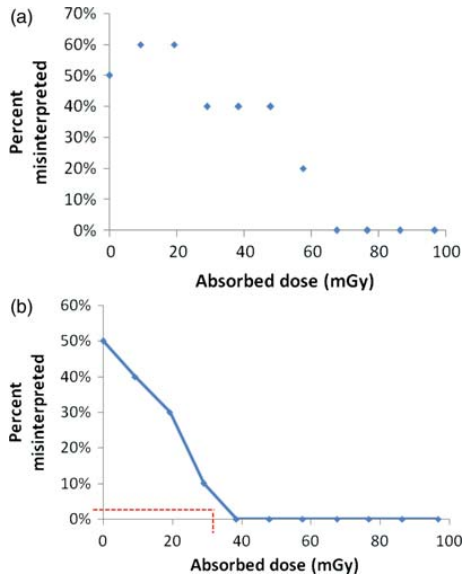

Figure 4. (a) Results for the participants when asked to visually rank the exposed films from the lowest to the highest dose. (b) Results when participants ranked exposed films placed next to unexposed. Five per cent likelihood of misinterpretation is marked in the plot.

increasing the number of layers. A relationship in NOD squared is observed when stacking film together (Figure 3b.). As the pathlength increases more light will be absorbed for a given absorbed dose value, resulting in a larger signal in terms of NOD, thus enhancing the signal-to-noise ratio of the measurement and improving the performance of the detector. As the OD of the background films increases a saturation will occur and eventually the effect of increasing the number of layers will become smaller. The radiation dose required to produce a NOD of 0.1 decreases from 210 mGy for a single-layer film to 90 mGy for a triple-layer film. The change in OD per unit-absorbed dose is increased by stacking films together, thus reducing the detectable dose limit by the densitometer. These results show that the multilayer technique enhances the film sensitivity and expands its application to lower dose regions. The results are in good agreement with the data published by Cheung *et al.*[6]. Due to inter-batch variability of Gafchromic films and variation in the background ODs of film sheets, the increase in sensitivity can vary considerably.

Influence of environmental conditions

To determine how the RTQA2 responds to different environments a field study was applied. For the film without protection placed outdoors the results showed that there was an increase in OD by 0.1 when measured by densitometer. This shows that if not protected, the performance is affected by environmental factors such as humidity and dust. The film encased in a polyethylene plastic case, however, showed no colouration effects or changes in OD. The other films placed indoors showed no colouration of the film and there were no density growth when measured, thus showing insensitivity to conventional room light. The RTQA2 appears to be unaffected in the various environments, but used outdoors, it requires some protection from humidity and dust.

Visual readout

The results of the 10 observers when asked to visually grade the exposed films from lowest to highest absorbed dose are shown in Figure 4a. There is a variation in visual interpretation and the grade of misinterpretation decreases at higher doses. The performance of the visual readout tests were improved

Figure 5. Visual comparison of an unexposed film and an exposed (47 mGy), shown side-by-side where the exposed film is shown to the right.

when the subjects were asked to identify exposed films placed next to an unexposed film, Figure 4b. A criterion value of 0.05 would mean that 5 % of the observed results would be false negatives at ~35 mGy. Thus, at absorbed doses above 35 mGy, this yields a >95 % probability that the film is identified as being exposed to radiation above the background level. For visual comparison, an unexposed film (NOD=0) and a film exposed to 47 mGy (with a NOD=0.03) is shown in Figure 5. Using the densitometer to determine the absorbed dose through NOD, a minimum detectable absorbed dose of 9 mGy was observed. The results show that basic qualitative analysis can be performed visually by comparing the colour of the exposed film with colours of unexposed film, down to ~35 mGy. Using a portable densitometer can depress the detection limit by almost a factor of 4.

CONCLUSION

This study demonstrates that the Gafchromic film RTQA2 withstands various normal environmental conditions and that it can be used as an indicator of dose, giving a visual qualitative absorbed dose estimate down to 35 mGy (corresponding to a risk of 5 % false negative). The colour change is obtained instantaneously and is essentially independent of the radiation energy and quality. The measurable change in OD against radiation dose can be increased by layering films together. Its sensitivity is sufficient for accurate measurements of doses in the range of 50–500 mGy, which is a dose range adequate for monitoring radiation in emergency situations.

FUNDING

This work was supported by a grant from the Swedish Radiation Safety Authority.

REFERENCES

1. Riel, G. K., Winters, P., Patel, G. and Patel, P. *Self-indication radiation alert dosimeter (SIRAD)*. Radiat. Prot. Dosim. **120**(1–4), 259–262 (2006).
2. Butson, M. J., Yu, P. K., Cheung, T. and Metcalfe, P. *Radiochromic film for medical radiation dosimetry*. Mater. Sci. Eng. R. **41**, 61–120 (2003).
3. Devic, S., Seuntjens, J., Hegyi, G., Podgorask, E. B., Soares, C. G., Kirov, A. S., Ali, I., Williamson, J. F. and Elinzondo, A. *Dosimetric properties of improved Gafchromic films for seven different digitizers*. Med. Phys. **31**, 2392–2401 (2004).
4. Niroomand-Rad, A., Blackwell, C. R., Coursey, B. M., Gall, K. P., Galvin, J. M., McLaughlin, W. L., Meigooni, A. S., Nath, R., Rodgers, J. E. and Soares, C. G. *Radiochromic film dosimetry: recommendations of AAPM Radiation Therapy Committee Task Group 55. American Association of Physicists in Medicine*. Med. Phys. **25**(11), 2093–2115 (1998).
5. Butson, M. J., Yu, P. K. and Metcalfe, P. *Effects of readout light sources and ambient light on radiochromic film*. Phys. Med. Biol. **49**, N371–N376 (1998).
6. Cheung, T., Butson, M. J. and Yu, P. K. *Use of multiple layers of Gafchromic film to increase sensitivity*. Phys. Med. Biol. **46**, 235–240 (2001).
7. Cheung, T., Butson, M. J. and Yu, P. K. *Experimental energy response verification of XR type T radiochromic film*. Phys. Med. Biol. **49**(21), N371–N376 (2004).

Paper II

CAN AN ENERGY-COMPENSATED SOLID-STATE X-RAY DETECTOR BE USED FOR RADIATION PROTECTION APPLICATIONS AT HIGHER ENERGIES?

Ünal Ören, Lars Herrnsdorf, Mikael Gunnarsson, Sören Mattsson and Christopher L. Rääf

This is a pre-copyedited, author-produced PDF of an article accepted for publication in Radiation Protection Dosimetry following peer review. The version of record [*Ünal Ören, Lars Herrnsdorf, Mikael Gunnarsson, Sören Mattsson and Christopher L. Rääf* ***CAN AN ENERGY-COMPENSATED SOLID-STATE X-RAY DETECTOR BE USED FOR RADIATION PROTECTION APPLICATIONS AT HIGHER PHOTON ENERGIES?*** *Radiat Prot Dosimetry (2016) 169(1-4): 292-296.* First published online: November 29, 2015] is available online at: http://rpd.oxfordjournals.org/content/169/1-4/292

Radiation Protection Dosimetry (2016), Vol. 0, No. 0, pp. 0-0 *SECTION TITLE HERE*
DOI: 10.1093/rpd/nc0000

CAN AN ENERGY-COMPENSATED SOLID-STATE X-RAY DETECTOR BE USED FOR RADIATION PROTECTION APPLICATIONS AT HIGHER ENERGIES?

Ünal Ören[1,*]Lars Herrnsdorf[1], Mikael Gunnarsson, Sören Mattsson and [1]Christopher L. rääf[1]
[1]Medical Radiation Physics, Department of Translational Medicine, Lund University, Skåne University Hospital, SE-205 02 Malmö, Sweden

Received month date year, amended month date year, accepted month date year

The objective of this study was to investigate the characteristics of a solid-state detector commonly available at hospitals for parallel use as a real-time personal radiation monitor following radiation emergency situations.
A solid-state detector probe with an inherent filtration (R100, RTI Electronics AB, Mölndal, Sweden) was chosen for evaluation. The energy dependence and the linearity in signal response with kerma in air were examined and the detector was exposed to both X-ray beams using a conventional X-ray unit with effective photon energies ranging between 28.5-48.9 keV and to γ-rays: 1.17 and 1.33 MeV from ^{60}Co. The R100 exhibited approximately 1.7 times over-response at the lowest X-ray energy relative to the ^{60}Co source. The detector demonstrated a linear response (R^2=1) when irradiated with ^{60}Co to air kerma values in the range of 20-200 mGy. The conclusion is that high-energy photons such as those from ^{60}Co can be detected by the R100 with an energy response within a factor < 2 over the energy range examined and that the detector can provide real-time dose measurements following nuclear or radiological events.

INTRODUCTION

A large quantity of radionuclides could be released into the environment following nuclear or radiological disasters, such as accidents in nuclear power plants or malevolent acts, which results in large numbers of people being exposed to ionizing radiation. There are also a number of sources of radionuclides in hospital and university laboratories that can lead to various exposure pathways to people. Radiation emergency situations in such facilities can range from spills that can cause external exposure to both staff and patients in the vicinity. Fires and explosions can result in major airborne releases of radionuclides used or stored in hospital facilities. In such scenarios there is a need to quickly detect elevated radiation in the localities and to instantly monitor potentially affected individuals. Moreover, this will require real-time monitoring of the exposures to the rescue workers who must operate in an unknown radiation environment.

In hospitals as well as in universities, conventional personal radiation monitoring techniques such as thermoluminescence (TL)/optically stimulated luminescence (OSL) dosemeters are commonly used for individual monitoring of the external dose of workers. These dosemeters are passive detectors requiring a posteriori signal read-out and thus do not provide real time information about the radiation exposure, resulting in a delayed information regarding the amount of accumulated absorbed dose. These techniques are also time consuming in preparation and assessment and they include laborious processing steps such as light or heat stimulation and readout. It follows therefore that such instrumentation is not suitable for use in radiation emergency situations where real time assessments of dose and dose rate is needed.

On the other hand, radiation detectors based on semiconductors such as silicon (Si) are commonly used as active dosemeters with instant reading [1]. Electronical dosemeters (EPD) contain silicon diodes and they are preferred in emergency situations since they provide real-time reading on the dose and dose rate. Silicon based dosemeters are also common in for example medical fields such as conventional radiotherapy and radiology, proton and heavy charged particle radiotherapy [2, 3, 4, 5, 6, 7]. Other areas where silicon diodes are used are in nuclear spectroscopy and high-energy physics [8, 9].

Silicon detectors have gained in popularity due to the inherent advantage of Si such as the ionization energy (3.62 eV [at 300 K]) required for an electron-hole pair production compared to e.g. 34 eV for an ion-pair production in an ionization chamber filled with air. The density of Si is also 1800 times higher than for air resulting in an 18000 larger current production per unit detector volume and thus allowing smaller volumes of Si that are more practical for use in personal monitoring [10].

The aim of this study was to investigate the potential use of a Si x-ray detector, which is widely available at hospitals and is used for quality assurance of diagnostic X-ray equipment, as a dosemeter for radiation safety purposes. This was done by investigating the energy

dependence of the number of registrations in terms of collected charge (nC) per unit of air kerma in air in the photon energy range of interest for radiation emergency situations, and by investigating the linearity between number of registrations and kerma.

MATERIALS AND METHODS

Dosemeter R100

A solid-state detector probe with a 10x10 mm^2 sensitive area (R100, RTI Electronics AB, Mölndal, Sweden), dedicated for quality assurance in diagnostic x-ray applications, was chosen for evaluation. The R100 has a built-in energy correction filter allowing the detector to automatically compensate for different photon energies in the energy range of conventional diagnostic X-rays. The energy dependence and the linearity in signal response for the solid-state detector were now examined for a broader photon energy range. Neither information about the filter material nor the filter dimensions of the R100 were available from the manufacturer.

Energy response, linearity and reproducibility

The R100 detector was exposed to X-ray beams and high-energy gamma photons from ^{60}Co under free air conditions and the exposure was expressed in terms of air kerma. A calibrated cylindrical ionization chamber with a 6 cm^3 active volume (Model 10X5-6, Radcal, Monrovia, Ca, USA) was used for the air kerma measurements. The R100 and the ionization chamber were connected to an electrometer (Barracuda, RTI, Mölndal, Sweden) for readout and were simultaneously irradiated. The Si-detector was operated in the photovoltaic mode (zero bias), whereas a high-voltage (300 V) was applied to the ionization chamber, and the measured charge in terms of nC was used to determine the dosimetric characteristics of the detector.

In order to assess the energy response, irradiations were carried out using a conventional X-ray unit (A-196, Varian Medical Systems, USA) as well as high-energy photons (1173 and 1333 keV) using a ^{60}Co (Gammatron-3, Siemens, Germany) gamma ray unit. For the X-ray measurements, the source-to-detector distance was set to 1 m. Five different tube voltages of 40 kVp, 60 kVp, 80 kVp, 100 kVp and 120 kVp were used and the corresponding effective photon energies for each were estimated to 28.5 keV, 30.9 keV, 40.3 keV, 45.7 keV and 48.9 keV. The effective photon energies for the X-ray measurements were determined from measuring the half-value layer (HVL) for each tube voltage and subsequently using mass attenuation coefficient data from the National Institute of Standards and Technology (NIST) database [11]. Measurements for HVL determinations were made using a silicon based detector (Unfors RaySafe Xi R/F, Billdal, Sweden). For the ^{60}Co irradiations, the detector was mounted 0.5 m from source, which is the distance that the ^{60}Co beam is calibrated at. Furthermore, at the ^{60}Co irradiations the ionization chamber was covered with a build-up cap made of 0.5 cm polymethylmethacrylate (PMMA) in order to acquire charge-particle equilibrium. The ionization chamber has a ± 5% variation of response within the energy range from 30 keV up to 1333 keV when a build-up cap is used for ^{60}Co gamma energies [12]. The R100 detector was also covered with 0.5 cm thick PMMA plate for ^{60}Co exposures in order to position the detector at the depth of maximum dose. The response for the detector per unit air kerma was normalized to the ^{60}Co readout value. Furthermore, the response of the detector was compared to the calculated ratio of the mass energy-absorption coefficients taken from the NIST database [11] of silicon to that of dry air in order to acquire a qualitative interpretation of the results.

To study the linearity of the detector signal with increasing air kerma, the detector was exposed to ^{60}Co gamma rays for the following air kerma values by varying the ^{60}Co irradiation time: 21; 41; 82 and 208 mGy. This range of air kerma represents the external exposures relevant for radiological protection of workers in both normal and accidental scenarios [13]. The response for each air kerma value was calculated as the average of five consecutive measurements. The reproducibility of the detector was calculated as the coefficients of variation (COV) of the five measurements for each exposure, i.e. the ratio of the standard deviation to their mean.

RESULTS AND DISCUSSION

Energy response, linearity and reproducibility

The detector response for the effective X-ray energies between 28.5 to 48.9 keV, in terms of collected charge, was normalized to that of ^{60}Co and is shown as a function of photon energy in Fig. 1. The response showed a weak dependence on the photon energy with a sensitivity that increases with decreasing photon energy. A peak region for the sensitivity is observed at the low energy photon range, with a maximum over-response of approximately 1.8 times at 48.9 keV relative to ^{60}Co. Other authors reported maximum sensitivities at photon energies in the range of approximately 30-50 keV for both energy-compensated and bare silicon detectors [14,15,16]. However, those

*Corresponding author: unal.oren@med.lu.se

studies resulted in over-responses in the range of 3.5-5 for energy-compensated silicon detectors when normalized to ^{60}Co, which is between a factor of approximately 2 - 3 times higher than observed for the R100 detector studied here. Also, the over-responses between low-photon energies (40 keV) and ^{60}Co of the unfiltered silicon detectors were as high as 7.5, which is a factor 4 times higher than observed for the R100 detecor

The dominant interaction of photons at lower energies is the photoelectric effect and this result in higher induced charge per unit kerma compared to high energies such as from those from ^{60}Co. The sensitivity for the Si-detector varies from 44 nC mGy^{-1} (28.5 keV) to 26 nC mGy^{-1} at ^{60}Co (1173 and 1333 keV), resulting in an over-response by a factor of 1.7 for the lowest energy (28.5 keV) relative to ^{60}Co. The energy response of the R100 is also approximately 4 times lower than the predicted response calculated based on the ratio of mass energy-absorption of silicon to that of dry air when the response is normalized to ^{60}Co. Thus, the expected over-response at low photon energies is reduced, due to the energy-compensating filter for the R100, compared to unfiltered silicon-based detectors and compared to the ratio of mass energy-absorption in silicon/dry air. The decrease in the response below 30 keV might be due to absorption of the photons in the cover layer of the detector material. If the energy response of the detector is known then a correction factor can be applied and a more accurate evaluation of the dose can be obtained if the photon energies of the source involved in a radiological incident differ from the energy used for calibration of the detector.

The observed sensitivity in terms of collected charge per unit air kerma for the R100 detector at ^{60}Co photon beams is also larger, compared to previously published results for unfiltered diodes where a sensitivity of approximately 1 nC mGy^{-1} has been reported [6]. This is mainly due to the much larger sensitive area of the R100 diode.

Fig. 2 represents the collected charge (nC) of the Si detector as a function of air kerma, when exposed to ^{60}Co gamma photons. Each point on the curve is the average of five measurements. The detector response was found to be linear, as expected, in the air kerma range studied with a correlation coefficient (R^2) equal to 1.0 of the linear fit. This behavior is in accordance with previously published results for silicon based detectors [17, 18].

In Table 1 the reproducibility of the R100 diode under ^{60}Co irradiation is displayed. The reproducibility test yielded coefficient of variations between 0.04% and 0.43% at ^{60}Co, indicating high degree of reproducibility and thus allowing accurate measurements of the dose levels.

This study presents some limitations, such as irradiation with other gamma sources emitting photons relevant for radiological protection, such as from ^{131}I and ^{137}Cs, and further investigations are necessary in order to better cover the entire investigated range of photon energies. Also, in order to obtain an even flatter energy response, the filter configuration could be optimized further in collaboration with the manufacturer.

The dose rate and angular dependence will also be examined since those are important parameters for dosemeters used for personal monitoring or in accidental scenarios. However, although the R100 is optimized for X-ray measurements in conventional radiology, it also appears promising for radiation protection purposes thanks to its energy-compensating filter, ability to detect high-energy photons such as those from ^{60}Co and real-time operation.

CONCLUSION

The feasibility of an energy-compensated X-ray detector, used for quality assurance in conventional diagnostic radiology, was investigated for radiation emergency purposes. The ability of detecting high-energy gamma photons such as from ^{60}Co opens up the application of the R100 to be used in radiation emergency scenarios. We believe that the R100 could be a suitable real-time dosemeter for measurements in radiation emergency situations, due to its linearity in the response and fairly weak energy dependence with a maximum of 1.8 times over-response per unit air kerma for X-ray energies (eff energy 48.9 keV) compared to photons from ^{60}Co. This means that a R100 unit in most relevant radiological and nuclear accident scenarios may provide gamma absorbed dose rates that are accurate within a factor of 2 regardless of the photon energy used for calibration.

FUNDING

This work was supported by the Swedish Radiation Safety Authority [Grant no SSM 2013-1436].

REFERENCES

1. Bolognese-Milsztajn, T., Ginjaume, M., Luszik-Bhadra, M., Vanhavere, F., Wahl, W., and Weeks, A. Active personal dosemeters for individual monitoring and other new developments. Radiat. Prot. Dosim. 112(1): 141-68 (2004)

2. AAPM. Diode in vivo dosimetry for patients receiving external beam radiation therapy. AAPM report no. 87. Report of AAPM Task Group 62 of the Radiation Threapy Committe. College Park, MD, USA (2005)

3. Herrnsdorf, L., Björk, M., Cederquist, B., Mattsson, C.G., Thungström, G. and Fröjdh, C. Point dose profile

measurements using solid-state detectors in characterization of computed tomography systems. Nucl. Instr. Meth. A. 607: 223-25 (2009)

4. Palm, Å., Nilsson, E. and Herrnsdorf L. Absorbed dose and dose rate using the Varian OBI 1.3 and 1.4 CBCT system. J. Appl. Clin. Med. Phys. 11: 3085 (2010)

5. Åsard, P.E. and Baarsen. G. Commercial photodiodes as gamma and roentgen ray dosimeters. Acta. Radiol. Ther. Phys. Biol. 7: 49-58 (1968)

6. Kaiser, F.J., Bassler, N. and Jäkel, O. COTS silicon diodes as radiation detectors in proton and heavy charged particle radiotheraphy 1. Radiat. Environ. Biophys. 49(3): 365-71 (2010)

7. Grusell, E. and Medin, J. General characteristics of the use of silicon diode detectors for clinical dosimetry in proton beams. Phys. Med. Biol. 45: 2573-82 (2000)

8. Gramsch, E., Lynn, K.G., Weber, M., DeChillo, B. and McWilliams, J.R. Silicon PIN photodetectors in high resolution nuclear spectroscopy. Nucl. Instr. And Meth. A. 311(3): 529-38 (1992)

9. Lindström, G., Moll, M. and Fretwurst, E. Radiation hardness of silicon detectors - challenge from high-energy physics Nucl. Inst. and Meth. A 426: 1-15 (1999)

10. Dixon, R. L. and Ekstrand, K. E. Silicon diode dosimetry. Int. J. Appl. Radiat. Isotop. 33: 1171-6 (1982)

11. Hubbell, J.H., Seltzer, S.M. Tables of X-Ray mass attenuation coefficients and mass energy-absorption coefficients (Version 1.4). National Institute of Standards and Technology, Gaithersburg, MD (online) Available. http://physics.nist.gov/xaamdi (2004).

12. Available at http://www.radcal.com/10x5-6-detail

13. SSMFS 2008:51 Strålsäkerhetsmyndighetens föreskrifter om grundläggande bestämmelser för skydd av arbetstagare och allmänhet vid verksamhet med joniserande strålning. 2009 (In Swedish) Available at www.stralsakerhetsmyndigheten.se

14. Rikner, G. and Grusell, E. Selective shielding of a p-Si detector for quality independence. Acta Radiol. Oncol. 24: 65-9 (1985)

15. Gilar, P. and Petro, I. Silicon photodiodes as a detector of exposure rate. Nucl. Instr. Meth. A. 234: 566-72 (1984)

16. Gager, L.D., Wright, A.E., Almond, P.R. Silicon diode detectors used in radiological physics measurements. Part I: Development of an energy compensating shield. Med. Phys. 4: 494-8 (1977)

17. Batista, E., Khoury, H.J., Melo, F.A., Barros, V. and da Silva, E.F Jr. The performance of commercial photodiodes for dosimetry in mammography. Radiat. Prot. Dosim. 115: 391-3 (2005)

18. Khoury, H.J., Hazin, C.A., Masccarenhas, P.A. and da Silva, Jr E.F. Low cost silicon photodiode for elelctron dosimetry. Radiat. Prot. Dosim. 84: 341-43 (1999)

Table 1. Reproducibility results for the R100 exposed to ^{60}Co. Mean, standard deviation (σ) and coefficient of variation (COV) for five repeated measurements at four different doses.

Air kerma (mGy)	Mean value (nC)	σ	COV (%)
21	5.3E+02	2.3E+00	4.3E-01
41	1.1E+03	2.5E+00	2.4E-01
82	2.1E+03	7.6E-01	3.6E-02
208	5.3E+03	7.2E+00	1.4E-01

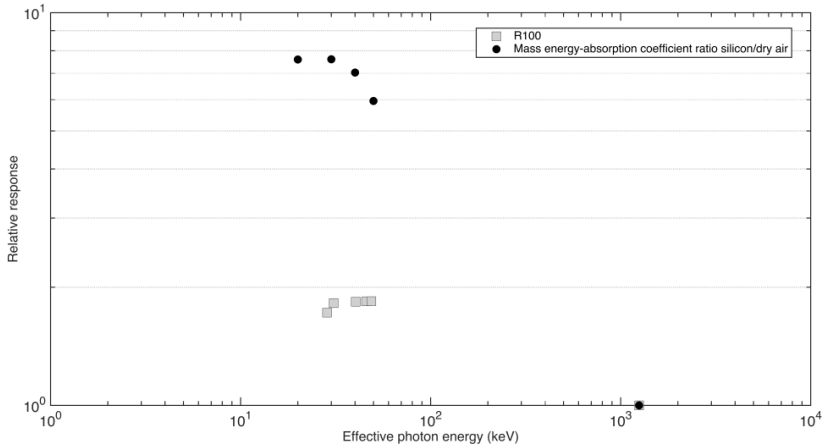

Figure 1. The relative energy response of the R00 detector normalized to the 1173 and 1333 keV photons (^{60}Co) as well as values for the ratio of the mass energy absorption coefficients in silicon to those of dry air.

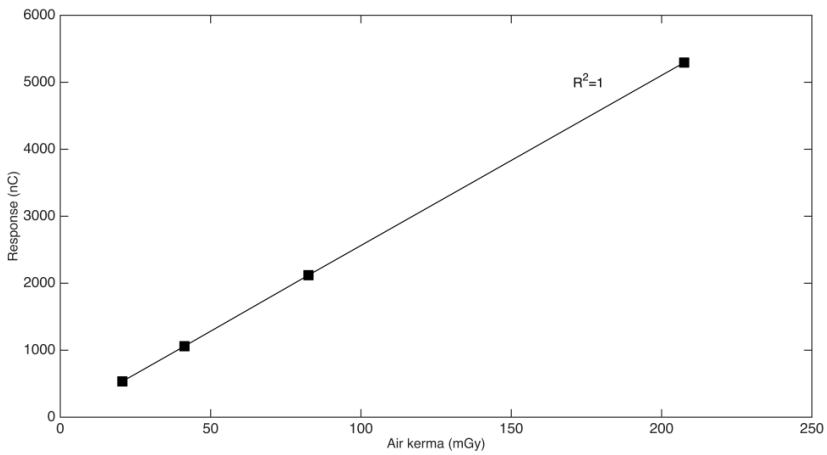

Figure 2. Response of the R100 detector versus air kerma for a ^{60}Co beam.

Paper III

SILICON DIODE AS AN ALPHA PARTICLE DETECTOR AND SPECTROMETER FOR DIRECT FIELD MEASUREMENTS

Ünal Ören, Jonas Nilsson, Lars Herrnsdorf, Christopher L. Rääf and Sören Mattsson

Radiation Protection Dosimetry (2016), Vol. 0, No. 0, pp. 0-0
DOI: 10.1093/rpd/nc0000

SILICON DIODE AS AN ALPHA PARTICLE DETECTOR AND SPECTROMETER FOR DIRECT FIELD MEASUREMENTS

Ünal Ören[1,*], Jonas Nilsson, Lars Herrnsdorf[1], Christopher L. rääf[1] and Sören Mattsson[1]
[1]Medical Radiation Physics, Department of Translational Medicine, Lund University, Skåne University Hospital, SE-205 02 Malmö, Sweden

Received month date year, amended month date year, accepted month date year

A windowless silicon (Si) diode (4 mm2) was evaluated as alpha particle detector and spectrometer for field measurements. It was irradiated with alpha particles from a ^{241}Am (2.3 kBq) and a ^{210}Po (9 kBq) source at source-detector distances (SDD) of 0.5, 1.0, and 1.8 cm. The energy resolution in terms of full width at half maximum (FWHM) was 281 keV, 148 keV, and 113 keV for SDD of 0.5, 1.0, and 1.8 cm, respectively. The minimum detectable activity increased from 0.08 Bq to 0.83 Bq when the SDD increased from 0.5 to 1.8 cm. The detector has the potential for several alpha spectrometric applications, such as monitoring for wound, skin, and surface contamination at nuclear fuel facilities, nuclear power plants, and facilities handling radioactive waste. Other areas are environmental surveys following releases of actinides at accidents in nuclear power plants and in connection with other radiological or nuclear scenarios.

INTRODUCTION

Following a nuclear or radiological accident or a deliberate dispersion of radioactive material, individuals could become contaminated with various radionuclides on their skin and in wounds. Alpha-emitting radionuclides are particularly hazardous, as they are difficult to detect and have large dose coefficients (Sv per Bq) for uptake through open wounds compared with gamma and beta emitters[1].

The principal monitoring instruments for alpha contamination are scintillation detectors, such as those based on zinc sulfide (ZnS[Ag]) and gas-filled detectors. A drawback of these devices is their inability to ascertain the energy distribution of the alpha particles. In particular, if the goal is to identify the contaminants as soon as possible in order to take appropriate measures, for example in the decontamination and cleaning of wounds, then spectrometric alpha particle measurements are required.

There have been only a few studies describing in situ alpha spectrometry, and these studies in most cases were performed under laboratory conditions in transportable laboratories equipped with evacuated chambers or canisters for the measurement of air filters[2-5]. These studies used field-portable prototype spectrometers based on silicon surface barrier detectors and ion-implanted planar silicon detectors. However, the constructed portable instruments were all intended for measurements on collected samples. A more rapid and direct method for identification and activity quantification is therefore needed for radiation emergency situations.

The aim of this study was to investigate the feasibility that a silicon (Si) solid state detector, available in hospitals in Sweden as well as in other countries and used for the control of computed tomography (CT) equipment, could be used as a portable handheld alpha particle spectrometer for field measurements under ambient conditions.

MATERIALS AND METHODS

Experimental setup

The detector is a silicon sensor, referred to here as a Si diode, which was originally fabricated for point dose profile measurements in computed tomography systems (CT Dose Profiler, RTI Electronics AB, Mölndal, Sweden)[6]. The Si diode had a thickness of 300 μm and an active area of 4 mm^2. It has also been applied as a directly readable dose meter for emergency radiation situations[7]. In that study, the author suggested the possibility it could be used to detect the higher photon energy ranges associated with nuclear or radiological emergencies, rather than the X-ray energies used in diagnostic radiology applications. It was also suggested that it might be feasible to detect alpha particles with the Si diode. The standard CT Dose Profiler was modified by the manufacturer to construct a shorter version (length 15 mm, diameter 12 mm). A hole (2.5 mm diameter) was milled in the package cap of the Si diode to uncover the radiation sensitive silicon and thus facilitate the detection of

*Corresponding author: unal.oren@med.lu.se

alpha particles. A BNC connector was attached to the Si diode to adapt the detector connection to a preamplifier (Canberra, Model 2003BT, Meriden, CT, USA) and a handheld digital multichannel analyzer (MCA, DigiDart™, Ortec, Oak Ridge, TN, USA) for a spectrometric evaluation (Figure 1). The Si diode was covered by 3 µm thick aluminum Mylar foil in order to protect it from contamination and ambient light. This enabled *in situ* measurements in a normal light environment. Commercial software (ORTEC, Gammavision 32 v-6.01) was used to analyze the MCA data. All measurements were performed at normal (ambient) air pressure and room temperature. No bias voltage was applied to the detector due to restrictions in the MCA for setting the low-level bias voltages usually applied to silicon diodes.

Detector response and energy resolution

Changes in energy resolution as a function of source-detector distance (SDD) were investigated for the Si diode. The detector was exposed to alpha particles from a 2.3 kBq ^{241}Am standard source from the National Institute for Standards and Technology (NIST; Gaithersburg, MD, USA) and had a circular active area of 33 mm^2. The ^{241}Am was electroplated onto a 0.16 mm thick platinum foil. ^{241}Am emits alpha particles with 5443 keV and 5486 keV energies and yields per decay of 0.13 and 0.845, respectively. A sequence of pulse height distributions were collected at the 0.5, 1.0, and 1.8 cm SDD, and the energy resolution of the alpha peaks was specified as full width at half maximum (FWHM) in terms of energy (keV). The data acquisition time was 100 s per measurement.

The detector response to alpha particles from a 9 kBq ^{210}Po source (E_α=5304 keV and yield per decay =1), originating from a static electricity elimination brush with dimensions 5 mm x 18 mm and coated with 3 µm Au, was also evaluated at the three distances.

Detection efficiency and minimum detectable activity

The detection efficiency (ε) for the Si diode and as a function of the source-detector distance was calculated by

$$\varepsilon(\%) = \frac{N}{A_\alpha \cdot t} \cdot 100 \quad (1)$$

where N and A_α are the total number of counts registered under the peak and the activity (in Bq) for a given radionuclide, respectively, and t is the measurement time (100 s). The 2.3 kBq ^{241}Am source was used for efficiency measurements of the 0.5, 1.0, and 1.8 cm SDD; thus, the efficiency values are valid for contamination areas comparable to the ^{241}Am source area (33 mm^2). The regions of interest (ROI) for the peaks were defined between channel numbers 11-142, 11-128, and 11-102 for the 0.5, 1.0, and 1.8 cm SDD, respectively.

The minimum detectable activity (MDA) of the particular source-detector geometries, expressed in Bq and defined at the 95% confidence level, was calculated by the following[8]:'

$$MDA=(2.71+4.65\sqrt{B})/t\varepsilon \quad (2)$$

where B is the number of background counts, t is the measurement time (100 s), and ε is the efficiency value obtained with the ^{241}Am source. Background measurement time of 11200 s was selected. MDA values were determined for all studied source-detector distances.

RESULTS

Detector response and energy resolution

Figure 2 shows the Si diode detector response after exposure to alpha particles from the ^{241}Am source at a 0.5 cm SDD for a 100 s measurement time, and compares it to the background measurement (acquired for 11200 s). A clear peak is observed, indicating that the miniature Si diode is capable of detecting and sorting the alpha particles by energy. The countrate in the background pulse height distribution below channel 10 are from electronic noise and the rest of the background pulse height distribution contains very few additional counts. Thus, it is possible to measure alpha particles in ambient air temperature and pressure during field operations using equipment available in most hospitals.

Figure 3 shows the pulse height distribution from the ^{241}Am and ^{210}Po sources at various distances using the Si diode. For ^{241}Am, the pulse height distribution exhibits a peak at channel 130 for 0.5 cm SDD with an energy resolution of 281 keV. At 1.0 cm and 1.8 cm, the resolution is 148 keV and 113 keV, respectively. For ^{210}Po a more pronounced broadening effect is observed, compared to the ^{241}Am source, due to interactions and energy loss of the alpha particles as they pass through the 3 µm thin gold protective foil of the source. Even at very small depths, the self-absorption causes both a peak shift in the channel axis as well as a broadening of the alpha peak due to a higher fraction of the ^{210}Po alphas being energy straggled in the metallic foil when reaching the detectors.

Detection efficiency and minimum detectable activity

Figure 4 shows the source-specific detection efficiency vs. source-detector distance for the Si diode irradiated with alpha particles from a 33 mm^2 area ^{241}Am source. The maximum efficiency for the Si diode was 1.0% at a source-detector distance of 0.5 cm, and it decreased to 0.1% at a distance of 1.8 cm.

The calculated MDA values for a 100 s measurement, specific to the particular source diameter (33 mm^2 area for the ^{241}Am source), were 0.08 Bq, 0.28 Bq, and 0.83 Bq at the 0.5, 1.0, and 1.8 cm SDD, respectively. These MDA values are applicable to measurements of shallow contamination spots and of sizes in the same order of magnitude as the investigated ^{241}Am source. MDA was also calculated in terms of Bq/cm^2 and these values were 0.24 Bq/cm^2, 0.85 Bq/cm2, and 2.5 Bq/cm^2 for the 0.5, 1.0, and 1.8 cm SDD, respectively.

DISCUSSION

A portable alpha spectrometer was tested by combining a handheld MCA with a Si diode for the spectrometric detection of alpha particles. The response and energy resolution of alpha particle detectors depend on parameters such as the SDD, the detector diameter, the thicknesses of the source and its protective cover, and the air pressure. The detector response in terms of number of counts per unit activity of the source decreased with increasing SDD, and the alpha particle peak channels also shifted to the lower side of the pulse height distribution.

The energy resolution improved as the air gap between the source and the detector increased. This was due to a larger fraction of the emitted alpha particles entering the detector perpendicularly at larger SDD. In contrast, the resolution was degraded as the SDD decreased due to the increased solid angle, as this results in a larger fraction of obliquely impinging alpha articles. This fraction of the particles is more energy degraded upon reaching the detector, and they also traverse a longer distance in the detector dead layer. This in turn causes more energy dispersion of the alpha particles and the subsequent broadening of the alpha peak in the spectrum. Thus, the energy resolution, in terms of the FWHM, was best (113 keV) at the longest SDD (1.8 cm). This is also consistent with other observations[9]. The energy resolution could also be improved using collimation of the detectors in order to account for the geometry factor, although this would be at the expense of decreased detection efficiency[5]. The asymmetric shape of the alpha peaks, with the characteristic tail on the lower energy side, was also due to the energy degradation of the alpha particles due to energy losses in the air gap between the source and the detector, in the source material, and in the detector dead layers.

The detection efficiency of the Si diode for irradiation by ^{241}Am alpha particles was very small due to the small detector surface. The maximum observed efficiency was 1.0% at the shortest measurement distance (0.5 cm SDD). The efficiency decreased with higher SDD values, which is why it was necessary to place the detector very close to the contaminated surface (area). The distance must, however, be relatively well defined for proper identification of the alpha emitter, since a variation in the air gap results in an alpha peak shift.

For 100 s measurements and a background measurement time of 11200 s, the MDA values were in the range of 0.08-0.83 Bq. Beginning with the shortest SDD at 0.5 cm, the MDA values increase as the SDD increases. The MDA is also dependent on the background measurement time, and lower MDA values can be achieved using longer counting times. However, a tradeoff is necessary between the higher detection efficiency obtained at a shorter measurement distance and the lower MDA occurring at the expense of a degraded resolution.

The National Council on Radiation Protection (NCRP) states that, for skin contamination by alpha emitters, intervention is advisable when the levels are >100 Bq/cm^2 and is required when the levels exceed 1000 Bq/cm^2[10]. The derived MDA values for the portable detector system using the Si diode (0.24-2.5 Bq/cm^2 for 0.5-1.8 cm SDD) indicate that it is possible to detect activities far below the aforementioned intervention levels.

The rapid and straightforward method described in this study could have several alpha spectrometric applications, such as monitoring for wound, skin, or surface contamination at nuclear fuel facilities, nuclear power plants, and facilities handling radioactive waste. Other areas are environmental surveys following the release of actinides from accidents at nuclear power plants and other radiological or nuclear scenarios.

CONCLUSION

The capability of alpha spectrometry using a portable system based on a Si diode, available in hospital departments, was examined. It was demonstrated that in situ alpha spectrometric measurements are possible under ambient air pressure and temperature. The best energy resolution (113 keV) was achieved at 1.8 cm SDD. The detection efficiency of the small Si diode was 1.0% at 0.5 cm SDD for a ^{241}Am disk-shaped source (33 mm^2), with an MDA of 0.08 Bq. The detector would be useful in radiation surveys following nuclear or radiological events where individuals and

surfaces have been contaminated with alpha-emitting radionuclides.

FUNDING

This work was supported by the Swedish Radiation Safety Authority [grant number SSM2013-5381].

ACKNOWLEDGEMENTS

The authors express their thanks to Urban Albinsson at RTI Electronics, Mölndal, Sweden, for the CAD design and adaption of a BNC connector for the shorter version of the CT Dose Profiler, enabling connection to an MCA. The authors also thank Göran Thungström (at Mid Sweden University and MidDec Scandinavia AB, Sundsvall, Sweden) for manufacturing the shorter CT Dose Profiler version.

REFERENCES

1. Spencer, D. and Smith, D. Practical system to detect and assess consequences of radioactivity in a wound. Radiat. Prot. Dosim. 105(1–4), 463-465 (2003)

2. Lidström, K. and Tjärnhage, Å. A method for field measurements using alpha-spectrometry. Journal of Radioanal. and Nucl. Chem. 248(3), 555-60 (2001)

3. Martín Sánchez, A. and de la Torre Pérez, J. Portable alpha spectrometer. Appl. Radiat. and Isotopes 70, 2267-2269 (2012)

4. Pöllänen, R., Peräjärvi, K., Siiskonen, and Turunen, T. In-situ alpha spectrometry from air filters at ambient air pressure. Radiat. Measurements 53-54, 65-70 (2013)

5. Pöllänen, R., Peräjärvi, K., Siiskonen, T. and Turunen, J. High-resolution alpha spectrometry at ambient pressure-towards new applications. Nucl. Inst. and Methods A 694, 173-78 (2012)

6. L. Herrnsdorf, M. Björk, B. Cederquist, C.G. Mattsson, G. Thungström, and C. Fröjdh, Point dose profile measurements using solid-state detectors in characterization of computed tomography systems. Nuclear Instruments and Methods A 607, 223-25 (2009)

7. Herrnsdorf, L. A directly readable personal dosemeter for radiation emergency situations-a design approach. In:Proc. Int. Conf. Medical Physics in the Baltic States 2012 (Ed. By D. Adlienė), Technologija, Kaunas, Lithuania

8. Currie, L.A. Limits for qualitative detection and quantitative determination. Application to radiochemistry. Analytical Chemistry 40(3) 586-93 (1968)

9. Vaninblat, N., Pelled, O., German, U., Haquin, G., Tshuva, A, and Alfassi, Z.B. Determination of parameters relevant to alpha spectrometry when employing source coating. Appl. Radiat. and Isotopes 61 307-11 (2004)

10. National Council on Radiation Protection and Measurement. Management of persons contaminated with radionuclides. NCRP Report No. 161. Bethesda, Md, USA: National Council on Radiation Protection and Measurement; (2009)

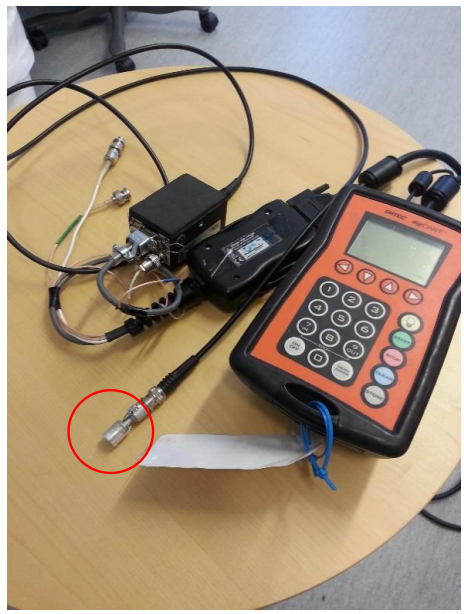

Figure1. The 4 mm^2 Si diode, indicated by a circle, connected to a charge-sensitive preamplifier (2003BT) and a digital portable multichannel analyzer (DigiDart™).

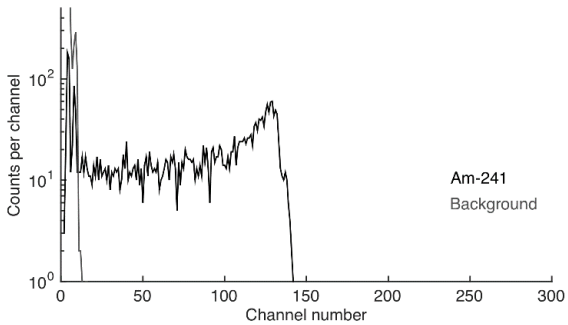

Figure 2. Pulse height distribution for a ^{241}Am (E_α= 5486 and 5443 keV) source measured with the Si diode at 0.5 cm SDD, compared to a background measurement (N.B. – a logarithmic y-axis).

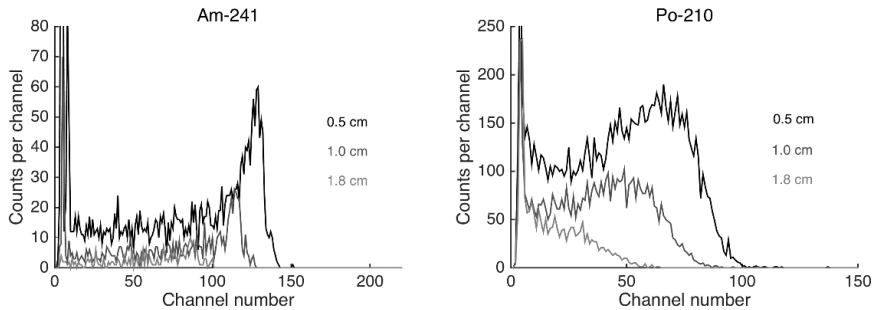

Figure 3. Pulse height distribution measured with the Si diode for a ^{241}Am source (E_α= 5486 and 5443 keV) (left) and a ^{210}Po (E_α= 5304 keV) (right) at three different distances: 0.5, 1.0, and 1.8 cm.

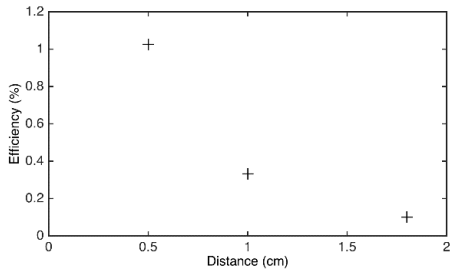

Figure 4. The efficiency of the Si diode versus the source-detector distance for the ^{241}Am source (33 mm^2).

Paper IV

IOP Publishing | Society for Radiological Protection Journal of Radiological Protection

J. Radiol. Prot. **34** (2014) 231–247 doi:10.1088/0952-4746/34/1/231

Detection of radioactive fragments in patients after radiological or nuclear emergencies using computed tomography and digital radiography

Ü Ören, M Hansson, S Mattsson and C L Rääf

Medical Radiation Physics, Department of Clinical Sciences Malmö, Lund University, Skåne University Hospital, SE-205 02 Malmö, Sweden

E-mail: unal.oren@med.lu.se

Received 24 July 2013, in final form 18 November 2013
Accepted for publication 20 December 2013
Published 24 February 2014

Abstract

A comparison has been carried out between standard-dose computed tomography, non-diagnostic computed tomography and digital radiography with respect to their suitability for detecting radioactive fragments associated with nuclear or radiological events such as debris from radiological dispersal devices. The purpose was to investigate if radiographic imaging is justified for the detection and localisation of radioactive fragments in affected patients.

Fragments of uranium (U), copper (Cu), iron (Fe) and volcanic ash with effective diameters ranging from (approximately) 100 to 700 μm were selected. The fragments were positioned at two different locations on an anatomical torso phantom and images were produced with standard-dose CT, non-diagnostic CT and digital radiography. Capsules with radionuclides of ^{137}Cs, ^{60}Co and ^{99m}Tc were also positioned in the phantom and the effective doses were estimated for radionuclide exposures as well as for standard-dose CT, non-diagnostic CT and digital radiography. For standard-dose CT and digital radiography, U, Cu and Fe fragments were detected in sizes down to 100–180, 250–300 and 300–400 μm respectively. For the non-diagnostic CT the results were 180–250 μm (for U), 300–400 μm (for Cu) and 400–500 μm (for Fe). The effective dose from the standard-dose CT, non-diagnostic CT and digital radiography was 5.6, 1.9 and 0.76 mSv. Corresponding doses from ^{137}Co, ^{60}Co and ^{99m}Tc positioned at the site of fragments were in the range of 0.07–0.1, 0.32–0.45 and 0.08–0.09 mSv per MBq during 24 h. We conclude that, for a number of gamma emitters with activity levels on the order of magnitude of megabecquerel, imaging using ionising radiation can be justified since the effective dose from the radionuclides will exceed the dose from the radiological examination.

1. Introduction

A significant fraction of the radioactive material released as a consequence of nuclear weapons testing or nuclear power plant accidents, such as the Chernobyl and Fukushima events, is associated with highly radioactive particles or fragments, commonly referred to as hot particles. These radioactive fragments present potential health hazards with different risk profiles compared to a uniform exposure, leading to less predictable outcomes in terms of radiation effects (Pöllänen 2002).

Another scenario which may result in a substantial dispersion of radioactive substances is an antagonistic event where radioactive material is dispersed deliberately, e.g. through a detonation of a radiological dispersal device (RDD). In such a scenario, small metallic particle fragments included in the explosives could be contaminated with radionuclides. These contaminated fragments could penetrate the skin and also be embedded in critical human organs and soft tissues. Metallic fragments are in some cases difficult to surgically retrieve, and are thus sometimes left in the human body because the removal procedure could be laborious, destructive of surrounding tissues and scarring may occur (Kane *et al* 2009). In such a situation, the trade-off between intervention or not, is further complicated by competing issues of the radiation dose received from the imaging modality and the radiation dose associated with letting the radioactive fragment remain in the tissue. In general, surgery is not indicated in most cases where patients are harboring non-radioactive foreign metallic fragments, because metals often remain inert and do not cause damage (Benjaminov *et al* 2006). A reason for surgical retrieval could however be the possible radiological effects (Koenig *et al* 2005, Rojas-Palma *et al* 2009) or chemical toxicity of the embedded material (Eylon *et al* 2005). An accurate detection, localisation and characterisation of a radioactive fragment would thus be crucial in the surgical management of the injury.

It has previously been reported that the size of radioactive particles associated with nuclear events is log-normally distributed, resulting in a few large particles carrying most of the activity (Shevchenko 2004). There is no clear definition of hot particles regarding the size, activity and composition but the United States National Council on Radiation Protection and Measurements (NCRP 1999) states that hot particles are 'larger than 10 μm but smaller than 3000 μm in any dimension'. They further state that hot particles smaller than 10 μm may be treated as general contamination. Charles and Harisson (2007) state that particles of diameters up to 10 μm can be inhaled. Other publications state that particles of sizes even up to 200 μm can be inhaled (Dale *et al* 2008). In addition, particles may also contaminate the skin or enter the body following inadvertent ingestion, resulting in possible radiation damage to the alimentary tract (Charles and Harisson 2007). Another exposure pathway is by deliberate poisoning of food or by the hand-to-mouth route.

Residual fragments in patients have been imaged by conventional radiography, computed tomography (CT), sonography, angiography and fluoroscopy (Sosna *et al* 2005, Mosheiff *et al* 2004, Benjaminov *et al* 2006) and fragments removed from wounds have been characterised using scanning electron microscopy combined with energy-dispersive x-ray analysis (SEM-EDXA) and infra red spectroscopy (IR) (Maggio *et al* 2008). Factors such as material composition, size, location and available imaging techniques determine the possibility of detecting embedded radioactive fragments.

Results from several previous studies have shown that imaging techniques such as single-photon emission computed tomography (SPECT) scanners and gamma cameras could be of value for emergency purposes where measurements of internal contamination are necessary (Hansson and Rääf 2011, Wallström *et al* 1998). Imaging modalities such as CT and digital radiography in hospitals could potentially also be a part of the hospital's disaster

Table 1. Fragments used in this study.

	Fragment material			
	Volcanic ash	Fe	Cu	U
Density (g cm^{-3})	2.65	7.87	8.96	19.1
Sieve aperture size range (μm)		700–500		
		500–400		
		400–300		
		300–250		
		250–180		
		180–100		

preparedness for patient management in the event of radiological or nuclear emergencies, where rapid measurements of internal contamination are required and when radioactive fragments have been inhaled, ingested or penetrated human tissue or organs. An initial survey of the patient for possible contamination could be made with hand instruments, whole-body counters or the above-mentioned techniques. This is followed by nuclide identification, activity estimation and a subsequent dose assessment is made in order to determine appropriate treatments.

The aim of this study was to examine whether it, from a radiation risk perspective, is justified to use imaging techniques utilising ionising radiation to detect radioactive fragments. This was done by (i) determining the effective dose needed from the imaging modality to detect fragments of different sizes and densities and (ii) to compare this dose level with the effective dose from radioactive point sources simulating radioactive fragments. This in turn enables establishment of the relationship between the effective dose from the imaging modality and the averted dose if a surgical extraction of a radioactive fragment is carried out.

2. Material and methods

2.1. Fragments

A set of nonradioactive fragments, surrogates of radioactive material, of different densities and sizes have been used to evaluate the visibility in the studied imaging modalities and to assess the detectable minimum size of the particles. The fragment material is summarised in table 1. The copper (Cu) and iron (Fe) specimens were obtained from a wire by rasping appropriate size fragments. The volcanic ash particles, selected in order to represent dispersible low-density particles, originated from the 2010 eruptions of the Eyjafjallajökull volcano, Iceland, and consisted mainly of silicon dioxide (SiO_2), (Gislason *et al* 2011). The uranium (^{238}U) metal fragments were chosen due to their high density and they were obtained from the Department of Nuclear Physics, Lund University. The samples were sieved, to retain particle size distributions in intervals from over 700 μm down to about 100 μm, through squared mesh sieves with 200 mm cartridges. The range of the sieve aperture sizes expressed in μm is specified in table 1. Radioactive fragments and particles reported in the literature show a wide spectrum in size, varying from mm down to several μm (Lang *et al* 1995, Aragon *et al* 2008, Salbu 2011). Analysis of military personnel injured in a combat environment by foreign entities originating from explosives, shows that the particle sizes vary from a diameter <1 mm to cross sections of 12×14 mm^2, with the most common type of material being metals (Thach *et al* 2005).

2.2. Imaging and quantitative analysis

The ability of a standard-dose CT (Somatom Definition AS+, Siemens, Erlangen, Germany), non-diagnostic CT (SPECT/CT, Symbia Truepoint, Siemens, Erlangen, Germany) and digital

radiography (A-196, Varian Medical Systems, USA) to detect fragments has been evaluated using an Alderson–Rando nuclear medicine thorax phantom (Radiology Support Devices, Long Beach, CA, USA). The phantom is equivalent to an average male adult and consists of components simulating anatomical structures (two lungs, liver, chest bones and the spinal cord) within the phantom with the corresponding attenuation properties. The phantom was filled with water to produce tissue attenuation and the fragments, positioned 1 cm apart from each other, were placed at two different locations at the phantom to represent an individual that is contaminated with radioactive material in the lungs and in the abdomen. First, the fragments were placed on the inner surface in the abdomen region of the Alderson–Rando phantom. This was done in order to represent a bomb survivor with penetrated objects in his/her body. Injury profiles of surviving terror attack victims show that the main body regions injured severely are the skin, thorax, abdomen, head and the limbs (Aharonson-Daniel *et al* 2006), where the main effect is penetrating trauma caused by flying bomb fragments such as shrapnel and other metallic objects that have been incorporated in the explosive, for instance nails, screws, and bolts (Sosna *et al* 2005). The second position of the fragments were on the costal surface of the right lung of the phantom in order to mimic a deep penetrating or inhalation scenario, although it is unlikely that high-density particles reach the lungs via the respiratory tract.

The size threshold for detection of fragments was estimated by imaging a line of varying sized particles with a series of tube voltage and tube load combinations. First, conventional standard-dose CT scans of the phantom were performed, containing the above-mentioned material. The standard dose was selected because a desired image quality can be achieved by increasing the milliampere-second (mAs) settings. The tube potential was set at 100, 120 and 140 kVp and for each fixed tube potential various effective mAs settings (defined as tube current-time product/pitch by Siemens Medical Solutions) were applied. Second, non-diagnostic CT imaging was performed using the 2-slice CT unit of the hybrid SPECT/CT (Symbia Truepoint, Siemens, Erlangen, Germany). Image acquisition parameters for the non-diagnostic CT were a tube potential of 130 kVp and a tube load of 17 mAs, which are the default settings for the non-diagnostic CT protocol currently used at the clinic (SUS Malmö). The classification as a non-diagnostic CT is due to the restraints regarding scanning parameters such as the tube current-time product, and there are also no requirements regarding the image quality. The field of view was 50×50 cm^2 and a matrix of 512×512 pixels was used for both standard-dose CT and non-diagnostic CT. Next, digital radiography (A-196, Varian Medical Systems, USA) imaging of the phantom was performed with different tube voltages (70, 90, 110 and 130 kVp) in combination with various tube loads (10, 20, 40, 80, 160 mAs). Anterior–posterior (AP) images of the phantom placed in the supine position were obtained and the measurements were done at a 110 cm source-to-detector distance with a 43×43 cm^2 field size. The volume CT dose index ($CTDI_{vol}$(mGy)) and dose–area product (DAP (mGy cm^2)) values were recorded from the equipment user interface after each exposure. The specific examination protocol parameters used for the imaging modalities are shown in table 2.

A quantitative assessment of the detection threshold (DT) for fragments was performed and a fragment was flagged, for a 95% confidence level, as detectable if the mean pixel value of the fragment was more than $3.29\sigma_\mu$ over the mean of the background, where σ_μ is the standard deviation of the mean of the background pixel value (Hsieh 2009). For a 0.05 significance level the critical value is 1.645 and the means of two distributions would be separated by 3.29 standard deviations of the measured means.

Measurements were made by placing circular regions of interest (ROIs) on the axial images encompassing the fragments. For CT imaging, the ROIs measured approximately 4 mm^2 for

Table 2. Acquisition parameters used for the 2-slice non-diagnostic CT, the conventional standard-dose 64-slice CT, and for the digital radiography system

	Non-diagnostic CT	Standard-dose CT	Digital radiography
Scan parameters (units)			
Tube voltage (kVp)	130	100, 120, 140	70, 90, 110, 130
Effective mAs (CT) and mAs (DR)	17	90, 120, 150, 180, 210, 230	10, 20, 40, 80, 160
Scan time (s)	96	3.5	
Slice (mm)	1.0	0.6	
Rotation time (s)	0.8	0.5	
Pitch	1.5	1.2	

the fragments and 107 mm^2 for the phantom background (taken from homogeneous parts of the phantom containing neither tissue boundaries nor metal fragments) and the mean pixel values ($\pm$SD) were recorded. For digital radiography, the ROIs for the fragments and background measurements were 0.1 and 0.9 mm^2 respectively. The ROIs, with a constant shape and size, were placed in identical locations for each series of images and detection thresholds were calculated for each set of scanning parameters, since the detection threshold would vary with the tube potential and tube load. The mean pixel values of the fragments (MPV_{frag}) were compared with the detection threshold by means of their quotient, MPV_{frag}/DT, i.e. fragments with a quotient higher than unity were considered as detectable. All image processing was performed utilising ImageJ (http://rsb.info.nih.gov/ij/).

2.3. Radiation dose measurements

2.3.1. Radiological imaging dose measurements. Lithium fluoride thermoluminescent dosemeters, LiF:Mg, Ti (Harshaw TLD-100, Thermo Fisher Scientific Inc, Erlangen, Germany), with dimensions of $3.2 \times 3.2 \times 0.9$ mm^3, were used to record the absorbed dose required to detect the fragments in the Alderson–Rando phantom by the different imaging modalities. For each procedure, two batches with twenty TLDs in each batch were used. The individual sensitivity of each TLD was determined by irradiations to known absorbed doses from a ^{60}Co gamma ray source, with a calibration traceable to the Secondary Standards Laboratory at the Swedish Radiation Safety Authority. Four reference TLDs from each batch were set aside and irradiated from the same source to obtain calibration coefficients and two TLDs from each batch were used to correct for background radiation. The additional 28 TLDs were used for absorbed dose measurements with the different imaging modalities. They were individually encased in plastic (polyvinyl chloride) bags, labeled and distributed throughout the Alderson–Rando phantom with two dosemeters for each anatomical position (figure 1). The TLDs were evaluated within 24 h after radiation exposure following a standard protocol as outlined elsewhere (Davis *et al* 2006) and using a TLD reader (Harshaw 5500, Gammadata Bycron NE, Wermelskirchen, Germany).

From the protocols in table 2, the combination of tube voltage and tube load which optimised detection of the fragments and which resulted in the lowest $CTDI_{vol}$ and DAP values, were chosen for the TLD measurements. Energy correction factors, accounting for the difference between the TLD response in the calibration beam quality and measurement beam quality, were applied. The uncertainty of the TLD measurements is estimated to about 3%.

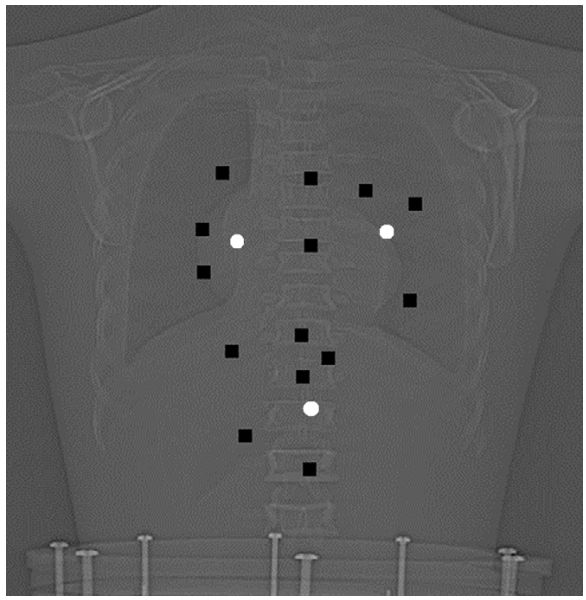

Figure 1. A CT scout radiography of the Alderson–Rando phantom showing the approximate locations of the TLDs (indicated as black squares) and the radionuclide positions (indicated as white circles).

2.3.2. Radionuclide dose measurements. The radioactive fragment geometries of the Alderson–Rando phantom were also mimicked using gamma-emitting point sources of ^{137}Cs (γ energy [E_γ] 662 keV; physical half-life [$t_{1/2}$] 30.2 y), ^{60}Co (γ energy [E_γ] 1173 and 1333 keV; half-life [$t_{1/2}$] 5.27 y) and ^{99m}Tc (γ energy [E_γ] 141 keV; half-life [$t_{1/2}$] 6.01 h). The radionuclides, covering a broad range of photon energies and commonly available in research departments and hospitals, were selected on the basis of their interest in radiological or nuclear emergency situations. The ^{137}Cs (31.7 MBq) and ^{60}Co (15.5 MBq) sources were encapsulated in nipple screws of stainless steel with a 3 mm thickness. For ^{99m}Tc (97 MBq), a sphere with a diameter of 15 mm was filled with a solution of ^{99m}Tc-pretechnetate and the activity was measured using an activity meter (CRC-15R, Capintec Inc, Ramsey, NJ, USA).

The TLDs were positioned at the same locations as at the aforementioned measurements with two TLDs at each position. In addition, the radionuclides were also placed on the surface of the torso in order to mimic skin deposition (figure 1). The absorbed dose due to the gamma radiation from the radionuclides was measured using TLDs, where each experiment was repeated for a specific radionuclide. The irradiation time for the radionuclides was 24 h and the subsequent TL-reading procedure was the same as for the radiographic imaging of the phantom. For organs where measurements were not possible, for example such as the salivary glands, brain and prostate, the dose was calculated from dose attenuation in water derived from the TLDs at different distances from the source, as described elsewhere (Van Laere *et al* 2000). For the imaging modality and radionuclide exposures the equivalent organ doses were calculated using the absorbed doses and radiation weighting coefficients as defined by ICRP publication 103 (ICRP 2007) and the effective dose values were estimated.

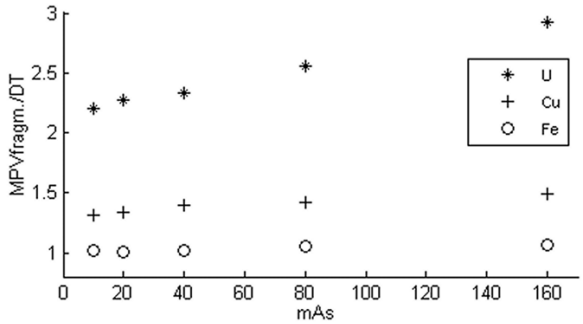

Figure 2. Graph shows the MPV_{frag}/DT quotient versus tube load for a fixed tube potential of 90 kVp for digital radiography and for fragment sizes in the range of 500–700 μm positioned on the right lung.

3. Results

3.1. Imaging and quantitative analysis

The detection threshold for fragments, in terms of mean-pixel Hounsfield numbers and with a 95% confidence level, has been evaluated for a standard-dose CT, and a non-diagnostic CT. The numbers in the tables are expressed as MPV_{frag}/DT, where the detection threshold (DT) is defined as $3.2\sigma_{bkg}$ from the mean of the background, as described in the previous section. A summary of the results for fragments of different size and atomic composition positioned at the lung and inner abdomen surface are shown for the standard-dose CT (table 3). The metallic fragments were detected at all tube potentials and the detection threshold was 100–180, 250–300 and 300–400 μm for U, Cu and Fe respectively for the standard-dose CT. The standard-dose CT failed to detect Cu and Fe fragments below these sizes with increased tube load.

The result of this work shows that for lung and abdominal positioning of the fragments using the tube voltage and effective tube load combination of kVp = 100 and eff. mAs = 180 resulted in the smallest detectable fragments at lowest dose (in terms of $CTDI_{vol}$). Therefore these scanning parameters were chosen when performing absorbed dose measurements with TLDs for the standard-dose CT.

Table 4 summarises the results for the measurements for the default acquisition parameters for the non-diagnostic CT. The results show that U, Cu and Fe fragments were detectable in the range of 180–250, 300–400 and 400–500 μm respectively. Below these levels the fragments are indistinguishable from the background and these observations indicate that smaller fragments would be missed in non-diagnostic CT imaging.

For digital radiography, the detection thresholds were determined to be 100–180 μm for U fragments and 300–400 μm for Cu and Fe fragments at the right lung (table 5). The results suggest that for the abdomen position, the detection threshold was similar for U and Cu. For Fe, fragments 400–500 μm in size were detected at the inner abdomen surface.

The effects of varying the tube load on the MPV_{frag}/DT quotient are shown in figure 2. For a fixed tube potential (90 kVp) and fragment sizes (500–700), the detection of the different material is improved with increasing material density and increasing tube load.

Overall for all the positions, a 20 mAs tube load and 90 kVp tube potential resulted in the detection of the smallest fragments at lowest dose levels. These exposure parameters

Table 3. Mean pixel value normalised to the image specific background pixel value (MVP_{frag}/DT) for fragments embedded in an Alderson phantom for the standard-dose CT. The results are at 100, 120 and 140 kVp and fragments flagged as detected by the quantitative analysis are indicated in shaded fields.

Right lung												
	U			Cu			Fe			Ash		
kVp	100	120	140	100	120	140	100	120	140	100	120	140
eff. mAs	180	210	230	180	210	230	180	210	230	180	210	230
$CTDI_{vol}$ (mGy)	6.99	14.12	23.60	6.99	14.12	23.60	6.99	14.12	23.60	6.99	14.12	23.60
Size												
700–500	24.91	33.30	39.99	8.35	10.67	10.48	6.47	7.05	8.22	0.52	0.44	0.26
500–400	13.75	18.64	22.27	3.15	3.59	3.66	2.32	2.85	3.18	0.36	0.18	0.39
400–300	6.41	8.78	10.00	1.28	2.05	2.01	1.10	1.00	1.01	0.07	0.02	0.00
300–250	3.50	4.18	5.22	1.24	1.19	1.27	0.40	0.38	0.55	0.14	0.37	0.57
250–180	2.56	3.46	3.77	0.88	0.65	0.86	0.35	0.24	0.11	0.24	0.54	0.30
180–100	1.03	1.72	1.60	0.48	0.66	0.20	0.22	0.19	0.51	0.05	0.37	0.12
Inner abdomen												
	U			Cu			Fe			Ash		
kVp	100	120	140	100	120	140	100	120	140	100	120	140
eff. mAs	180	230	210	180	230	210	180	230	210	180	230	210
$CTDI_{vol}$ (mGy)	6.99	15.47	21.54	6.99	15.47	21.54	6.99	15.47	21.54	6.99	15.47	21.54
Size												
700–500	18.41	23.55	24.20	14..02	16..90	15..05	4..33	4..65	4..44	0.44	0.22	0.00
500–400	16.01	19.73	19.33	3.99	5.21	4.31	3.33	2.92	3.22	0.34	0.12	0.30
400–300	8.71	10.67	10.14	2.15	2.51	2.54	1.40	1.22	1.08	0.03	0.08	0.21
300–250	3.68	4.39	4.41	1.64	1.18	1.94	0.67	0.66	0.51	0.23	0.32	0.37
250–180	1.64	2.06	1.90	0.77	0.94	0.69	0.48	0.41	0.34	0.25	0.18	0.12
180–100	1.01	1.42	1.26	0.52	0.64	0.31	0.32	0.13	0.29	0.16	0.19	0.23

were therefore used in the subsequent TLD measurements of the absorbed dose for digital radiography.

Neither computed tomography nor digital radiography were capable of detecting the ash fragments.

3.1.1. Radiological imaging dose measurements. Absorbed doses generated by the imaging modalities were recorded with TLDs and the scanning parameters were derived from the protocols mentioned before. On the basis of the lowest measured $CTDI_{vol}$ (6.99 mGy), in combination with the smallest detected fragments, the following scanning protocol was chosen for dose measurements for the standard-dose CT; a tube potential of 100 kVp and 180 eff. mAs, scan time 3.5 s, rotation time 0.5 s, slice thickness 0.6 mm. For measurements with the non-diagnostic CT the scanning parameters were; eff. mAs = 17, kV = 130, scan time = 96 s, rotation time of 0.8 s and a slice thickness of 1 mm, resulting in a $CTDI_{vol}$ of 1.45 mGy. For digital radiography, the Alderson–Rando phantom equipped with the TLD chips was irradiated at 20 mAs and 90 kVp, yielding a DAP of 1732 mGy cm^2. The equivalent organ and effective doses for the imaging modalities are given in detail in table 6. The relationship between the effective dose from the imaging modalities and smallest detected fragment types positioned in the inner abdomen region is indicated in figure 3. The effective doses required for detection

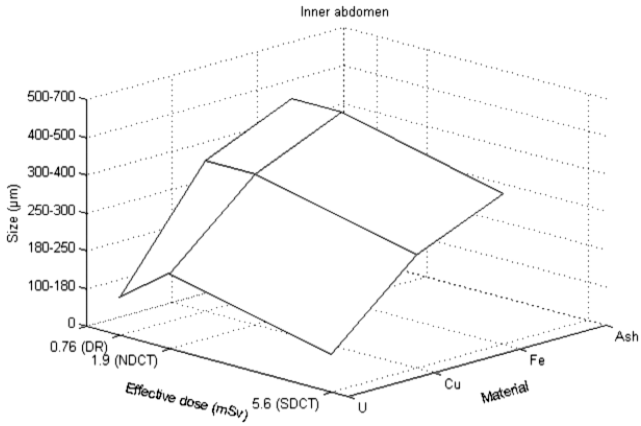

Figure 3. The relationship between the smallest fragments detected and the effective doses from digital radiography (DR), non-diagnostic CT (NDCT) and standard-dose CT (SDCT).

Table 4. As in table 3 but for non-diagnostic CT. Detected fragments are indicated in shaded fields.

	U	Cu	Fe	Ash
Right lung				
kVp	130	130	130	130
eff. mAs	17	17	17	17
$CTDI_{vol}$ (mGy)	1.45	1.45	1.45	1.45
Size				
700–500	11.43	3.48	1.32	0.12
500–400	8.24	1.35	1.19	0.14
400–300	2.91	1.14	0.69	0.17
300–250	2.03	0.62	0.56	0.03
250–180	1.73	0.53	0.41	0.18
180–100	0.72	0.39	0.25	0.17
Inner abdomen				
kVp	130	130	130	130
eff. mAs	17	17	17	17
$CTDI_{vol}$ (mGy)	1.45	1.45	1.45	1.45
Size				
700–500	12.66	4.40	2.29	0.11
500–400	4.16	1.67	1.05	0.00
400–300	2.73	1.29	0.70	0.01
300–250	1.86	0.81	0.43	0.23
250–180	1.75	0.62	0.39	0.07
180–100	0.78	0.44	0.33	0.15

of the smallest fragments for the standard-dose CT was 5.6 mSv, approximately seven times higher than for digital radiography, where the effective dose was 0.76 mSv. Non-diagnostic CT resulted in an effective of 1.9 mSv. The equivalent organ doses from the standard-dose and non-diagnostic CT examinations were also higher than those from digital radiography, as illustrated in table 6. For example, the equivalent lung doses from standard-dose CT and

Table 5. As in table 3 but for digital radiography where the detected fragments are indicated in shaded fields.

	U				Cu				Fe				Ash			
Right lung																
kVp	70	90	110	130	70	90	110	130	70	90	110	130	70	90	110	130
mAs	20	10	10	10	10	10	10	10	10	10	10	10	20	10	10	10
DAP (mGy cm^2)	1055	876	1241	1652	533	876	1241	1652	533	876	1241	1652	1055	876	1241	1652
Size																
700–500	2.71	2.20	1.86	1.71	1.58	1.32	1.23	1.13	1.25	1.11	1.02	1.04	0.88	0.87	0.86	0.84
500–400	1.86	1.59	1.52	1.40	1.32	1.25	1.17	1.08	1.23	1.02	1.02	1.03	0.86	0.79	0.82	0.85
400–300	1.88	1.54	1.42	1.22	1.27	1.23	1.24	1.08	1.07	1.05	1.05	1.02	0.85	0.90	0.91	0.94
300–250	1.25	1.15	1.09	1.06	0.79	0.83	0.86	0.86	0.93	0.94	0.94	0.93	0.76	0.81	0.77	0.81
250–180	1.49	1.40	1.21	1.16	0.82	0.86	0.84	0.87	0.88	0.87	0.94	0.94	0.79	0.82	0.91	0.93
180–100	1.00	1.03	1.01	1.02	0.93	0.93	0.97	0.98	0.79	0.78	0.88	0.84	0.82	0.92	0.90	0.93
Inner abdomen																
kVp	70	90	110	130	70	90	110	130	70	90	110	130	70	90	110	130
mAs	160	20	40	40	40	20	20	20	40	20	10	10	160	20	40	40
DAP (mGy cm^2)	8392	1732	4842	6289	2103	1732	1241	1652	2103	1732	1241	1652	8392	1732	4842	6289
Size																
700–500	1.60	1.39	1.38	1.36	1.21	1.12	1.11	1.10	1.10	1.08	1.05	1.05	0.91	0.90	0.94	0.95
500–400	1.55	1.31	1.29	1.23	1.04	1.02	1.02	1.00	1.02	1.03	1.01	1.00	0.87	0.91	0.91	0.94
400–300	1.38	1.23	1.22	1.21	1.01	1.01	1.01	1.02	0.88	0.99	0.95	0.93	0.93	0.93	0.96	0.96
300–250	1.25	1.11	1.13	1.11	0.91	0.92	0.94	0.93	0.92	0.93	0.93	0.94	0.93	0.94	0.97	0.97
250–180	1.10	1.01	1.06	1.02	0.88	0.93	0.94	0.95	0.86	0.92	0.89	0.92	0.93	0.93	0.95	0.96
180–100	1.01	1.00	1.01	1.02	0.89	0.92	0.94	0.95	0.86	0.90	0.92	0.96	0.92	0.88	0.92	0.94

non-diagnostic CT were 8.8 and 2.7 mSv, whereas the dose from digital radiography was 1.1 mSv.

3.2. Radionuclide dose measurements

The organ equivalent and effective doses for the point sources are reported in mSv per MBq for the first 24 h (mSv MBq^{-1} d^{-1}). The results are displayed in table 6. For a ^{137}Cs source, with an activity of 31.7 MBq and placed at the right lung, the equivalent organ doses ranged from 0.008 to 0.33 mSv MBq^{-1} d^{-1}. The highest equivalent organ dose (0.33 mSv MBq^{-1} d^{-1}) was delivered to the lung followed by the liver (0.13 mSv MBq^{-1} d^{-1}). The estimated effective dose was 0.07 mSv MBq^{-1} d^{-1}. For the^{137}Cs-source placed in the inner abdomen surface region the effective dose was 0.08 mSv MBq^{-1} d^{-1}. The liver received the highest equivalent organ dose (0.5 mSv MBq^{-1} d^{-1}), followed by the stomach (0.21 mSv MBq^{-1} d^{-1}). For source position on the left breast surface the highest equivalent organ dose was received by the breast (0.63 mSv MBq^{-1} d^{-1}) followed by the skin (0.2 mSv MBq^{-1} d^{-1}). The effective dose was 0.1 mSv MBq^{-1} d^{-1}. The effective doses for ^{60}Co placed at the lung, inner abdomen surface and on the breast were 0.32, 0.42, 0.45 mSv MBq^{-1} d^{-1} respectively. When the ^{60}Co source was positioned at the lung the equivalent dose was 1.3 mSv MBq^{-1} d^{-1} for the lung followed by 0.52 mSv MBq^{-1} d^{-1} received by the liver. The dose to the liver was 3.3 mSv MBq^{-1} d^{-1} and a stomach dose of 0.95 mSv MBq^{-1} d^{-1} was noted when the ^{60}Co source was placed in the abdomen region. For the breast surface position, the equivalent breast dose was 2 mSv MBq^{-1} d^{-1} whereas the skin received 0.67 mSv MBq^{-1} d^{-1}. The associated effective dose for ^{99m}Tc was 0.008, 0.009 and 0.009 mSv MBq^{-1} d^{-1} for the lung, inner abdomen surface and breast positions respectively. Maximum equivalent organ doses were 0.33 (lungs), 0.059 (liver) and 0.052 mSv MBq^{-1} d^{-1} (breast) at the corresponding positions.

For ^{137}Cs and ^{60}Co the highest effective doses were estimated when the radionuclides were placed on the skin whereas for ^{99m}Tc the effective dose was highest at the abdomen position.

4. Discussion

4.1. Imaging and quantitative analysis

The result of this work demonstrates that the standard-dose CT and digital radiography are superior to non-diagnostic CT in the detection of embedded fragments, allowing sub-millimeter visualisation of high-density particles. In general for digital radiography and standard-dose CT, the quantitative analysis revealed that the quotient between the mean pixel values for the fragments and the detection threshold, MPV_{fragm}/DT, decreased as expected with decreasing fragment size.

Although not plotted for all the various tube voltage and tube load combinations, for a given tube potential, the MVP_{frag}/DT quotient increased with increasing tube load. This is illustrated in figure 2 for digital radiography and for U, Cu and Fe fragments in the size range of 500–700 μm positioned on the right lung. This was more pronounced for U fragments, followed by Cu, due to the increase in mean pixel values with increased density of the fragment, and as a consequence of reduction of the quantum noise with increased dose.

Figure 3 was plotted to compare the detection ability of the imaging modalities with respect to material type and size. It shows, as expected, that there is a clear tendency for all the imaging modalities that smaller fragments can be detected as the material density increases. These results indicate that the factors affecting the detection of fragments in human subjects are not only size but also the composition of the material.

Table 6. Equivalent organ and effective doses (E) in millisievert (mSv) estimated using TLDs when the phantom was imaged by the standard-dose CT, non-diagnostic CT and digital radiography. In addition are given values for equivalent and effective dose values per megabecquerel and day (mSv MBq d^{-1}) for the organs using radionuclides of ^{137}Cs, ^{60}Co and ^{99m}Tc placed (i) on the mediastinal part of the right lung (ii) on the inner surface of the abdomen and (iii) on the breast surface of the phantom.

	Imaging modalities			Point sources								
				Tc-99m			Cs137			Co60		
	SDCT	NDCT	DR	Right lung	Inner abdomen	Breast surface	Right lung	Inner abdomen	Breast surface	Right lung	Inner abdomen	Breast surface
Organs												
Gonads	0.0×10^{0}	0.0×10^{0}	0.0×10^{0}	5.3×10^{-4}	1.1×10^{-3}	1.5×10^{-5}	4.0×10^{-3}	8.6×10^{-3}	1.5×10^{-4}	2.7×10^{-2}	5.3×10^{-2}	8.3×10^{-4}
Red bone marrow	8.2×10^{0}	2.3×10^{0}	3.7×10^{-1}	6.2×10^{-3}	1.1×10^{-2}	1.5×10^{-3}	3.6×10^{-2}	8.7×10^{-2}	1.4×10^{-2}	2.2×10^{-1}	3.8×10^{-1}	7.0×10^{-2}
Lung	8.8×10^{0}	2.7×10^{0}	1.1×10^{0}	3.3×10^{-2}	2.8×10^{-3}	7.0×10^{-3}	3.3×10^{-1}	2.7×10^{-2}	8.5×10^{-2}	1.3×10^{0}	1.3×10^{-1}	4.6×10^{-1}
Colon	9.3×10^{-1}	5.9×10^{-1}	2.0×10^{-1}	1.5×10^{-3}	5.7×10^{-3}	1.3×10^{-3}	1.2×10^{-2}	4.9×10^{-2}	1.1×10^{-2}	7.4×10^{-2}	2.6×10^{-1}	6.4×10^{-2}
Stomach	2.0×10^{0}	1.2×10^{0}	2.2×10^{-2}	3.1×10^{-3}	2.2×10^{-2}	1.2×10^{-3}	2.5×10^{-2}	2.1×10^{-1}	1.3×10^{-2}	1.4×10^{-1}	9.5×10^{-1}	7.3×10^{-2}
Breast	1.1×10^{1}	4.8×10^{0}	2.7×10^{0}	4.2×10^{-3}	1.3×10^{-3}	5.2×10^{-2}	4.1×10^{-2}	1.9×10^{-2}	6.3×10^{-1}	2.6×10^{-1}	1.0×10^{-1}	2.0×10^{0}
Bladder	0.0×10^{0}	0.0×10^{0}	0.0×10^{0}	7.0×10^{-4}	1.8×10^{-3}	3.3×10^{-5}	5.3×10^{-3}	1.4×10^{-2}	3.4×10^{-4}	3.5×10^{-2}	8.4×10^{-2}	1.9×10^{-3}
Liver	1.1×10^{1}	3.3×10^{0}	1.3×10^{0}	1.5×10^{-2}	5.9×10^{-2}	2.9×10^{-3}	1.3×10^{-1}	5.0×10^{-1}	3.2×10^{-2}	5.2×10^{-1}	3.3×10^{0}	1.6×10^{-1}
Esophagus	1.1×10^{1}	3.0×10^{0}	1.4×10^{0}	6.4×10^{-3}	1.5×10^{-3}	4.5×10^{-3}	5.5×10^{-2}	1.2×10^{-2}	4.8×10^{-2}	2.9×10^{-1}	7.1×10^{-2}	2.7×10^{-1}
Thyroid	1.5×10^{-2}	0.0×10^{0}	0.0×10^{0}	2.2×10^{-3}	1.1×10^{-3}	2.6×10^{-3}	2.1×10^{-2}	8.2×10^{-3}	2.3×10^{-2}	1.2×10^{-1}	5.1×10^{-2}	1.3×10^{-1}
Skin	1.1×10^{1}	3.8×10^{0}	1.7×10^{0}	6.6×10^{-3}	4.4×10^{-3}	1.6×10^{-2}	6.9×10^{-2}	6.1×10^{-2}	1.8×10^{-1}	3.4×10^{-1}	3.1×10^{-1}	6.7×10^{-1}
Bone surface	8.2×10^{0}	2.3×10^{0}	3.7×10^{-1}	6.2×10^{-3}	1.1×10^{-2}	1.5×10^{-3}	3.6×10^{-2}	8.7×10^{-2}	1.4×10^{-2}	2.2×10^{-1}	3.8×10^{-1}	7.0×10^{-2}
Brain	0.0×10^{0}	0.0×10^{0}	0.0×10^{0}	9.9×10^{-4}	4.8×10^{-4}	4.0×10^{-4}	7.7×10^{-3}	3.6×10^{-3}	4.2×10^{-3}	4.8×10^{-2}	2.4×10^{-2}	2.3×10^{-2}
Salivary glands	0.0×10^{0}	0.0×10^{0}	0.0×10^{0}	2.1×10^{-3}	8.7×10^{-4}	1.6×10^{-3}	1.7×10^{-2}	6.7×10^{-3}	1.7×10^{-2}	1.0×10^{-1}	4.2×10^{-2}	9.4×10^{-2}
Remainder	4.8×10^{0}	1.4×10^{0}	5.2×10^{-1}	5.8×10^{-3}	1.0×10^{-2}	2.8×10^{-3}	5.3×10^{-2}	9.6×10^{-2}	3.0×10^{-2}	2.6×10^{-1}	4.5×10^{-1}	1.7×10^{-1}
E	5.6×10^{0}	1.9×10^{0}	7.6×10^{-1}	7.7×10^{-3}	9.2×10^{-3}	9.0×10^{-3}	7.0×10^{-2}	8.2×10^{-2}	1.0×10^{-1}	3.2×10^{-1}	4.3×10^{-1}	4.5×10^{-1}

The results in this work (see tables 3–5) match previous published studies where detection of metal fragments down to sizes of 0.5–1.00 mm have been reported (Lakits *et al* 2000, Dass *et al* 2001). Other studies found threshold volumes of 0.048 and 0.07 mm^3 (corresponding to a diameter of 0.36 and 0.4 mm respectively) for metallic foreign entities (Chacko *et al* 1997, Otto *et al* 1992).

Concerning the anatomical positions of the fragments in the Alderson–Rando phantom, the standard-dose CT provides information about the precise localisation of the fragments. In digital radiography on the other hand, determination of the fragment position is more difficult because the technique creates a two-dimensional image of a three-dimensional volume. This is shown in table 5, where the detection of the 400–500 μm Fe fragment in the abdomen region, in contrast to the lung position, fails since its appearance is obstructed due to the radiopaque spinal cord background at that particular position. Moreover the detectability is influenced by overlaying tissue (anatomical noise). Other authors have suggested that detectability in digital radiography is more affected by the anatomical background than the quantum noise (Brettle *et al* 2007, Båth *et al* 2005) and that this is more pronounced for digital radiography than for CT (Månsson *et al* 2005). However, an additional radiographic lateral projection of the concerned volume would facilitate the visualisation of the fragment in three dimensions.

The drawback of using the standard-dose CT is the higher radiation doses compared to digital radiography. Further optimisation of the CT scanning parameters such as rotation time, scanning length and beam collimation could be done with respect to the radiation dose. Another drawback with the standard-dose CT is the image artifacts generated by high-density fragments that could obscure smaller particles that otherwise would be detectable. A possibility to overcome this problem could be to use cone-beam computed tomography (CBCT) or dual-energy computed tomography (DECT) which are associated with lower metal artifacts than a conventional CT (Von See *et al* 2009, Zhang *et al* 2007, Bamberg *et al* 2011).

The advantages of the standard-dose CT over the non-diagnostic CT include superior detectability and shorter acquisition times. Besides poorer detection capability, longer imaging times associated with the nondiagnostic CT are more likely to introduce patient motion artifacts, resulting in a degraded image quality and potentially blurring smaller objects that would have otherwise been detected.

The volcano ash particles, due to their low attenuation, were not detectable with any of the imaging techniques used in this study. If the fragment, such as ash, has attenuation properties close to the surrounding material, it cannot be easily differentiated from the background structures and may remain undetected. The failure of computed tomography and digital radiography to detect potentially highly radioactive low-density fragments that would require prompt surgical removal could lead to potential health hazards. Thus, non-radiopaque material in the size range as in this study may remain undetected and the limitations of the imaging modalities used must be considered given that dispersible low-density particles were not detectable. Other imaging modalities that have proved successful in detecting radiolucent foreign bodies, such as ultrasonography (Aras *et al* 2010) and, if metallic composition of the foreign entity has been ruled out, magnetic resonance imaging (LoBue *et al* 1988) may be needed in such cases. Ultrasonography may, however, fail to detect non-superficial fragments (embedded deeper than 2 cm) due to the range of ultrasound waves (Turkcuer *et al* 2006).

In case of a radiation disaster scenario where individuals are internally contaminated or injured by contaminated fragments, we propose that a pilot digital radiography should be the first imaging technique of choice in evaluating patients at an initial stage. The reason for this is: (i) the radiation dose required to detect the fragments is smaller compared to the standard-dose CT, (ii) the sizes of dirty bomb fragments are likely to be greater than those in this study of

minimum detectable fragments and (iii) the availability of digital radiography units are higher and the cost lower than of CTs.

4.2. Dose measurements

The mSv MBq^{-1} per day factors in table 6 are based on radionuclides located in specific body sites, resulting in a nonhomogenous exposure. The values enable us to assess the effective doses for internally and externally deposited radioactive material following nuclear or radiological events. For ^{60}Co placed in the right lung, inner abdomen region and left breast surface, the 5.6 mSv effective dose from the standard-dose CT equates to a 24 h exposure with activity levels of 18, 13 and 12 MBq respectively. The effective dose from the non-diagnostic CT (1.9 mSv) and digital radiography (0.76 mSv), corresponds to activity levels in the range of 4–6 MBq and 1.7–2.4 MBq for the different ^{60}Co positions. For ^{137}Cs and for a 24 h exposure it takes 56–80 MBq to reach the 5.6 mSv levels of the standard-dose CT, depending on the radionuclide position. To equal the effective dose levels of non-diagnostic CT and digital radiography the activities of ^{137}Cs are in the range of 19–27 MBq and 8–11 MBq respectively.

The organ equivalent and effective doses are affected by various factors such as distance from the radiation source and attenuation of photons inside the body, with closest organs receiving the highest doses. The exposures within the phantom are lower for low-energy gamma emitters due to higher attenuation coefficients in water, such as (0.15 cm^{-1}) for 141 keV γ rays of ^{99m}Tc compared to the penetrating gamma rays from ^{60}Co (0.07 cm^{-1}) and ^{137}Cs (0.09 cm^{-1}). The dose is reduced rapidly with increasing distance from the source due to the inverse square law and attenuation in the phantom. The effect seen, in general, for gamma-emitting radionuclides is that higher penetrating gamma rays deliver higher doses to distant organs compared to radionuclides emitting low-energy photons, since an increase in photon energy decreases the probability of a photoelectric effect.

According to IAEA and for patients internally contaminated with ^{137}Cs, medical treatment is recommended if the activity exceeds 5 MBq (IAEA 1994). For comparison, the action level for internal contamination specified by the TMT Handbook at 24 h for ingestion and inhalation (Type S) of ^{60}Co are 42 MBq and 5 MBq respectively. The action levels for ^{137}Cs and specified at 24 h, are set to 18 MBq (inhalation, Type F) and 15 MBq (ingestion) (Rojas-Palma *et al* 2009). Other authors state that treatments for internal contaminations less than one annual limit of intake for ^{137}Cs (7.4 MBq from inhalation and 3.7 MBq from ingestion) is not indicated (Koenig *et al* 2005).

The ICRP recommends an annual effective dose limit of 1 mSv for members of the public, a level that equates, for ^{137}Cs fragments positioned at the different locations in this study, to an annual exposure with activity levels in the range of 27–39 kBq. For ^{60}Co the corresponding levels are 6–9 kBq. Other available data suggest that for a whole-body activity in the range of 20–50 kBq for ^{137}Cs equals an effective dose less than 1 mSv (Rahola *et al* 2006). However, considering the negligible cancer risk at an effective dose of 1 mSv, it would not be justified to utilise radiological examinations resulting in additional effective doses exceeding 1 mSv.

Emergency response plans state that radioactive fragments should be removed as soon as possible (Rojas-Palma *et al* 2009), while another study states the potential future health problems should be taken in account when dealing with embedded radioactive fragments and considering a treatment strategy (Edmond and Kalinich 2012). Besides the associated radiation exposure, depending on the half-life, type and amount of the radioactive material, the potential chemical toxicity of the fragments has to be taken into consideration.

In this work, the effective doses from the imaging modalities are comparable to those from relatively high-energy gamma-emitting radionuclides with activity levels >MBq. The effective

dose from such a source would clearly outweigh the effective dose from an radiographic examination within days. To avoid unnecessary exposure from radioactive fragments deposited in human subjects, surgical removal would be justified and imaging systems utilising ionising radiation would be of benefit for the patient's health with respect to averted dose if the fragment is excised.

5. Conclusion

The detection limits have been demonstrated for different small fragments using various imaging modalities. This study concludes that standard-dose CT and digital radiography are reliable methods and equal in sensitivity regarding detection of metallic fragments. They have the potential to be useful tools, used by emergency clinicians to detect and locate high-density fragments, down to sizes in the range of 100–180 μm. The material type, size and location affects the detection ability of the imaging modalities. The particle position can be identified easier with the standard-dose CT for a removal if decided so by the clinical surgeon. However, digital radiography requires a lower radiation dose in order to detect the same fragment size and should be considered as a first alternative for localising radioactive fragments *in vivo*, since standard-dose CT is accompanied by a higher effective dose. The associated effective dose from radiographic imaging is low enough to justify the procedure in view of the anticipated dose from, if not removed, high-energy gamma-emitting radioactive fragments with activities above MBq levels. The results obtained from the study can be applied in emergency situations where individuals have been contaminated with radioactive fragments originating from radiological or nuclear events.

Acknowledgment

This work was supported by the Swedish Radiation Safety Authority (grant no SSM 2009/4591).

References

Aharonson-Daniel L, Klein Y, Peleg K and ITG 2006 Suicide bombers form a new injury profile *Ann. Surg.* **244** 1018–23

Aragon A, Espinosa A, De la Cruz B and Fernandez J A 2008 Characterization of radioactive particles from the Palomares accident *J. Environ. Radioact.* **99** 1061–7

Aras M H, Miloglu O, Barutcugil C, Kantarci M, Ozcan E and Harorli A 2010 Comparison of the sensitivity for detecting foreign bodies among conventional plain radiography, computed tomography and ultrasonography *Dentomaxillofac. Radiol.* **39** 72–8

Bamberg F, Dierks A, Nikolaou K, Reiser M F, Becker C R and Johnson T R C 2011 Metal artifact reduction by dual energy computed tomography using monoenergetic extrapolation *Eur. Radiol.* **21** 1424–9

Båth M, Håkansson M, Börjesson S, Hoeschen C, Tischenko O, Kheddache S, Vikgren J and Månsson L G 2005 Nodule detection in digital chest radiography: effect of anatomical noise *Radiat. Prot. Dosim.* **114** 109–13

Benjaminov O, Sklair-Levy M, Rivkind A, Cohen M, Gabi B and Stein M 2006 Role of radiology in evaluation of terror attack victims *Am. J. Roentgenol.* **187** 609–16

Brettle D S, Berry E and Smith M A 2007 The effect of experience on detectability in local area anatomical noise *Br. J. Radiol.* **80** 186–93

Chacko J G, Figueroa R E, Johnson M H, Marcus D M and Brooks S E 1997 Detection and localization of steel intraocular foreign bodies using computed tomography. A comparison of helical and conventional axial scanning *Ophthalmology* **104** 319–23

Charles M W and Harisson J D 2007 Hot particle dosimetry and radiobiology—past and present *J. Radiol. Prot.* **27** 97–109

Dale P, Robertson I and Toner M 2008 Radioactive particles in dose assessments *J. Environ. Radioact.* **99** 1589–95

Dass A B, Ferrone P J, Chu Y R, Esposito M and Gray L 2001 Sensitivity of spiral computed tomography scanning for detecting intraocular foreign bodies *Ophthalmology* **108** 2326–8

Davis S D, Ross C K, Mobit P N, Van der Zwan L, Chase W J and Shortt K R 2006 The response of LiF thermoluminescence dosemeters to photon beams in the energy range from 30 kV x rays to ^{60}Co gamma rays *Radiat. Prot. Dosim.* **106** 33–43

Edmond C A and Kalinich J F 2012 Biokinetics of embedded surrogate radiological dispersal device material *Health Phys.* **102** 124–36

Eylon S, Mosheiff R, Liebergall M., Wolf E, Brocke L and Peyser A 2005 Delayed reaction to shrapnel retained in soft injury *Injury* **36** 275–81

Gislason S R *et al* 2011 Characterization of Eyjafjallajökull volcanic ash particles and a protocol for rapid risk assessment *Proc. Natl Acad. Sci. USA* **108** 7307–12

Hansson M and Rääf L R 2011 Visualisation and quantification of lung content of radionuclides associated with nuclear and radiological emergencies *Radiat. Prot. Dosim.* **145** 341–50

Hsieh J 2009 *Computed Tomography Principles, Design, Artifacts* (Bellingham, WA: SPIE Optical Engineering Press) pp 158–9 (Hoboken, NJ: Wiley)

ICRP 2007 Recommendations of the International Commission on Radiological Protection *ICRP Publication 103*; *Ann. ICRP* **37**

IAEA 1994 Rapid monitoring of large groups of internally contaminated people following a radiation accident *IAEA-TECDOC-746* (Vienna: IAEA)

Kane M A, Kasper C E and Kalinich J F 2009 Protocol for the assessment of potential health effects from embedded metal fragments *Mil. Med.* **174** 265–9

Koenig K L, Goans R E, Hatchett R J, Mettler F A Jr, Schumacher T A, Noji E K and Jarett D G 2005 Medical treatment of radiological casualties: current concepts *Ann. Emerg. Med.* **45** 643–52

Lang S, Servomaa K and Rytömaa T 1995 Biokinetics of nuclear fuel compounds and biological effects of nonuniform radiation *Environ. Health. Perspect.* **103** 920–34

Lakits A, Prokesch R, Scholda C, Nowotny R, Kaider A and Bankier A 2000 Helical and conventional CT in the imaging of metallic foreign bodies in the orbit *Acta Ophthalmol. Scand.* **78** 79–83

LoBue T D, Deutsch T A, Lobick J and Turner D A 1988 Detection and localization of nonmetallic intraocular foreign bodies by magnetic resonance imaging *Arch. Ophthalmol.* **106** 260–1

Maggio K L, Kalasinsky V F, Lewin-Smith M R and Mullick F G 2008 Wound fragments from cutaneous sites of US Military personel deployed in operation Iraqi Freedom: clinical aspects and pathologic characetrizations *Dermatol. Surg.* **34** 475–82

Mosheiff R, Weil Y, Khoury A and Liebergall M 2004 The use of computerized navigation in the treatment of gunshot and shrapnel injury *Comput. Aided Surg.* **9** 39–43

Månsson L G, Båth M and Mattsson S 2005 Priorities in optimisation of medical x-ray imaging—a contribution to a debate *Radiat. Prot. Dosim.* **114** 298–302

NCRP 1999 *Biological Effects and Exposure Limits for 'Hot Particles'* Recommendations of the National Council on Radiation Protection and Measurements *NCRP Report 130* (Bethseda, MD: NCRP)

Otto P M, Otto R A, Virapongse C, Friedman S M, Emerson S, Li K C, Malot R, Kaude J V and Staab E V 1992 Screening test for detection of metallic foreign objects in the orbit before magnetic resonance imaging *Invest. Radiol.* **27** 308–11

Pöllänen R 2002 Nuclear fuel particles in the environment—characteristics, atmospheric transport and skin doses *Academic Dissertation* Helsinki, Finland STUK-A188

Radiology Support Devices, (RSD) 1904 East Domingez Street, Long Beach, CA 90810, USA. www.rsdphantoms.com/nm_heart.htm

Rahola T, Muikku M, Falk R, Johansson J, Liland A and Thorshaug S 2006 Assessment of internal doses in emergency situations *Report NKS-128* Roskilde, Denmark (available at www.nks.org)

Rojas-Palma C, Liland A, Jerstad A N, Etherington G, Pérez M R, Rahola T and Smith K 2009 *TMT Handbook—Triage, Monitoring and Treatment of People in the Event of Malevolent Use of Radiation* (Österås, Norway: Norwegian Radiation Protection Authority) (available at www.tmthandbook.org)

Salbu B 2011 Radionuclides released to the environment following nuclear events *Integr. Environ. Assess. Manag.* **7** 362–4

Shevchenko S V 2004 On the uncertainty in activity measurements for samples containing 'hot particles' *Appl. Radiat. Isot.* **61** 1303–6

Sosna J, Sella T, Shaham D, Shapira C. S, Rivkind A, Bloom A I and Libson E 2005 Facing the new threats of terrorism: radiologists' perspectives based on experience in Israel *Radiology* **237** 28–36

Thach A B, Ward T P, Dick J S 2nd, Bauman W C, Madigan W P Jr, Goff M J and Thordsen J E 2005 Intraocular foreign body injuries during operation Iraqi freedom *Ophthalmology* **112** 1829–33

Turkcuer I, Atilla R, Topacoglu H, Yanturali S, Kiyan S, Kabakci N, Bozkurt S and Cevik A A 2006 Do we really need plain and soft-tissue radiographies to detect radiolucent foreign bodies in the ED? *Am. J. Emerg. Med.* **24** 763–8

Van Laere K, Koole M, Kauppinen T, Monsieurs M, Bouwens L and Dierck R 2000 Nonuniform transmission in brain SPECT using ^{201}Tl, ^{153}Gd, and ^{99m}Tc static line sources: anthropomorphic dosimetry studies and influence on brain quantification *J. Nucl. Med.* **41** 2051–62

Von See C, Bormann K H, Schumann F, Goets F, Gellrich N C and Rücker M 2009 Forensic imaging of projectiles using cone-beam computed tomography *Forensic Sci. Int.* **190** 38–41

Wallström E, Alpsten M and Mattsson S 1998 A gamma camera for measurements of internal contamination after a radiological accident *J. Radiol. Prot.* **19** 143–54

Zhang Y, Zhang L, Zhu X R, Lee A K, Chambers M and Dong L 2007 Reducing metal artifacts in cone-beam CT images by preprocessing projection data *Int. J. Radiat. Oncol. Biol. Phys.* **67** 924–32

Paper V

A phantom for determination of calibration coefficients and minimum detectable activities using a dual head gamma camera for internal contamination monitoring following radiation emergency situations

Ünal Ören, Martin Andersson, Christopher L. Rääf and Sören Mattsson

This is a pre-copyedited, author-produced PDF of an article accepted for publication in Radiation Protection Dosimetry following peer review. The version of record [*Ünal Ören, Martin Andersson, Christopher L. Rääf and Sören Mattsson* ***A PHANTOM FOR DETERMINATION OF CALIBRATION COEFFICIENTS AND MINIMUM DETECTABLE ACTIVITIES USING A DUAL-HEAD GAMMA CAMERA FOR INTERNAL CONTAMINATION MONITORING FOLLOWING RADIATION EMERGENCY SITUATIONS.*** *Radiat Prot Dosimetry. 2016 Jun;169(1-4):297-302.* First published online: January 13, 2016] is available online at: http://rpd.oxfordjournals.org/content/169/1-4/297

Radiation Protection Dosimetry (year), Vol. 0, No. 0, pp. 0–0
DOI: 10.1093/rpd/nc0000

A PHANTOM FOR DETERMINATION OF CALIBRATION COEFFICIENTS AND MINIMUM DETECTABLE ACTIVITIES USING A DUAL HEAD GAMMA CAMERA FOR INTERNAL CONTAMINATION MONITORING FOLLOWING RADIATION EMERGENCY SITUATIONS

Ünal Ören, Martin Andersson, Christopher L. Rääf and Sören Mattsson

Received month date year, amended month date year, accepted month date year

The purpose of this study was to derive calibration coefficients (in terms of cps kBq^{-1}) and minimum detectable activities, MDA, (in terms of kBq and corresponding dose rate) for the dual head gamma camera part of a SPECT/CT-instrument when used for *in-vivo* internal contamination measurements in radiation emergency situations.

A cylindrical-conical PMMA-phantom with diameters in the range of 7-30 cm was developed in order to simulate different body parts and individuals of different sizes. A series of planar gamma camera investigations were conducted using a SPECT/CT modality with the collimators removed for ^{131}I and ^{137}Cs; radionuclides potentially associated with radiation emergencies. Energy windows of 337-391 keV and 490-690 keV were selected for ^{131}I and ^{137}Cs respectively.

The measurements show that the calibration coefficients for ^{137}Cs range from 10 to 19 cps kBq^{-1} with MDA values in the range of 0.29 kBq to 0.55 kBq for phantom diameters of 10-30 cm. The corresponding values for ^{131}I are 12 to 37 cps kBq^{-1} with MDA values of 0.08 to 0.26 kBq.

An internal dosimetry computer program was used for the estimation of minimum detectable dose rates. A thyroid uptake of 0.1 kBq ^{131}I (representing MDA) corresponds to an effective dose rate of 0.6 µSv/day. A ^{137}Cs source position representing the colon with a MDA of 0.55 kBq corresponds to an effective dose rate of 1 µSv/year.

This method using a simple phantom for the determination of calibration coefficients and MDA levels can be implemented within the emergency preparedness plans in hospitals with nuclear medicine departments. The derived data will help to quickly estimate the internal contamination of humans following radiation emergencies.

INTRODUCTION

The radioactive fallout associated with nuclear accidents, as those in Fukushima and Chernobyl, could lead to internal contamination of humans with gamma-emitting fission products such as ^{131}I and ^{137}Cs. The radionuclide ^{131}I is important considering short-term exposure whereas ^{137}Cs is of concern from a long-term perspective[1]. Humans could also be exposed to radiation from similar gamma emitting radionuclides (fission and neutron activation products) in other scenarios such as antagonistic events where radioactive material is dispersed deliberately or accidents such as that in Goiana in 1987[2,3,4]. Early detection of internal contamination following nuclear or radiological events is crucial in order to take appropriate countermeasures. Rapid examinations for screening purposes are thus needed when internal contamination is suspected in individuals. Low-background level whole body counters (WBC) are normally used for individual monitoring of internal contamination. However, whole body counters are rarely found in most hospitals and the lack of availability limits the throughput of individuals when rapid measurements are required for a large number of people. Other methods such as in vitro monitoring, i.e. analysis of urine, faeces, teeth, hair, nails, saliva and blood, are also time consuming and special laboratories for sample preparation are required. On the other hand, nuclear medicine gamma cameras and hybrid instruments such as single photon emission computed tomography/computed tomography (SPECT/CT) are available at most hospitals with nuclear medicine departments and could be implemented in radiation emergency plans. Gamma cameras and SPECT/CTs are designed for diagnostic purposes and they are therefore optimized and calibrated for radionuclides such as ^{99m}Tc and ^{123}I.

The potential of gamma cameras has been previously recognized for radiation emergency applications[5,6,7]. However, studies with different body sizes and body parts are rare. Wallström et al.[6] determined calibration coefficients and minimum detectable activities (MDA) using homogenous solutions for different body sizes whereas Hansson and Rääf[7] used both homogenous solutions and point sources. However, the latter study was mainly aimed for acute lung uptakes.

The aim of this study is to provide general calibration coefficients and determine the MDA values, for ^{131}I and ^{137}Cs when using dual–headed gamma cameras in a SPECT/CT-instrument and for different body sizes ranging from 10-30 cm in diameter. The results would therefore enable more generalized calibration data for various organ uptakes.

MATERIALS AND METHODS

Phantoms

An in-house developed PMMA (polymethyl methacrylate) phantom was used to simulate humans and body parts of different sizes (Fig. 1a and b). It consists of one cylindrical and one conical part where the cylindrical part of the phantom has an axial length of 40 cm and a diameter of 30 cm. The length of the cone-shaped phantom is 60 cm and the diameter is 30 cm in the base and 7 cm in the top. There are three drilled holes through for each phantom, one at the centre and two holes separated 5 cm apart, where radionuclide sources can be inserted. Each hole is 15 mm in diameter.

The Alderson-Rando (Fig. 1c) nuclear medicine thorax phantom (Radiology Support Devices, Long Beach, Ca, USA) was used to verify the calibration coefficients obtained with the conical-cylindrical phantom. The phantom corresponds to an average male adult (74 kg) and it includes organs mimicking the lungs, liver, chest bones and the spinal cord with attenuating properties comparable with those of human anatomical structure.

Calibration coefficients and minimum detectable activities

The dual-headed gamma camera in a hybrid SPECT/CT scanner (Symbia TruePoint T2, Siemens Medical Solutions, Erlangen, Germany) was employed to determine the count rates per unit activity from a point source located at various phantom diameters and depths in the cone shaped phantom, referred to as calibration coefficients, and to determine the minimum detectable activity (MDA) for these source-phantom geometries. Each head of the SPECT system has a thallium-activated sodium iodide detector with a rectangular field-of-view of 53.3x38.7 cm^2 and a detector thickness of 9.5 mm.

Static planar gamma camera acquisitions were performed with a 180º detector configuration and with the collimators removed. The acquisition time was set to 300 s. For simplicity and for easy use in an emergency situation, the count rates from the dual-headed gamma camera were just added. It has previously been shown that a 300 s acquisition time has given sufficient counting statistics in cases of emergency situations where a rapid investigation of internally contaminated individuals is necessary[7].

The radionuclides ^{131}I (737 kBq [22 Dec 2014]) and ^{137}Cs (167 kBq [22 Dec 2014]) were selected on basis of their potential risk in radiation emergency situations. The activity of ^{131}I was measured using an activity meter (CRC-15R, Capintec Inc, Ramsey, NJ, USA) and the activity of ^{137}Cs was measured using a high-purity germanium (HPGe) detector (EG&ORTEC, Berwyn, PA, USA). Sealed point shaped sources of each of these radionuclides were inserted in the central drill hole in the cylindrical and conical phantom one at a time. When primarily the quantification of activity is considered rather than spatial resolution, short detector-surface distance without collimators is preferred[7]. The phantom-surface detector distance was therefore set at the shortest practical distance (2.5 cm) for all measurements[6].

The count rates were registered for five phantom diameters, i.e. 10, 15, 20, 25 and 30 cm. Count rates for ^{137}Cs were measured with the energy window centered symmetrically around 588 keV with a 34% window width, corresponding to an energy window of 490-690 keV. This energy window could not be centered around the 661 keV peak from ^{137}Cs, but was chosen as 690 keV was the upper limit of the pulse height analyzer (PHA) of the signals from the gamma cameras. For ^{131}I, an energy window was set at 364 keV with a 15 % window width (energy window of 337 - 391 keV). From this, calibration coefficients were calculated as the ratio between the background-corrected count rate (counts per second [cps]) and the activity of the radionuclides (kBq).

The MDA was defined as three times the standard deviation of the background count rate (SD_{bkg}) for a 300 s measurement time t_m:

$$MDA(t_m)=3/(t_m \cdot \varepsilon) \cdot SD_{bkg} \quad (1)$$

where ε refers to the calibration coefficients (cps kBq^{-1}) as defined previously. Next, in order to acquire calibration coefficients for various depths, measurements were performed by placing the radionuclides in the drilled holes at the following radial positions in the phantom: 0 cm (surface of the phantom of the 30 cm diameter part of the phantom), 5 cm, 10 cm and 15 cm (central drill hole); Figure 1a).

Verification measurement

The accuracy of the calibration coefficients was determined with an additional measurement using the Alderson-Rando phantom in order to verify the determined calibration coefficients. The ^{137}Cs source was placed on the right lung surface of the Alderson-Rando phantom which was subsequently filled with water. The lung inserts of the phantom contain frigolite beads to achieve a density roughly corresponding to human lungs. The measurement was performed using the same acquisition mode as previously with an energy window of 490-690 keV and a 300 s measurement time. The detector-phantom surface distance was 4 cm due to practical limitations. The anterior-posterior distance of the phantom at the lung position was 23 cm.

*Corresponding author: unal.oren@med.lu.se

Estimation of absorbed dose rate

The absorbed dose rate from the MDA was estimated for both ^{131}I and ^{137}Cs. To perform the absorbed dose rate estimations a source position representing the thyroid (12 cm in diameter with a MDA of 0.1 kBq) was used for ^{131}I and a phantom position representing the colon (30 cm in diameter with a MDA of 0.55 kBq) was used for ^{137}Cs uptake. The absorbed dose rate estimations were performed using the internal dosimetry computer program IDAC 2.0[8], which uses the ICRP/ICRU computational reference adult voxel phantoms[9], and the tissue weighting factors from ICRP publication 103[10].

RESULTS

Calibration coefficients and minimum detectable activities

The calibration coefficients, in terms of cps Bq^{-1}, for the radionuclides for the different phantom diameters are summarized in Figure 2. The calibration coefficients for ^{131}I ranged from 12 cps kBq^{-1} (30 cm phantom diameter) to 37 cps kBq^{-1} (10 cm phantom diameter). The corresponding values for ^{137}Cs were 10 cps kBq^{-1} (30 cm phantom diameter) to 19 cps kBq^{-1} (10 cm phantom diameter). The largest calibration coefficients were observed for the smallest phantom diameter as shown in Fig. 2.

The MDA values for ^{131}I and ^{137}Cs are presented in Fig. 3 for the different phantom diameters. For ^{137}Cs, the MDA values varied between 0.29 kBq (10 cm diameter) and 0.55 kBq (30 cm diameter). The corresponding MDA values for ^{131}I were between 0.08 kBq (10 cm diameter) and 0.26 kBq (30 cm diameter).

Fig. 4 and Fig. 5 illustrate the calibration coefficients and the MDA values at various distances from the central drill hole for the 30 cm diameter cylindrical phantom, representing different depth deposition of the contaminants. The calibration coefficients are highest (49 and 100 cps kBq^{-1} for ^{137}Cs and ^{131}I, respectively) and the MDAs are lowest (0.11 and 0.03 kBq ^{137}Cs and ^{131}I) when the radionuclides are placed on the surface, nearest to one of the detectors.

Verification measurement

For the Alderson phantom with the ^{137}Cs source positioned on the lung surface, a total count rate of 2794 cps was registered for the two detectors and corrected for the background. This value was converted to activity using a calibration coefficient of 13 cps kBq^{-1}, corresponding to 23 cm anterior-posterior distance for the Alderson-Rando phantom (derived from Fig. 2). The result was an activity estimation of 215 kBq, which overestimates the true activity by 29 %.

Estimation of absorbed dose rate

A ^{131}I uptake in the thyroid at the MDA-level of 0.1 kBq (found for the conical phantom at a 10 cm diameter) was estimated to give a mean absorbed dose rate in the thyroid of 14 μGy/day and 16 μGy/day for the male and the female phantom, respectively. The effective dose rate was 0.6 μSv/day. For a ^{137}Cs uptake in the colon at the MDA level of 0.55 kBq, the mean absorbed dose rate to the colon was estimated to 10 μGy/year and 11 μGy/year for the male and the female phantom, respectively, corresponding to an effective dose rate of 1 μSv/year.

DISCUSSION

This study demonstrates the feasibility of obtaining calibration coefficients and MDA values, for gamma emitting radionuclides associated with radiation emergency situations, using a cylindrical-and cone-shaped phantom which mimics different patient sizes and body parts,. The calibration coefficients and the MDA values obtained are useful for estimating the activity in internally contaminated individuals following nuclear accidents.

The size of the phantom affects the calibration coefficients and the MDA values. As anticipated the calibration coefficients decreased as the phantom diameter increased. The MDA values, which are affected by the background levels and the measurement time, increase with increasing phantom diameter from 10 to 30 cm. This is due to the fact that a thicker phantom attenuates a larger portion of the emitted gamma rays. Also, as the photon energy increases, the probability of energy deposition in the NaI(Tl)-detectors of the gamma camera decreases, resulting in a lower efficiency at higher photon energies and thus higher MDA values for ^{137}Cs.

The verification measurement for ^{137}Cs using the derived calibrations coefficient from the conical-cylindrical phantom did not differ by more than 29 % when comparison was made with the Alderson-Rando phantom. The difference can be attributed to parameters such as different densities between PMMA and water, the different detector-phantom surface distance which affects the sensitivity of the gamma camera and depth in the phantoms for the ^{137}Cs source position. However, we can with this approach convert with an uncertainty within 30% the count rate into activity estimations for individuals who are internally contaminated with radionuclides such as ^{137}Cs or ^{131}I following radiological or nuclear events. Published results show that better estimations (±8%) of the activity concentrations can be achieved using whole body monitors[11].

The calibration coefficients provided by this simple method are in good agreement with previously published data. Wallström et al.[6] obtained calibration

coefficients for solutions of ^{137}Cs in the range of 2.2 – 12 cps kBq^{-1}, distributed in phantoms weighting between 14 – 93 kg and using an energy window of 550-750 keV and a 5 cm detector-surface distance. The discrepancies are probably associated with the fact that the conical-cylindrical phantom used in this study has a different shape, material and density compared to phantoms used in the study by Wallström et al. We also used radionuclide point sources whereas Wallström et al. used solutions of nuclides homogenously distributed in the phantoms. The energy window and the detector-surface distance used in this study are also different compared to published data. Other authors obtained, for lung deposited ^{137}Cs, a calibration coefficient of 210 cps kBq^{-1} for an Alderson-Rando average male phantom and using the whole photon energy window (24-690 keV)[7].

Dantas et al.[12] obtained, for a thyroid phantom using a gamma camera without a collimator and a 10 cm detector-surface distance, a calibration coefficient value of 39 cps kBq^{-1} using a ^{133}Ba source as a ^{131}I surrogate. This is in good agreement with the 37 cps kBq^{-1} for ^{131}I in this study for the 10 cm phantom diameter, which could be approximated to a thyroid phantom diameter. They also obtained a MDA value of 0.081 kBq which is in good agreement with the 0.082 kBq obtained in this study.

Internal dose rate calculations were performed to present the dose level corresponding to the MDA values which could be achieved when using the added pulses from the dual-headed gamma camera heads for detection. For example, the MDA values for a thyroid uptake of ^{131}I and ^{137}Cs uptake in the colon results in effective dose rates of 0.6 μSv/day and 3 μSv/year, respectively. Thus, utilizing gamma cameras with 5 min measurements times results in the detection of internal contamination of ^{131}I and ^{137}Cs with effective dose rate levels below the annual effective dose limit of 1 mSv for members of the public as recommended by the ICRP[10].

Reported MDA values for WBCs in the Nordic countries are in the range of approximately 0.04-0.15 kBq for ^{137}Cs and for a phantom representing a 70 kg man[13]. The MDA values for the WBCs are thus approximately 4 to 14 times lower compared to the results obtained with the gamma camera in this study for the 30 cm phantom diameter. The much lower MDA values between the WBCs and gamma cameras can be explained by the low background in the WBCs, differences in detector types, phantom shapes and measurement times.

Published data also show that average whole-body content in adults of highly contaminated areas in the Bryansk region following the Chernobyl accident was in the range of 3-60 kBq[14]. These values are much higher than the MDA values obtained for the gamma cameras in this study, indicating that gamma cameras can be used for internal contamination monitoring especially in cases where the contaminants are in the form of point sources such as hot particles.

The limitation of this study is that the phantom is only an approximation of a human body and there is absence of specific organs of different densities and different attenuation properties. The nuclides used in the present study were also point sources whereas more homogenous uptakes can be expected in several organs. Further, another limitation using gamma cameras is the background activity in the nuclear medicine department originating from patients, activity transport and contamination. Also, the derived calibration coefficients and minimum detectable activities are only valid for the specific gamma camera type used in this study. However, the methodology could be used as a template for other vendors.

Nevertheless, gamma camera imaging will have a place in large scale monitoring of *in-vivo* contamination to alleviate the patent flow to WBC in case of a radiological or nuclear emergency, and the method presented in this study of using a simple phantom for making approximate calibration coefficients for various body sizes and organ depths of intake can be of great value for such *in-vivo* measurements.

CONCLUSION

Calibration coefficients and MDA values have been derived, using a SPECT/CT system for stationary gamma camera imaging and a conical-cylindrical phantom simulating different body sizes for the two fission products ^{131}I and ^{137}Cs, which are associated with nuclear and radiological emergencies. Dual planar gamma camera imaging with its collimators removed could provide a rapid and direct measurement of the nuclide in the patient when whole body counters are not available. The results can be applied in situations where individuals have been internally contaminated following radiation emergency or accident situations.

ACKNOWLEDGEMENTS

The authors acknowledge Mats Hansson for help with the initial measurements with the cylindrical-conical phantom.

FUNDING

This work was supported by the Swedish Radiation Safety Authority [Grant number SSM2008-3130].

REFERENCES

1. UNSCEAR. Annex A: In: *UNSCEAR 2013 Report Vol I: Sources, effects and risks of ionizing radiation.* Vienna,

Austria: United Nations Scientific Committee on the Effects of Atomic Radiation; 2013:1-321 Available at: http://www.unscear.org/unscear/en/publications/2013_1.html

2. Musolino, S.V. and Harper, F.T. Emergency response guidance for the first 48 hours after the outdoor detonation of an explosive radiological dispersal device. Health Phys. 90(4), 377-85 (2006)
3. Smith, J.M, Ansari, A. and Harper F.T. Hospital management of mass radiological casualties: reassessing exposures from contaminated victims of an exploded radiological dispersal device. Health Phys. 89(5), 513-20 (2005)
4. International Atomic Energy Agency (IAEA), 1998. Dosimetric and medical aspects of the radiological accident in Goiania in 1987, IAEA-TECDOC-1009, Vienna
5. Rojas-Palma, C., Liland, A., Ness Jerstad, A., Etherington, G., del Rosarion Perez, M., Rahola, T. and Smith, K. TMT Handbook; Triage monitoring and treatment of people exposed to ionising radiation following a malevolent act. ISBN (printed version): 978-82-90362-27-5. Print: Lobo Media AS. Available on http://www.tmthandbook.org/
6. Wallström, E., Alpsten, M. and S. Mattsson, S. A gamma camera for measurements of internal contamination after a radiological accident. J. Radiol. Prot. 19(2), 143-54 (1999)
7. Hansson, M. and Rääf, C.L. Visualisation and quantification of lung content of radionuclides associated with nuclear and radiological emergencies. Radiat. Prot. Dosim. 145(4), 341-50, (2011)
8. Andersson, M., Johansson, L., Minarik, D., Mattsson, S. and Leide-Svegborn S. An internal radiation dosimetry computer program, IDAC 2.0, for estimation of patient doses from radiopharmaceuticals. Radiat Prot Dosim. 162(3): 299-305, (2014)
9. International Commission on Radiological Protection: ICRP publication 110: Adult Reference Computational Phantoms. Oxford: Elsevier; 2009.
10. The 2007 Recommendations of the International Commission on Radiological Protection. ICRP publication 103. Ann ICRP, 2007. 37(2-4): 1-332.
11. Andrási, A. Whole-body counter intercomparison as a tool of quality assurance. Radiat. Prot. Dosim. 89(3-4), 229-33 (2003)
12. Dantas, B. M., Lucena, E. A., Dantas, A. L., Araújo, F., Rebelo, A.M., Terán, M., Paolino, A., Hermida. J.C., Rojo, A.M., Puerta, J. A. et al. A protocol for the calibration of gamma cameras to estimate internal contamination in emergency situations. Radiat. Prot. Dosim. 127(1-4), 253-7 (2007)
13. Rahola, T., Muikky, M., Falk, R., Johansson, J., Liland, A. and Thorshaug, S. Assessment of internal doses in emergency situations. (Roskilde, Denmark: Report NKS-128) (2006). ISBN 87-7893-190-8. Available at www.nks.org
14. Zvonova, I. A., Jesko, T.V., Balonov, M.I., Danilova, I. O., Wallström, E., Alpsten, M., Thornberg, C. and Mattsson, S. ^{134}Cs and ^{137}Cs whole-body measurements and internal dosimetry of the population living in areas contaminated by radioactivity after the Chernobyl accident. Radiat. Prot. Dosim. 62(4), 213-21 (1995)

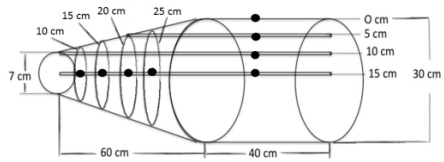

(a)

Figure 1a. A schematic representation of the cylindrical-conical phantom, used for determination of calibration coefficients, where the positions for the radionuclides are indicated in black circles.

(b)

(c)

Figure 1b and c. The cylindrical-conical phantom, used for determination of calibration coefficients and the Alderson-Rando phantom used for verification measurements.

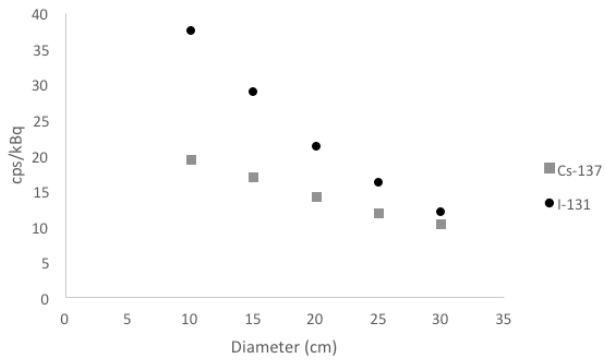

Figure 2. Variation of the calibration coefficients with phantom diameter for the cylindrical-conical phantom.

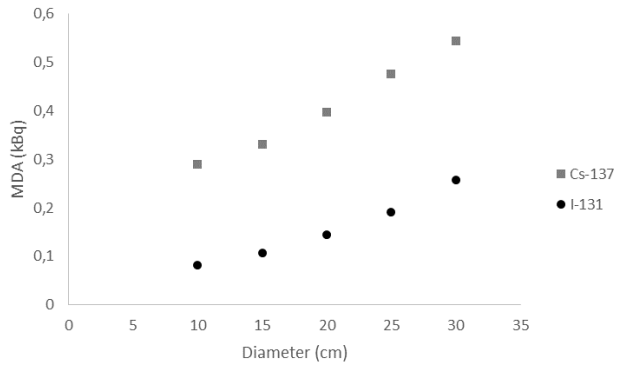

Figure 3. MDA values obtained with the conical-cylindrical phantom as a function of phantom diameter.

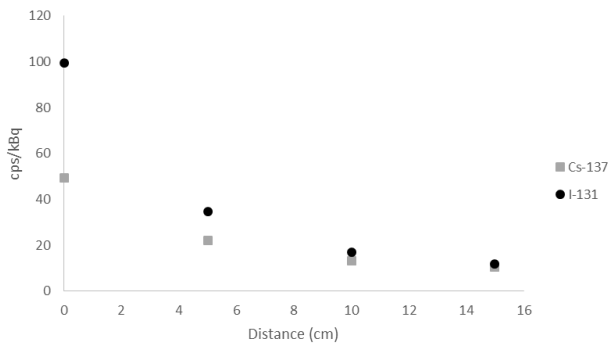

Figure 4. Calibration coefficients for the radionuclides as a function of different depths in the 30 cm diameter phantom where 0 cm corresponds to the phantom surface and 15 cm to the center of the phantom.

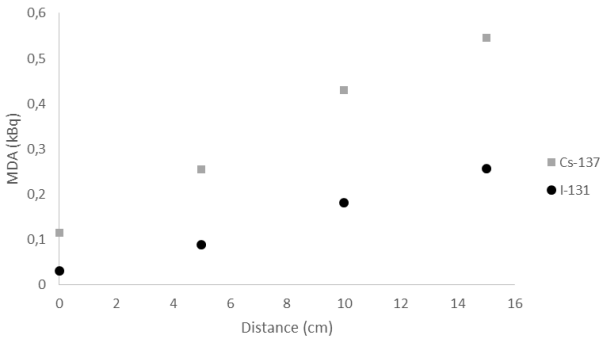

Figure 5. MDA values for the radionuclides placed at different depths in the 30 cm diameter phantom where 0 cm corresponds to the phantom surface and 15 cm to the center of the phantom.